# Carnegie Mellon University

## CARNEGIE INSTITUTE OF TECHNOLOGY

## THESIS

SUBMITTED IN PARTIAL FULFILLMENT OF THE REQUIREMENTS

FOR THE DEGREE OF Doctor of Philosophy

TITLE **Multi-Timescale Control of Energy Storage**

**Enabling the Integration of Variable Generation**

PRESENTED BY **Dinghuan Zhu**

ACCEPTED BY THE DEPARTMENT OF

**Electrical and Computer Engineering**

Gabriela Hug — 5/1/14
ADVISOR, MAJOR PROFESSOR — DATE

Jelena Kovacevic — 5/1/14
DEPARTMENT HEAD — DATE

APPROVED BY THE COLLEGE COUNCIL

Vijayakumar Bhagavatula — 5/1/14
DEAN — DATE

# Multi-Timescale Control of Energy Storage Enabling the Integration of Variable Generation

Submitted in partial fulfillment of the requirements for

the degree of

Doctor of Philosophy

in

Electrical and Computer Engineering

Dinghuan Zhu

B.S., Electrical Engineering, Zhejiang University (2009)

Carnegie Mellon University

Pittsburgh, PA

May, 2014

*This dissertation is dedicated to my parents and my beloved wife.*

# Abstract

A two-level optimal coordination control approach for energy storage and conventional generation consisting of advanced frequency control and stochastic optimal dispatch is proposed to deal with the real power balancing control problem introduced by variable renewable energy sources (RESs) in power systems. In the proposed approach, the power and energy constraints on energy storage are taken into account in addition to the traditional power system operational constraints such as generator output limits and power network constraints.

The advanced frequency control level which is based on the robust control theory and the decentralized static output feedback design is responsible for the system frequency stabilization and restoration, whereas the stochastic optimal dispatch level which is based on the concept of stochastic model predictive control (SMPC) determines the optimal dispatch of generation resources and energy storage under uncertainties introduced by RESs as well as demand. In the advanced frequency control level, low-order decentralized robust frequency controllers for energy storage and conventional generation are simultaneously designed based on a state-space structure-preserving model of the power system and the optimal controller gains are solved via an improved linear matrix inequality algorithm. In the stochastic optimal dispatch level, various optimization decomposition techniques including both primal and dual decompositions together with two different decomposition schemes (i.e. scenario-based decomposition and temporal-based decomposition) are extensively investigated in terms of convergence speed due to the resulting large-scale and computationally demanding SMPC optimization problem. A two-stage mixed decomposition method is conceived to achieve the maximum speedup of the SMPC optimization solution process. The underlying control design philosophy across the entire work is the so-called time-scale matching principle, i.e. the conventional generators are mainly responsible to balance the low frequency components of the power variations whereas the energy storage devices because of their fast response capability are employed to alleviate the relatively high frequency components. The performance of the proposed approach is tested and evaluated by numerical simulations on both the WECC 9-bus system and the IEEE New England 39-bus system.

# Acknowledgements

First of all, I would like to express my deepest gratitude to my advisor Prof. Gabriela Hug for the immeasurable amount of support, guidance and encouragement she has provided since the first day of my Ph.D. study in the Department of Electrical and Computer Engineering (ECE) at Carnegie Mellon University (CMU). It is her passion and enthusiasm that have been encouraging me to devote myself to research; it is her guidance and advice that have been pointing me to the in-depth thinking of my research topics; it is her insight and inspiration that have been enlightening my deep understanding of the field of electric energy systems. The training I received from her on professional skills such as writing, presentation, time management and leadership is going to have a profound influence on my life. The opportunity of working with Gabriela has been my greatest fortune and privilege.

Sincere gratitude is extended to my dissertation committee members – Prof. Bruce H. Krogh, Dr. Daniel F. Opila, Dr. Xiaoming Feng, and Prof. Zhi-Hong Mao for their generous time, invaluable advice, and insightful comments.

I would also like to show my appreciation toward other faculty members in the ECE and CS departments, including Prof. Marija D. Ilić, Prof. Xin Li, Dr. Jovan Ilić, Prof. Bruno Sinopoli, Prof. Soummya Kar, Prof. Ozan Tonguz, Prof. Franz Franchetti, Prof. Jian-Gang (Jimmy) Zhu, Prof. Hui Zhang, Prof. J. Zico Kolter, and Prof. David R. O'Hallaron. The constructive discussions with them not only helped me become a mature and qualified Ph.D. candidate but also assisted me to plan my future career development path.

Special thanks go to Ms. Claire E. Bauerle, and Ms. Carolyn Patterson. They made the Porter Hall B-Level a warm and pleasant place for me to work and study. I am also grateful to Ms. Samantha Goldstein and Ms. Elaine Lawrence in the ECE Graduate Programs Office. They are very knowledgable about the Ph.D. programs at CMU and always ready to help, which made each of my steps toward the degree easy to follow.

I am also so thankful to have a large group of excellent colleagues and friends who brought me lots of support, comfort, and fun along the stressful journey of my Ph.D. study, including Prof. Le Xie, Prof. Nermeen Mahmoud, Dr. Qixing Liu, Dr. Tao Cui, Dr. Juhua Liu, Dr. Chenye Wu, Dr. Mohsen Rahmani, Dr. Sanja Cività, Dr. Jhi-Young Joo, Dr. Milos Cvetković, Dr. Congzhong Guo, Dr. Can Ye, Dr. João Mota, Dr. Qiao Li, Dr. Yilin Mo, Rui Yang, Kyri Baker, Todd Ryan, Hameed Safiullah, Javad Mohammadi, Andrew Hamann, Xiao Zhang, Dmitry Shchetinin, Junyao Guo, Zhe Yu, Harald Franchetti, Hao Ming, Yang Weng, Jonathan Donadee, Joya Deri, Nipun Popli, Xia Miao, Kevin Bachovchin, Xiaoqi Yin, Andrew Hsu, Stefanos Baros, Nikos Aréchiga, Sérgio Pequito, Jiawei Shi, Yisu Nie, Yizhi Zheng, Liangyan Gui, Yue Ding, and others too numerous to name.

In addition, I would like to thank those people who led me into the wonderland of the electric power engineering during my undergraduate studies, including Prof. Yijia Cao, Prof. Quanyuan Jiang, and Prof. Chuangxin Guo of Zhejiang University and Prof. Alex Q. Huang of North Carolina State University.

However, no single piece of this dissertation would be possible without the solid support of my family. I want to express my profound thanks to my parents Yungen Ding and Dian Zhu for always standing by my side and encouraging me to pursue my dreams, no matter how far apart we are. I also want to thank my wife Lingling Xu for her enormous love and unwavering support for me. I very much appreciated her great effort to ensure a healthy and energetic me during my writing of this dissertation. My life becomes wonderful and full of miracles because of her!

The research work presented in this dissertation was supported by the following funding sources: the National Energy Technology Laboratory, the Philip and Marsha Dowd Engineering Seed Fund, Innovation Works, the Keystone Innovation Starter Kit grant from Pennsylvania's Department of Community and Economic Development, the National Science Foundation Grant ECCS-1027576, and the Department of Electrical and Computer Engineering at Carnegie Mellon University. I gratefully appreciate the financial support.

To close, earning the Ph.D. degree from CMU is a significant milestone for me and it also means a brand new start in my life. The spirit of CMU – "My heart is in the work" has been and will always be part of my DNA wherever I am and whatever I do.

# Contents

# List of Tables

# List of Figures

# Chapter 1

# Introduction

The work of this dissertation is essentially motivated by the fact that more and more variable renewable energy sources (RESs) such as wind and solar generators are added to the legacy electric power system, introducing large uncertainties and variations in the power supply side. This section briefly reviews the current industry practice of real power balancing control and further describes the motivation behind the development of the proposed control approach. In addition, the formal problem statement is given and the technical contributions made in this dissertation are stated.

## 1.1 Motivation

One of the main drivers for the transition to the smart grid is to enable a higher penetration level of renewable energy sources with the intention to gradually transform the current power grid into a green and sustainable energy ecosystem. The main difficulty of accommodating considerable amounts of RESs is that they introduce large variations and uncertainties in the power supply side. The RES generation cannot be dispatched like conventional generators because its power output is highly dependent on environmental factors such as wind speed and solar irradiation. Furthermore, the prediction accuracy of the output power from

RESs is significantly lower than the accuracy of load forecasts resulting in inefficient or even infeasible day-ahead scheduling of generation resources [6, 7]. As a result, the chance of having large power mismatches which have to be balanced in real time increases drastically. Ultimately, this increased imbalance between active power supply and consumption in power systems leads to increased frequency deviations from the nominal value. Large unattended frequency deviations could impede the performance of generating units by influencing the performance of their auxiliary electric motor drives and even lead to severe consequences such as blackouts [4]. Fortunately, the variability and intermittency introduced by RESs can be overcome by finding means to counterbalance the power output such as using storage devices, demand side management or flexible dispatchable generation resources [8, 9]. This dissertation concentrates on providing real power balancing control solutions in terms of energy storage devices. The large-scale energy storage is identified as a key enabler for a future with high penetration of renewable generation [10–12]. Energy storage devices such as flywheels, supercapacitors and batteries are suitable for real power balancing control because of their fast response capabilities and the breakthroughs in the area of power electronics [13]. However, the question of how to optimally and safely integrate energy storage into the power grid remains open.

As the current industry practice, a hierarchical real power balancing and frequency regulation mechanism consisting of primary, secondary and tertiary frequency control is employed to maintain the system frequency within specified limits. Primary control is based on speed droop controllers (proportional controllers) used locally by the generators to stabilize the frequency in the system whereas the centrally organized secondary control (a.k.a. automatic generation control or AGC) based on area control error (ACE) brings the frequency back to its nominal value and re-establishes the tie-line flows across control areas to the agreed values. The ACE is defined as a linear combination of the average frequency deviation from the nominal value and the net deviation of tie-line flows from their scheduled quantities, which is intended to be an indication of real power imbalance in a particular control area. Tertiary control is an optimization based generation resource dispatching task involving economic dispatch which is performed at every 5 to 15 minutes depending on the specific real-time electricity markets.

In the future with increased amounts of variable and intermittent resources, the aforementioned scheme may need to be revisited for three main reasons/issues: 1) it leads to increased fast ramping of conventional generators while still not being able to sufficiently reduce the frequency deviations because the traditional primary control is of proportional feedback type and the traditional secondary control is not designed to quickly respond to power imbalance; 2) it does not take into account the increased uncertainty caused by RESs at the tertiary level, very likely resulting in economically inefficient dispatch of generation resources; 3) it is not suitable for the integration of energy storage devices as not only the power output (MW) but also the provided energy (MWh) is limited.

## 1.2 Problem Statement

Before stating the problem itself, a few terms that appear in the dissertation and may lead to confusing if not properly defined are clarified first. The term “frequency control” in the remaining of this dissertation refers to the sole task of maintaining frequency in a tight band, while the meaning of the term “secondary control” or “secondary frequency control” includes the tie-line flow regulation task in addition to frequency control by following the current industry convention.

Given an interconnected power system (possibly consisting of multiple control areas) with high penetration of variable renewable energy sources and reasonable amount of installed energy storage capacity, the problem is to develop a systematic approach for real power balancing control under uncertainties for the entire system, which maintains a tight band of frequency deviations, ensures the safe operation of energy storage devices, and minimizes the total cost of providing energy for the system including the generation and ramping costs of generators subject to relevant physical constraints such as transmission line limits.

We restrict ourselves to the realtime and near realtime control aspects of the real power balancing task in power systems, i.e. the day-ahead unit commitment is out of scope of this dissertation. In addition, we assume that the interconnected power system consisting of multiple control areas can be treated as a single consolidated system and that the parameters for modeling the entire interconnected power system is available to the control design engineers.

## 1.3 Proposed Two-Level Approach

As previously mentioned, this dissertation is dedicated to developing a systematic control and optimization framework for real power balancing and frequency regulation in a new environment with variable renewable generation and energy storage. The traditional three-level framework is restructured and redesigned to address all of the three aforementioned issues. The redesigned framework consists of two levels, including the advanced frequency control (AFC) and the stochastic optimal dispatch. Advanced frequency control incorporates the primary control and the frequency regulation task in the secondary control. The level of stochastic optimal dispatch which is specifically based on the stochastic model predictive control (SMPC) method takes into consideration not only the uncertainty introduced by RESs and demand but also multiple time steps in a look-ahead horizon. We use the term "stochastic model predictive control based optimal dispatch" (short for "SMPC based optimal dispatch") and the term "stochastic optimal dispatch" interchangeably to refer to this level. In addition, the power and energy constraints associated with energy storage devices are taken into account in both of the two levels.

### 1.3.1 Design Philosophy

In the proposed framework, the coordination between conventional generation and energy storage is achieved by assigning the power balancing responsibilities to these resources according to their capabilities. The conventional generators are mainly responsible to balance the low frequency components of the power variations whereas the energy storage devices because of their fast response capability are employed to alleviate the relatively high frequency components. This is the underlying design philosophy across the entire work, which we term as the *time-scale matching*. The wear and tear effect of conventional generators caused by frequent high ramping operations is therefore reduced by smoothing out their power output [14].

### 1.3.2 Relation between the Two Levels

The relation between the two control levels shown in Fig. 1.1 follows the basic paradigm of hierarchical control. The stochastic optimal dispatch level collects all the relevant data from the physical power system to perform the stochastic optimization every 5 to 15 minutes, yielding the optimal generator and storage settings to be implemented by the advanced frequency control level for the current time interval. The advanced frequency control level adjusts the generator and storage power output set points once it is instructed by the stochastic optimal dispatch level and continuously takes the responsibility of maintaining frequency within a tight band by imposing physical control actions. Overall, the two-level control keeps the physical power system operating in a safe and most economical manner.

## 1.4 Contributions of this Dissertation

The technical contributions of this dissertation are as follows:

- **Development of a systematic approach for real power balancing control with safe and optimal integration of energy storage devices:** A two-level control approach including advanced frequency control and stochastic optimal dispatch is proposed. The control actions of both the two levels are determined through optimization processes with consideration of the power and energy limits of energy storage

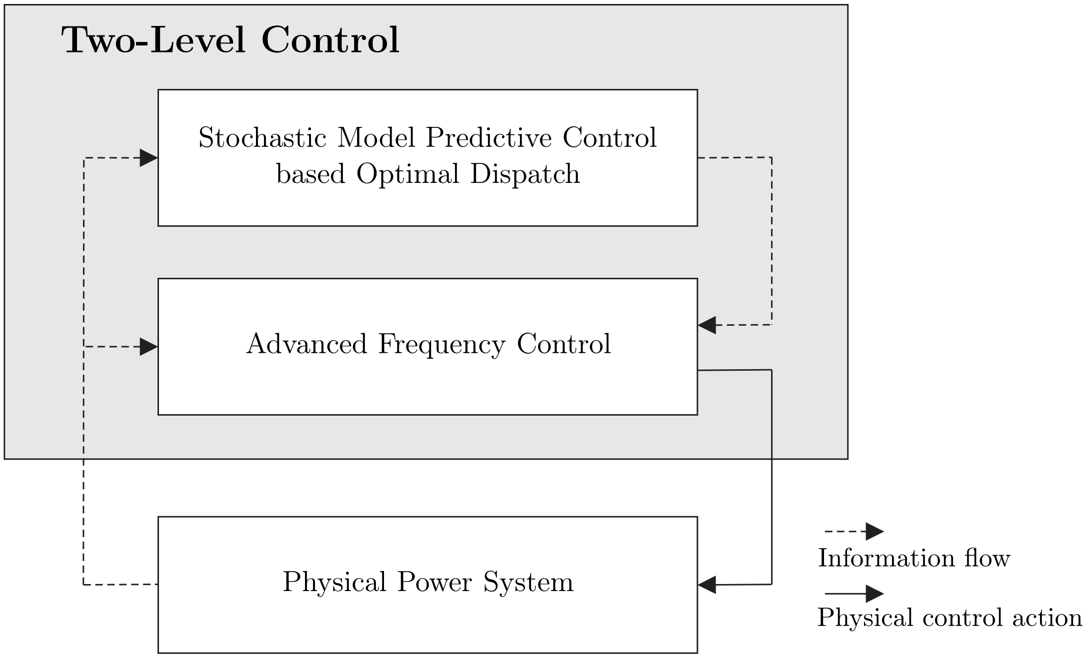


Figure 1.1: Interaction among the two control levels and the physical power system.

devices.

- **Introduction and implementation of the concept of time-scale matching for coordination between conventional generation and energy storage in real power balancing responsibilities:** The proposed time-scale matching principle states that the conventional generators are mainly responsible to balance the low frequency components of the power variations whereas the energy storage devices because of their fast response capability are employed to alleviate the relatively high frequency components. The time-scale matching is ensured in the advanced frequency control level via frequency dependent weighting functions and the stochastic optimal dispatch level achieves the principle by including quadratic ramping cost terms.

- **Development of an $H_\infty$ optimization approach for enhanced frequency control with energy storage:** The problem of integrating energy storage and renewable generation with respect to real power balancing is constructed as a multi-objective $H_\infty$ optimization problem. In addition to frequency dependent weighting functions, the decentralized static output feedback is applied to achieve task-specific but easily-implementable controllers. We also show that this $H_\infty$-based frequency control approach provides a promising means to design and coordinate decentralized proportional-integral (PI) controllers for multiple conventional generators which enables the return to the nominal frequency.

- **Development of a structure-preserving dynamic model for interconnected power systems:** The state-space model of an interconnected power system is systematically derived based on component-level models and the DC power flow model for the control design. In addition, a model to estimate the local frequency at non-generator buses is developed to facilitate the decentralized control scheme for advanced frequency control in the design stage.

- **Improvement of an existing iterative linear matrix inequality algorithm for optimal $H_\infty$ controller gain calculation:** The existing linear matrix inequality algorithm involves a non-convex generalized eigenvalue minimization problem. We improve the existing algorithm by convexifying this minimization problem via heuristics.

- **Proposal of the use of stochastic model predictive control for optimal dispatch considering energy storage in the future power systems:** The stochastic model predictive control is adopted to optimally and safely dispatch energy storage and conventional dispatchable generation under uncertainties for a certain period of look-ahead horizon.

- **Analysis of both primal and dual optimization decomposition techniques for solving the stochastic model predictive control based optimal dispatch in terms of speed and convergence:** Both the primal based (Benders decomposition) and dual based (Lagrangian relaxation decomposition and augmented Lagrangian decomposition) decomposition techniques are analyzed for the considered stochastic model predictive control problem in terms of problem formulation and convergence speed. The value of decomposition is demonstrated using the WECC 9-bus system and the IEEE New England 39-bus system.

- **Development and evaluation of three decomposition approaches for solving the stochastic model predictive control based optimal dispatch:** A temporal-based decomposition is introduced to achieve the tradeoff between convergence speed and subproblem size for the considered stochastic model predictive control problem. Simulation results indicate that the two-stage mixed decomposition scheme among the three proposed approaches has the best performance record in terms of convergence speed. To the best of our knowledge, this is the first time the mixed decomposition is proposed for two-stage stochastic model predictive control problems. Under such a two-stage decomposition, each subproblem in the first stage is associated with a specific scenario for the stochastic process. The second stage further decomposes each of the scenario-based subproblems into even smaller subproblems where each corresponds to a set of time steps in the optimization horizon. In addition, we resolve the singularity issues that arise in the three proposed decomposition approaches, which is applicable to the decomposition of general model predictive control problems.

## 1.5 Dissertation Organization

The rest of this dissertation is organized as follows. Chapter 2 reviews some basic concepts about real power balancing and frequency control in power systems and briefly introduces various important energy storage technologies. The advanced frequency control in the proposed two-level approach is throughly investigated in Chapter 3 whereas the stochastic optimal dispatch level is described in Chapter 4. Numerical simulation results of both the two control levels on the WECC 9-bus test system and the IEEE New England 39-bus test system are given in the end of those two chapters. Chapter 5 concludes this dissertation and points out some future directions.

# Chapter 2

# Background

This chapter reviews some basic concepts about power systems including an overview on the basics of real power balancing and frequency control in power systems and a brief introduction of various important energy storage technologies, in order for readers to better understand this dissertation.

## 2.1 Power System Frequency Control Basics

As briefly mentioned in Chapter 1, the real power balancing and frequency control in the current power industry follows the paradigm of hierarchical control consisting of three levels – primary, secondary and tertiary frequency control levels to regulate the system frequency within a tight band and provide electric energy for demands in a safe and most economical manner. The basic structure of this control scheme is visualized in Fig. 2.1. This section provides a more detailed introduction about each control level, serving as the background knowledge of the dissertation.

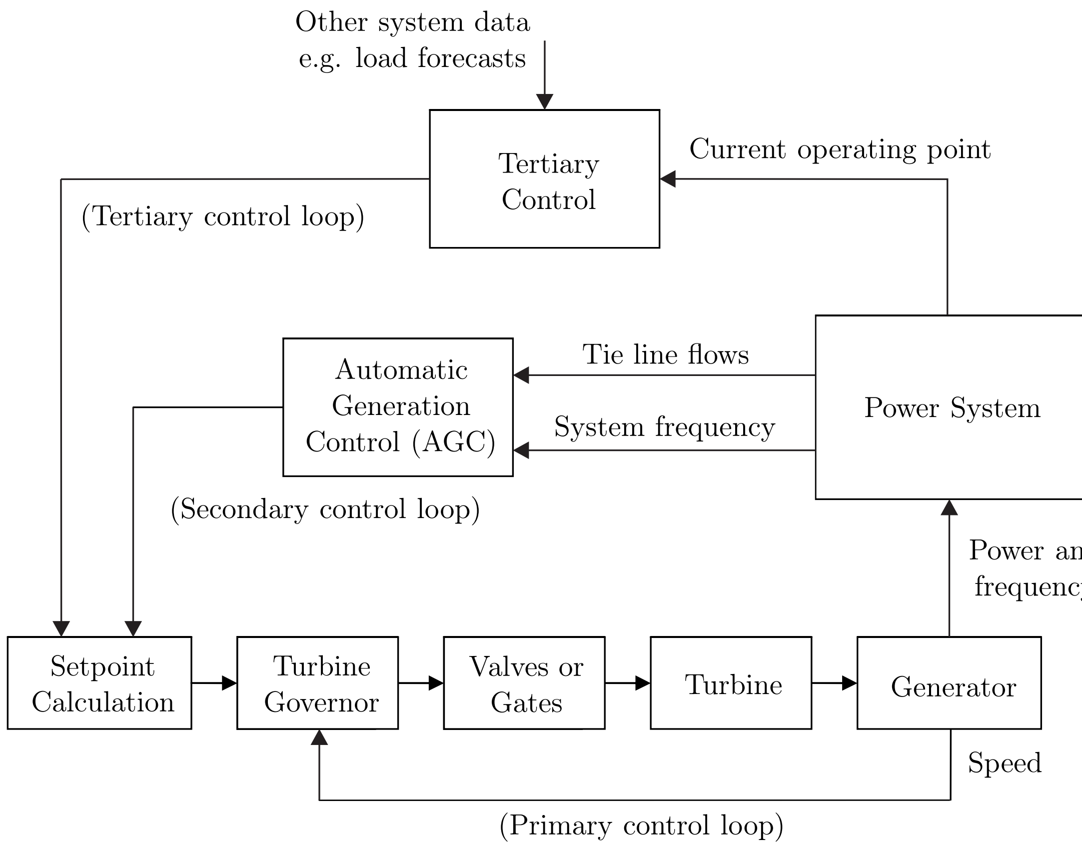


Figure 2.1: Basic structure of power systems frequency control (modified from [1]).

### 2.1.1 Primal Frequency Control

The primary control loop in Fig. 2.1 is a local control implemented by each generator in a power system to stabilize its rotating speed, which is the local frequency at that bus. The time scale of this level is on the order of seconds. If there is a sudden increase or decrease in the electric loads of the system, the kinetic energy stored in the rotating mass of each generator compensates for this change at the first place causing a frequency deviation from the nominal value. Without considering the load damping effect, the frequency deviation would keep increasing if no actions are taken by the generators. The primary control is used to adjust the mechanical power input of the generator based on a speed droop to arrest the frequency, avoiding large frequency deviations to occur due to such a load change. The static speed droop states a linear relation between the increased (or decreased) generator power output and the decrease (or increase) in the system frequency in steady state, allowing each generator to share the power balancing responsibility in a system.

The aforementioned speed droop is implemented by the turbine governor within a generator set (see Fig. 2.1). There are two common types of turbine governors – hydro-mechanical governor and hydro-electronic governor. The conceptual control block diagrams for generators equipped with the two types of governors are shown in Fig. 2.2 and Fig. 2.3, respectively. Due to the integral control behavior of the hydraulic servo actuators, a feedback is needed to transform it to a first order lag in order to implement the speed droop. $R$ in both figures represents the speed droop coefficient, whose typical value is 5% in North America. Both types of governors employ hydraulic servo actuators to physically change the opening of the valves or gates associated with the turbine. The main difference between the two is the way how they sense the rotating speed of the generator. Hydro-mechanical governors use flyweights to determine the speed at which the shaft is spinning while hydro-electronic governors utilize a magnetic pickup sensor to sense the speed. Because of this difference, the speed setpoints in hydro-mechanical governors are set via the speed adjusting screw position (see Fig. 2.2) compared to the hydro-electronic governors where speed signals are represented by electrical quantities such as voltages and currents. The speed setpoints are manipulated in the secondary frequency control to restore the system frequency back to its nominal value.

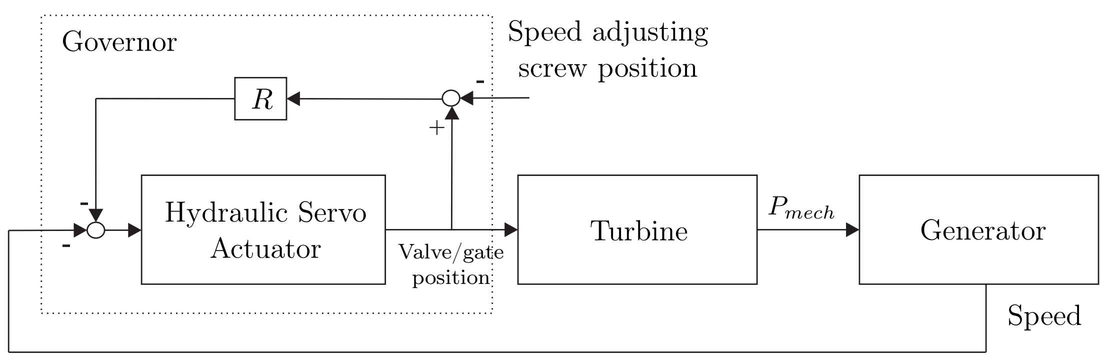


Figure 2.2: Conceptual control block diagram for generators with hydro-mechanical governors (modified from [2]).

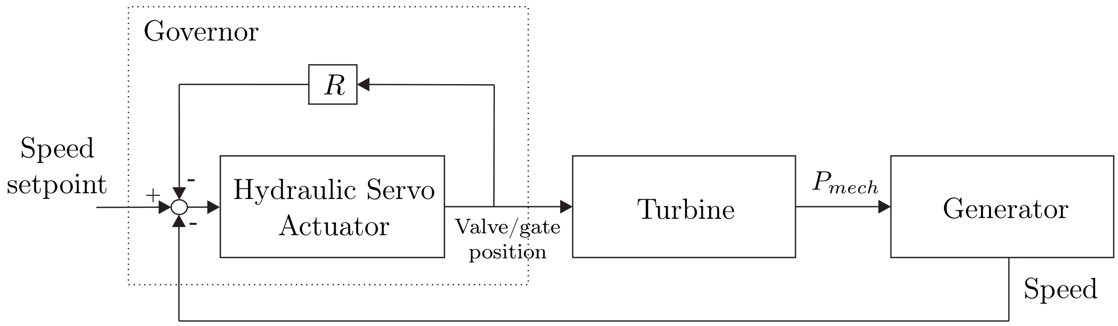


Figure 2.3: Conceptual control block diagram for generators with hydro-electronic governors (modified from [3]).

### 2.1.2 Secondary Frequency Control

The secondary frequency control (a.k.a. automatic generation control or AGC) is designed to bring the system frequency back to its nominal value and re-establish the tie-line flows across control areas to the agreed values. The time scale of this level is on the order of several seconds to several minutes. The conceptual control block diagram for this level is depicted in Fig. 2.4. This control level is centrally organized in the viewpoint of each control area. The control actions are determined based on the concept of area control error (ACE), which is intended to be an indication of real power imbalance in a particular control area. The ACE is defined as a linear combination of the average frequency deviation from the nominal value and the net deviation of tie-line flows from their scheduled quantities. As can be seen from Fig. 2.4, the centrally calculated control actions are distributed to each participating generators via a so-called participation factor $\alpha_i$. In addition, it is evident that the secondary control level is indeed an integral control.

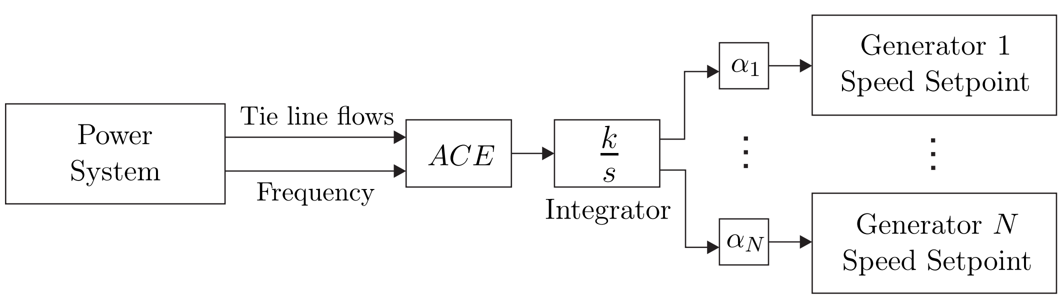


Figure 2.4: Conceptual control block diagram for secondary control (modified from [4]).

### 2.1.3 Tertiary Frequency Control

The tertiary control level is an optimization based generation resource dispatching task involving economic dispatch which is typically performed at every 5 to 15 minutes depending on the specific real-time electricity markets. Economic dispatch is aimed at optimizing the power output of the generating units to serve the forecasted system demand in the next time step in the most economical manner subject to constraints on the power balance and the transmission line limits. Based on that, the security constrained economic dispatch additionally takes into account the generation resource limits such as ramp rate limits in making resource dispatch decisions.

## 2.2 Energy Storage Technologies

This section provides a short overview over various energy storage technologies, including battery energy storage systems (BESSs), flywheel storage, supercapacitor storage, superconducting magnetic energy storage (SMES), pneumatic storage and pumped hydro storage [15–19].

### 2.2.1 Battery Energy Storage Systems (BESSs)

BESSs use electrochemical reactions to convert electrical energy into chemical energy when charging and vice versa. There are mainly five types of battery storage technologies at the moment: lead-acid batteries, nickel-based batteries, lithium-based batteries, sodium-based batteries and flow batteries [17, 18]. All the types of batteries above have been commercially deployed in power systems for various applications, such as frequency regulation, load leveling (peak load shaving) and voltage support [17]. Generally, the round trip efficiency for BESSs is in the range of 60% to 90% depending on the specific battery technology. The self-discharge rates (standby losses) are between 0% and 5% of rated capacity per month (except the nickel-based type with a minimum rate of 10%) [15, 17, 18]. The relatively low self-discharge rates make BESSs suitable for long-term energy applications.

### 2.2.2 Flywheel Storage

Flywheels store energy in the form of rotating kinetic energy which is enabled by their inertia. A typical flywheel storage system consists of three components: the flywheel, the rotor bearings and the power interface [18]. Flywheels can be accelerated to high velocities via the power interface in charging mode and slowed down to generate electricity in discharging mode. The overall round trip efficiency is between 80% and 85% [16]. The characteristics of the high charge/discharge rates and the long lifetime make flywheel storage appropriate for power applications such as frequency regulation. However, one main drawback is the large standby loss, which is reported as higher than 20% of the capacity per hour [18].

### 2.2.3 Supercapacitor Storage

Supercapacitors (ultracapacitors) are similar to regular capacitors but with significantly larger capacitance. Because there are no chemical reactions involved in charging and discharging these storage devices, supercapacitors have not only a fast response time but also great tolerance with respect to overcharging and deep discharging [18]. Their round trip efficiency is with $84-95\%$ quite high while the self-discharge rate is approximately equal to 14% of the nominal capacity per month [16, 18]. Due to the high power density of supercapacitors, they are capable of providing power quality control [19].

### 2.2.4 Superconducting Magnetic Energy Storage (SMES)

SMES systems store energy in the form of electromagnetic energy which is induced by the direct current flowing in the cooled superconducting coils [19]. The direct current is converted back to AC electricity via an inverter if power is needed in the grid. The round trip efficiency is extremely high, in the range of 95% to 98% [16]. However, they are still impractical for the industry sector due to the expensive superconducting coils as well as the uneconomical refrigeration system.

### 2.2.5 Pneumatic Storage

In pneumatic storage technologies, electrical energy is stored as compressed air or as compressed gas. The corresponding technologies include compressed air energy storage (CAES) technology and liquid-piston technology where the first one has already been employed in large-scale energy applications such as load leveling while the second one is not yet applied in the commercial sector [16, 18]. The round trip efficiencies for CAES and liquid-piston technology are around 85% and 73%, respectively [16, 18]. As a result of the required large air-tight underground caverns, CAES is severely dependent on geographical conditions, which greatly restricts the utilization of this technology. The main disadvantages for liquid-piston storage are the low energy density and significant self-discharge rate[18].

### 2.2.6 Pumped Hydro Storage

This type of storage has been widely used in the application of load leveling for a long time. Electrical energy in pumped hydro storage is transformed into potential energy by pumping water from a reservoir with a lower elevation to one with a higher elevation. The pumped hydro plant acts as a generator returning electricity back to the grid when needed. The round trip efficiency is reported as approximately $70-85\%$ [18]. Similar to CAES technology, the main drawback of pumped hydro storage is the special geographical requirements.

## 2.3 Summary

This chapter provides an overview on the current power system frequency control basics as well as various energy storage technologies that are suitable or promising for large-scale power and/or energy applications.

# Chapter 3

# Advanced Frequency Control

The advanced frequency control (AFC) is responsible for the system frequency stabilization and restoration, which addresses the first and the third issues mentioned in Chapter 1, i.e. the current frequency control scheme fails to quickly respond to power imbalance and it is not suitable for the integration of energy storage devices as not only the power output but also the provided energy is limited. The design of AFC aims to make full use of both the generator and energy storage assets according to their different capabilities in counteracting real power mismatches of the system. In essence, AFC is a unified control that integrates both the primary and secondary frequency controls of the hierarchy described in Chapter 2. The two most desirable properties – the paradigm of decentralized control in the traditional primary frequency control and the functionality of frequency restoration in the secondary frequency control are preserved in the proposed AFC. This level of control operates continuously in real time. The robust control theory and the decentralized static output feedback design are adopted in order to achieve the robustness and stability of the considered power system as well as the simplicity of the controllers. Another big advantage of robust control is that it allows the synthesis of frequency dependent weighting functions into the objective function facilitating the implementation of the time-scale matching objective. The objectives of this control level are threefold: 1) to minimize frequency deviations from the nominal value for all generator buses; 2) to minimize the use of energy storage devices in terms of state of charge; 3) to minimize the ramping required from conventional generators.

## 3.1 Background and Literature Review

Energy storage does not naturally fit into the conventional frequency control framework mentioned in Chapter 1, as not only the power output but also the energy capacity is limited for energy storage devices. In terms of frequency control, the energy storage devices in the current pilot projects are simply employed to follow the AGC signal [20, 21]. The physical limits on the state of charge (SOC) are ignored and consequently the storage devices are prone to hit their upper and lower limits.

The $H_\infty$-based robust control theory has recently attracted great attention in the power engineering community to counteract the frequency deviations because it can simultaneously achieve robustness and stability in a dynamic system subject to model uncertainties and/or bounded disturbances [22, 23]. Previous work such as [24–26] successfully applied $H_\infty$ control theory to power system frequency control problems but without consideration of energy storage. Essentially, the idea is to render the conventional generators much more responsive to the RES disturbances via either high-gain or dynamic controllers. However, this leads to an even higher burden on conventional generators equipped with the new controllers than with traditional controllers due to the increased ramping to follow the RES disturbances. High ramp rates are usually harmful to the lifetime of generators and could also cause a significant increase in air emissions [27]. In contrast, energy storage devices are taken into account in [28–31] for various other applications of $H_\infty$ control in electric energy systems such as tie-line flow control, inter-area damping control and transient stability improvement. However, none of these papers consider the limits on the SOC of storage devices. In addition, the main drawback of $H_\infty$ control is that the order of the yielding dynamic controllers is typically as high as that of the system model, which makes the controller implementation impractical especially with the increase of the system complexity. To deal with this issue, the decentralized static output feedback and the iterative linear matrix inequality (ILMI) approach are adopted in AFC design.

## 3.2 Feasibility of Decentralized PI Frequency Control

As mentioned in Chapter 2, decentralized control merely exists in the primary level of the current hierarchical frequency control framework in terms of each control area. In other words, there only exist decentralized proportional controllers (P controllers) in current power systems. As we learned from Chapter 2, the combination of the primary control and secondary control actually exhibits the behavior of proportional-integral controllers (PI controllers). We are thus wondering whether it is viable to integrate the primary and secondary control levels and design a unified decentralized PI frequency control scheme.

The two main technical barriers that currently hinder the application of decentralized PI control in power system frequency regulation are that 1) local frequency controllers are mostly designed based on the sole knowledge of the corresponding local generating unit model; 2) power sharing among generators in responding frequency deviations is not clear when multiple PI controllers are placed in the system even if the system stability is ensured. Due to the first barrier, multiple PI controllers designed in that way would very likely fight against each other and each tries to gain the dominance in regulating system frequency when they are interconnected, causing instability of the system. With respect to the second barrier, the underlying reason is because there is no precise time synchronization scheme implemented among different frequency controllers of different generators in a control area. The integration in all the PI controllers must start at the same time in order for the decentralized PI control to function properly. Otherwise, the power output of each generator depends on not only the power mismatches and the controller settings but also the time when the controller starts its integration process. The generators with the integral control part kicking in early might take more responsibility in balancing power mismatches.

In order to deal with the first barrier, a structure-preserving approach needs to be conceived where the interactions among generators via power transmission networks should be explicitly taken into account. Based on such a system-wide model, it is of more confidence that the yielding PI controllers are able to cooperate with each other to stabilize the system and bring the frequency back to its nominal value. On the other hand, the second barrier can be easily solved by employing the mature technology of phasor measurement units (PMUs) because of their embedded function of Global Positioning System (GPS) based time synchronization. Voltage angle information that is indeed the integral of the local frequency is directly measured with a precise GPS time stamp by PMUs so that a common time reference among generators that might be located far way from each other can be established.

**Definition 1** (Synchronization for PI Controllers)**.** Multiple PI controllers in a network are said to be synchronized if and only if the integral control part of each controller starts at the same time.

In terms of the voltage angle which is the integral of the frequency, the time synchronization of PI controllers ensures that the reference values for voltage angles at each bus are measured at the same time. For example, consider two voltage angles at two buses at time $t$ denoted by $\theta_1^t$ and $\theta_2^t$. If PI controllers are placed at these two buses, the control inputs at time $t$ in terms of deviations from their nominal values are given by

$$\begin{aligned} \Delta P_1^t &= -k_1 \Delta\omega_1^t - k_2 \left(\theta_1^t - \theta_1^{t1}\right) \\ \Delta P_2^t &= -k_3 \Delta\omega_2^t - k_4 \left(\theta_2^t - \theta_2^{t2}\right) \end{aligned} , \tag{3.1}$$

where superscripts $t1$ and $t2$ are the time instances when the two corresponding angle reference values were measured, respectively; $\Delta\omega_1^t$ and $\Delta\omega_2^t$ are the frequency deviations at time $t$ from the nominal value for Bus 1 and Bus 2, respectively; $k_1, k_2, k_3, k_4$ are positive control gains. In such a setting, the two controllers are said to be synchronized if and only if the condition $t1 = t2$ holds.

Before we develop the structure-preserving approach for system modeling, we first provide a theorem in the following to establish the uniqueness of the generator power sharing with synchronized multiple PI frequency controllers in a power network represented by the DC power flow model.

**Definition 2** (Uniqueness of Generator Power Sharing)**.** The steady-state generator power sharing for frequency control in a given power network is said to be unique if and only if the power output of each generator merely depends on the power mismatches of the system and the parameters of frequency controllers.

**Theorem 1** (Uniqueness Theorem of Generator Power Sharing under Decentralized PI Frequency Control)**.** *In a power network represented by the DC power flow model, the steady-state power sharing among generators in responding frequency deviations is unique under negative feedbacks via synchronized decentralized PI frequency controllers given that the closed loop system is stable.*

*Proof.* Without loss of generality, we assume that there are $(n+m)$ buses in the network and the first $n$ buses are generator buses and the remaining $m$ buses are load buses.

The DC power flow model which is widely adopted in the power system steady-state analysis yields the following relation between bus power injections and bus voltage angles:

$$\begin{bmatrix} \Delta P_G^1 \\ \vdots \\ \Delta P_G^n \\ -\Delta P_L^1 \\ \vdots \\ -\Delta P_L^m \end{bmatrix} = \mathbf{H} \cdot \begin{bmatrix} \Delta\theta_1 \\ \vdots \\ \Delta\theta_n \\ \Delta\theta_{n+1} \\ \vdots \\ \Delta\theta_{n+m} \end{bmatrix} = \begin{bmatrix} H_{1,1} & \dots & \dots & \dots & \dots & H_{1,n+m} \\ \vdots & \ddots & & & & \vdots \\ \vdots & & \ddots & & & \vdots \\ \vdots & & & \ddots & & \vdots \\ \vdots & & & & \ddots & \vdots \\ H_{n+m,n+m} & \dots & \dots & \dots & \dots & H_{n+m,n+m} \end{bmatrix} \cdot \begin{bmatrix} \Delta\theta_1 \\ \vdots \\ \Delta\theta_n \\ \Delta\theta_{n+1} \\ \vdots \\ \Delta\theta_{n+m} \end{bmatrix}. \quad (3.2)$$

where $\Delta P_G^i, \Delta P_L^j$ are the generator power output deviation at Bus $i$ and the load power deviation at Bus $(n+j)$, respectively; $\Delta\theta_k$ is the voltage angle deviation at Bus $k$ with respect to its reference value, i.e. $\Delta\theta_k = \theta_k - \theta_k^{t0}$ with $t0$ being the initial time when the controller synchronization was done; the matrix $\mathbf{H}$ is known as the admittance matrix. Three important properties associated with $\mathbf{H}$ are that 1) it is structurally singular; 2) it is diagonally dominant with positive diagonal elements; 3) its first minors associated with the diagonal elements $M_{i,i}$ are positive.

Since the closed loop system is stable, the power output of the generator with negative feedback PI control at Bus $i$ in steady state is proportional to the local voltage angle deviation, i.e. $\Delta P_G^i = -k_i \cdot \Delta\theta_i$ with $k_i > 0$. We therefore prove the theorem by proving the uniqueness of the vector for voltage angle deviations given deterministic load changes. The following two cases cover all the possibilities.

1. One single PI controller is installed.

   Without loss of generality, we assume that the first generator adopts the PI control. Thus, rearranging (3.2) gives us

$$\begin{bmatrix} 0 \\ \vdots \\ 0 \\ -\Delta P_L^1 \\ \vdots \\ -\Delta P_L^m \end{bmatrix} = \begin{bmatrix} H_{1,1}+k_1 & \dots & \dots & \dots & \dots & H_{1,n+m} \\ \vdots & \ddots & & & & \vdots \\ \vdots & & \ddots & & & \vdots \\ \vdots & & & \ddots & & \vdots \\ \vdots & & & & \ddots & \vdots \\ H_{n+m,n+m} & \dots & \dots & \dots & \dots & H_{n+m,n+m} \end{bmatrix} \cdot \begin{bmatrix} \Delta\theta_1 \\ \vdots \\ \Delta\theta_n \\ \Delta\theta_{n+1} \\ \vdots \\ \Delta\theta_{n+m} \end{bmatrix}. \tag{3.3}$$

   We denote the modified admittance matrix as $\bar{\mathbf{H}}$. Next, we are going to prove that $\bar{\mathbf{H}}$ is nonsingular. On the one hand, the Laplace expansion along the first row of the original admittance matrix $\mathbf{H}$ yields

$$0 = det(\mathbf{H}) = \sum_{j=1}^{n+m} (-1)^{1+j} H_{1,j} M_{1,j} = H_{1,1}M_{1,1} + \sum_{j=1, j\neq 1}^{n+m} (-1)^{1+j} H_{1,j} M_{1,j}. \tag{3.4}$$

   On the other hand, the determinant of $\bar{\mathbf{H}}$ can also be calculated by the Laplace expansion along its first row:

$$\begin{aligned} det(\bar{\mathbf{H}}) &= \sum_{j=1}^{n+m} (-1)^{1+j} \bar{H}_{1,j} M_{1,j} = \bar{H}_{1,1}M_{1,1} + \sum_{j=1, j\neq 1}^{n+m} (-1)^{1+j} H_{1,j} M_{1,j} \\ &= k_1 M_{1,1} + det(\mathbf{H}) = k_1 M_{1,1} > 0. \end{aligned} \tag{3.5}$$

From the third property of the admittance matrix and the condition of $k_i > 0$, $\bar{\mathbf{H}}$ is indeed nonsingular and more precisely positive definite so that the vector of voltage angle deviations is uniquely determined given deterministic load changes.

2. Multiple PI controllers are installed.

   We prove this case following the same idea in Case 1. Without loss of generality, we further assume that PI control is applied to the $i$th generator. Now, rearranging (3.2) gives us

$$\begin{bmatrix} 0 \\ \vdots \\ 0 \\ -\Delta P_L^1 \\ \vdots \\ -\Delta P_L^m \end{bmatrix} = \begin{bmatrix} H_{1,1}+k_1 & \dots & \dots & \dots & \dots & H_{1,n+m} \\ \vdots & \ddots & & & & \vdots \\ \vdots & & H_{i,i}+k_i & & & \vdots \\ \vdots & & & \ddots & & \vdots \\ \vdots & & & & \ddots & \vdots \\ H_{n+m,n+m} & \dots & \dots & \dots & \dots & H_{n+m,n+m} \end{bmatrix} \cdot \begin{bmatrix} \Delta\theta_1 \\ \vdots \\ \Delta\theta_n \\ \Delta\theta_{n+1} \\ \vdots \\ \Delta\theta_{n+m} \end{bmatrix}. \quad (3.6)$$

   Denote the newly modified admittance matrix as $\tilde{\mathbf{H}}$. On the one hand, the Laplace expansion along the $i$th row of $\bar{\mathbf{H}}$ in (3.3) gives:

$$0 < det(\bar{\mathbf{H}}) = \sum_{j=1}^{n+m} (-1)^{i+j} \bar{H}_{i,j} \bar{M}_{i,j} = \bar{H}_{i,i}\bar{M}_{i,i} + \sum_{j=1, j\neq i}^{n+m} (-1)^{i+j} \bar{H}_{i,j} \bar{M}_{i,j}. \quad (3.7)$$

   On the other hand, the determinant of $\tilde{\mathbf{H}}$ can be calculated as

$$\begin{aligned} det(\tilde{\mathbf{H}}) &= \sum_{j=1}^{n+m} (-1)^{i+j} \tilde{H}_{i,j} \bar{M}_{i,j} = \tilde{H}_{i,i}\bar{M}_{i,i} + \sum_{j=1, j\neq i}^{n+m} (-1)^{i+j} \bar{H}_{i,j} \bar{M}_{i,j} \\ &= k_i \bar{M}_{i,i} + det(\bar{\mathbf{H}}) > 0. \end{aligned} \quad (3.8)$$

   The positiveness of $\bar{M}_{i,i}$ can be established from the positiveness of $M_{i,i}$ and $k_1$. Therefore, $\tilde{\mathbf{H}}$ is indeed nonsingular and more precisely positive definite so that the vector of voltage angle deviations is uniquely determined given deterministic load changes.

Based on the foregoing proof, it is trivial to see that the theorem holds for the general case of multiple PI controllers by using mathematical induction.

For both the two cases, it can be shown that the vector of voltage angle deviations is uniquely determined by the power mismatches of the system and the parameters of PI frequency controllers. Therefore, the steady-state generator power sharing is unique as the steady-state power outputs of generators are proportional to local voltage angle deviations. This concludes the complete proof of the theorem. □

As long as the two aforementioned barriers are overcome and additionally the stability of the system is guaranteed, there should be no problems in implementing decentralized PI frequency controllers in power systems. In the following sections, we will develop the proposed AFC scheme step by step beginning with the system modeling.

## 3.3 System Modeling

Unlike the traditional frequency control investigation method where a uniformed frequency is assumed within each control area, a structure-preserving approach is developed in this section, which utilizes the DC power flow model to connect different components in the considered system retaining the frequency information at each individual generator bus. Following the general practice in power system analysis, all the following models are linearized around the operating point. Unless otherwise specified, all units are in per unit with respect to the power network base.

### 3.3.1 Conventional Generator

The conventional generators are assumed to be of non-reheat thermal type for illustration purpose, which is a fourth order governor-turbine-generator model including the dynamics of the speed droop governor and the turbine [4] and is given by

$$\begin{bmatrix} \Delta\dot{\omega} \\ \Delta\dot{\theta} \\ \Delta\dot{P}_m \\ \Delta\dot{Y} \end{bmatrix} = \begin{bmatrix} \frac{-k_D}{2H} & 0 & \frac{S_N}{2HS} & 0 \\ \omega_0 & 0 & 0 & 0 \\ 0 & 0 & \frac{-1}{T_{CH}} & \frac{1}{T_{CH}} \\ \frac{-S}{S_N T_G R} & 0 & 0 & \frac{-1}{T_G} \end{bmatrix} \begin{bmatrix} \Delta\omega \\ \Delta\theta \\ \Delta P_m \\ \Delta Y \end{bmatrix} + \begin{bmatrix} 0 \\ 0 \\ 0 \\ \frac{1}{T_G} \end{bmatrix} \begin{bmatrix} \Delta P_G^{ref} \end{bmatrix} + \begin{bmatrix} \frac{-S_N}{2HS} \\ 0 \\ 0 \\ 0 \end{bmatrix} \begin{bmatrix} \Delta P_e \end{bmatrix}. \tag{3.9}$$

The parameters and variables in this model are:

| | |
|---|---|
| $S_N$: power network VA base | $S$: generator VA base |
| $H$: inertia constant based on $S$ | $\omega$: rotor speed |
| $\Delta$: deviations from operating point | $\theta$: voltage angle in radians |
| $P_m$: mechanical power | $P_e$: electrical power |
| $k_D$: damping factor | $T_{CH}$: turbine time constant |
| $Y$: turbine valve position | $T_G$: governor time constant |
| $P_G^{ref}$: control input | $\omega_0$: nominal speed in rad/sec |
| $R$: speed droop coefficient | |

We denote the state space model (3.9) of the $i$th conventional generator in a compact form as

$$\dot{x}_{G,i} = A_{G,i} \cdot x_{G,i} + B_{G,i} \cdot u_{G,i} + E_{G,i} \cdot P_{e,i}. \tag{3.10}$$

If the traditional secondary control is in place in addition to the existing primary control loop, the control input is set to $\Delta P_G^{ref} = P_{AGC}$ where $P_{AGC}$ is the AGC signal of the secondary control loop.

### 3.3.2 Energy Storage Device

The storage device consists of the actual storage and the power electronic inverter connecting the device to the grid. The model for the storage captures the relationship between charging/discharging power and the energy level. The dynamics of the inverter can be modeled using a first order model with time constant $T_S$ capturing the response of the inverter to the control signal. Hence, the model for the storage device results in the second order model [32] given by

$$\begin{bmatrix} \Delta S\dot{O}C \\ \Delta \dot{P}_S \end{bmatrix} = \begin{bmatrix} 0 & \frac{-1}{E_{cap}} \\ 0 & \frac{-1}{T_S} \end{bmatrix} \begin{bmatrix} \Delta SOC \\ \Delta P_S \end{bmatrix} + \begin{bmatrix} 0 \\ \frac{1}{T_S} \end{bmatrix} \begin{bmatrix} \Delta P_S^{ref} \end{bmatrix}, \tag{3.11}$$

where the parameters and variables are:

| | |
|---|---|
| $E_{cap}$: energy capacity in p.u.sec | $T_S$: inverter time constant |
| $\Delta$: deviations from operating point | $SOC$: state of charge |
| $P_S$: storage power injection | $P_S^{ref}$: control input |

However, due to the fact that the time constant $T_S$ is typically on the order of milliseconds and is negligibly small relative to the time constants associated with the conventional generator, it is reasonable to use a reduced order model by neglecting the dynamics of the power electronics inverter [33]. In other words, the power injection $\Delta P_S$ can be changed instantaneously in the reduced order model resulting in

$$\begin{bmatrix} \Delta S\dot{O}C \end{bmatrix} = \begin{bmatrix} 0 \end{bmatrix} \begin{bmatrix} \Delta SOC \end{bmatrix} + \begin{bmatrix} \frac{-1}{E_{cap}} \end{bmatrix} \begin{bmatrix} \Delta P_S^{ref} \end{bmatrix}. \tag{3.12}$$

We further denote this reduced order model of the $i$th storage device in a compact form as

$$\dot{x}_{S,i} = A_{S,i} \cdot x_{S,i} + B_{S,i} \cdot u_{S,i}. \tag{3.13}$$

### 3.3.3 RES Generator

The main focus with regards to renewable energy sources is on wind and solar generation. Most of the modern wind and solar generation types such as doubly fed induction generator and photovoltaic generator are connected to the grid via power electronics [13, 34]. Typically, these power electronic devices are controlled by the maximum power point tracking algorithm to maximize the RES power output. In addition, usually wind and solar generators do not participate in frequency control. Hence, the RES generators are modeled as negative loads.

### 3.3.4 Frequency at Load Buses

The challenge which arises in AFC design if the storage is placed at a non-generator bus is that the local frequency is not part of the state variables in the traditional power system model. While measuring the frequency in operation is straightforward, a model of the local frequency needs to be derived for the design stage. Hence, a mathematical model is developed to estimate the local frequency at load buses as a function of the frequencies at generator buses. The modeling of the frequency at load or generally non-generator buses is crucial for the decentralized control design in situations where the storage device is located at a non-generator bus.

Recall the DC power flow model, which gives the relationship between the power injections and the voltage angles, i.e.

$$\begin{bmatrix} \Delta P_G \\ \Delta P_L \end{bmatrix} = \mathbf{H} \begin{bmatrix} \Delta \theta_G \\ \Delta \theta_L \end{bmatrix} \triangleq \begin{bmatrix} H_{GG} \; H_{GL} \\ H_{LG} \; H_{LL} \end{bmatrix} \begin{bmatrix} \Delta \theta_G \\ \Delta \theta_L \end{bmatrix}, \tag{3.14}$$

where $\Delta P_G$ and $\Delta P_L$ are vectors for power injections at generator buses and non-generator buses; $\Delta \theta_G$ and $\Delta \theta_L$ are vectors for voltage angles at generator buses and non-generator buses; $\mathbf{H}$ is the bus admittance matrix. Now making the assumption that the power injections at non-generator buses are differentiable, the load frequency can be expressed as

$$\Delta \omega_L = -H_{LL}^{-1} H_{LG} \Delta \omega_G + \frac{1}{\omega_0} H_{LL}^{-1} \Delta \dot{P}_L, \tag{3.15}$$

where $\Delta \omega_L$ and $\Delta \omega_G$ are vectors for the load frequencies and generator frequencies, respectively. Since (3.15) contains the differentiation of $\Delta P_L$ which is a disturbance input to the system, further simplification is needed. It is reasonable to assume that the frequency at load buses is mainly determined by the frequencies of the terminal voltages of synchronous generators in the grid [35]. Hence, the mathematical model to estimate the local frequency at load buses is given by

$$\overline{\Delta\omega}_L = -H_{LL}^{-1} H_{LG} \Delta\omega_G, \tag{3.16}$$

where $\overline{\Delta\omega}_L$ is the vector for the estimated load frequencies. This estimation model is used in the controller design stage in case the storage is located at a non-generator bus.

### 3.3.5 Overall System

By stacking all the states of the dynamic components represented by (3.10) and (3.13), we obtain the following preliminary model for the entire system:

$$\dot{x} = A_0 x + B_0 u + E_0 h, \tag{3.17}$$

where

$$\begin{aligned}
x &= [x_{G,1}^T, \cdots, x_{G,N_G}^T, x_{S,1}^T \cdots, x_{S,N_S}^T]^T, \\
u &= [u_{G,1}, \cdots, u_{G,N_G}, u_{S,1} \cdots, u_{S,N_S}]^T, \\
h &= [P_{e,1}, \cdots, P_{e,N_G}]^T, \\
A_0 &= diag(A_{G,1}, \cdots, A_{G,N_G}, A_{S,1}, \cdots, A_{S,N_S}), \\
B_0 &= diag(B_{G,1}, \cdots, B_{G,N_G}, B_{S,1}, \cdots, B_{S,N_S}), \\
E_0 &= [F_0^T \quad 0_{N_G \times N_S}]^T, F_0 = diag(E_{G,1}, \cdots, E_{G,N_G}),
\end{aligned}$$

$N_G$ and $N_S$ are the number of conventional generators and the number of energy storage devices, respectively.

Based on the DC power flow model, the electric power $h$ in (3.17) produced by generators can be given as a linear function of the states $x$, control inputs $u$ and RES disturbances $w$, i.e.

$$h = G_0 x + H_0 u + J_0 w, \tag{3.18}$$

where $G_0, H_0, J_0$ are coefficient matrices derived from the DC power flow model.

Hence, the structure-preserving state-space model of the entire system is derived by substituting (3.18) into (3.17) resulting in

$$\dot{x} = Ax + B_1 w + B_2 u, \tag{3.19}$$

where $A = A_0 + E_0 G_0$, $B_1 = E_0 J_0$, $B_2 = B_0 + E_0 H_0$. The model is consistent with the standard $H_\infty$ problem formulation, which is described in the following subsection.

## 3.4 $H_\infty$ Control Basics

The standard configuration of the $H_\infty$ control problem is depicted in Fig. 3.1, where $G(s)$ is the transfer function of the plant, $K(s)$ is the transfer function of the controller, $w$ is the exogenous input including disturbances, references and measurement noise, $u$ is the control input, $z$ is the performance vector that we want to minimize to satisfy the control objective and $y$ is the measurement vector [23, 36].

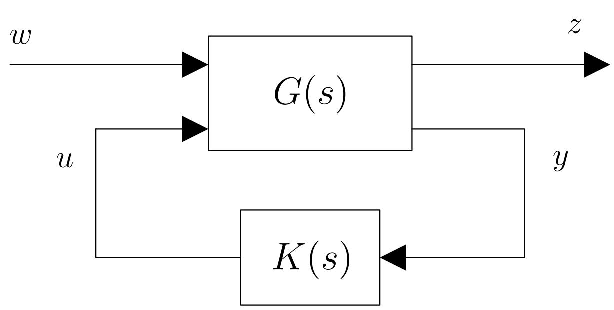


Figure 3.1: Standard $H_\infty$ problem configuration.

The corresponding state space model of the standard $H_\infty$ control problem in Fig. 3.1 is given as:

$$\dot{x} = Ax + B_1 w + B_2 u \tag{3.20}$$

$$z = C_1 x + D_{11} w + D_{12} u \tag{3.21}$$

$$y = C_2 x + D_{21} w + D_{22} u \tag{3.22}$$

where $x$ is the vector of internal states of $G(s)$. There exist two standard assumptions associated with the model [37]: 1) $(A, B_2, C_2)$ is stabilizable and detectable; 2) $D_{22} = 0$. The first assumption guarantees the existence of a solution to the $H_\infty$ control problem while the second one is typically made to simplify calculations without the loss of generality.

The objective of $H_\infty$ control is to find the optimal stabilizing controller $K(s)$ that minimizes the $H_\infty$ norm of the transfer function from $w$ to $z$, which is defined as the peak of the maximum singular value of the complex matrix $T_{zw}(j\omega)$ over all frequencies $\omega$, i.e.

$$\|T_{zw}(s)\|_\infty \triangleq \sup_{\omega} \overline{\sigma}(T_{zw}(j\omega)), \tag{3.23}$$

where $T_{zw}(s)$ is the closed loop transfer function from $w$ to $z$. It can also be proven that this $H_\infty$ norm $\|T_{zw}(s)\|_\infty$ is equivalent to the supremum of the quotient of the 2-norm of $z(t)$ and $w(t)$ in the time domain [36], i.e.

$$\sup_{\omega} \overline{\sigma}(T_{zw}(j\omega)) \;=\; \sup_{\|w(t)\|_2 \neq 0} \frac{\|z(t)\|_2}{\|w(t)\|_2}\ . \tag{3.24}$$

The equivalence above can be interpreted as that $H_\infty$ control gives a guaranteed bound on the performance vector $z$ for any bounded exogenous input $w$. In other words, the $H_\infty$ control design is independent of the size (norm) of the exogenous signal and instead to minimize the "amplification" effect of the closed loop transfer function from the exogenous input to the performance vector. Thus, $H_\infty$ control is widely applied to disturbance rejection problems. For the general closed form of the transfer function $T_{zw}(s)$ in terms of the system model (3.20)-(3.22), interested readers are referred to [37]. The feasible set of $K(s)$ may be restricted as well due to the specific control design requirements on the controller structure, e.g. the order of the resulting controller should be limited.

Consequently, $H_\infty$ control gives a guaranteed bound on the performance vector $z$ for any bounded exogenous input $w$, e.g. for wind power with given maximal root-mean-square (RMS) variations the resulting controller guarantees a bounded deviation in the energy level of the storage from its target value.

In order to achieve specific design requirements on control performance and to characterize the exogenous input signals based on their frequency spectrums, weighting functions are typically assigned to the performance vector $z$ and the exogenous input $w$. Thus, the resulting weighted $H_\infty$ control problem becomes

$$\min_{K(s)} \|W_z(s)T_{zw}(s)W_w(s)\|_\infty, \tag{3.25}$$

where $W_z(s), W_w(s)$ are matrix valued weighting functions for $z$ and $w$, respectively. The matrices allow defining the importance of the individual control objectives.

In summary, the general procedure of $H_\infty$-based robust control design includes:

- state space modeling of the system according to (3.20);
- selection of the performance vector $z$ with respect to disturbance attenuation in the form of (3.21);
- selection of the measurements $y$ in the form of (3.22);
- decision on the type and structure of the control law, e.g. the order of the resulting controller;
- determination of frequency dependent weighting functions in (3.25) based on control design objectives;
- solving the resulting optimization problem (3.25) to obtain the optimal controller $K^*(s)$.

## 3.5 $H_\infty$-based Controller Synthesis

There are three objectives in the proposed AFC design:

- to minimize the influence of RES variations on frequency deviations from the nominal value for all generator buses;
- to minimize the state of charge deviations of the storage devices in order to minimize the wear and tear effect due to deep cycling of SOC;
- to achieve the time-scale matching principle so that the ramp rates required from conventional generators are minimized for the purpose of minimizing the generator wear and tear effect caused by frequent high-ramping operations.

According to the aforementioned control objectives, the performance vector $z$ in (3.21) consists of the deviations in the local frequencies of the conventional generators, the SOCs of the energy storage devices and the power output of the two types of resources, i.e.

$$\begin{aligned} z = [\, & \Delta\omega_1, \cdots, \Delta\omega_{N_G}, \Delta SOC_1, \cdots, \Delta SOC_{N_S}, \\ & \Delta P_{m,1}, \cdots, \Delta P_{m,N_G}, \Delta P_{S,1}, \cdots, \Delta P_{S,N_S} \,]^T \, . \end{aligned} \tag{3.26}$$

For each of the elements in the performance vector, a frequency dependent weighting function $W_z(s)$ as defined in (3.25) needs to be chosen. These weighting functions are design parameters and reflect the importance of each of the objectives along the frequency spectrum of the respective performance element. The weighting functions for the frequency deviations $\Delta\omega_i$ and the state of charge deviations $\Delta SOC_i$ are chosen to be constant values, i.e. not frequency dependent. The values of these constants reflect the trade-off between tightly regulating the frequencies to their nominal values and to keep the SOCs of the energy storage devices close to a predefined value and away from the upper and lower limits of the storage devices.

The time-scale matching is achieved by choosing frequency dependent weighting functions for the power output of the two types of resources. For the power output from the conventional generators, higher penalties are put onto the high frequency region so that by minimizing the weighted power output the generators are less responsive to the high frequency components of the RES disturbances. For the power injection of the storage devices, higher weights are put on the low frequency region, which forces the storage to be less sensitive to the low frequency components in RES fluctuations. The general forms of the weighting functions for the $i$th conventional generator and the $i$th storage device under AFC are mathematically formulated as

$$W_{G,i}(s) = \frac{(10s + 20\pi f_c)^n}{m_{G,i}(s + 20\pi f_c)^n} \tag{3.27}$$

$$W_{S,i}(s) = \frac{(s + 2\pi f_c)^n}{m_{S,i}(s + 0.2\pi f_c)^n} \tag{3.28}$$

where $f_c$ is the cut-off frequency in time-scale matching, $n$ is the order of the weighting function, $m_{G,i}, m_{S,i}$ are the participation factors of the $i$th generator and the $i$th storage device under AFC, respectively. These variables are all design variables, which can be adjusted per specific control requirements. The participation factors are constrained by

$$\sum_{i \in G} m_{G,i} = 1, \quad \sum_{i \in S} m_{S,i} = 1, \tag{3.29}$$

where $G$ and $S$ are the sets of the generators and storage devices in AFC, respectively. Under the deregulated electricity market environment such as the PJM ancillary service market, the participation factors are determined according to the bids submitted by generators and storages. An example of weighting functions for conventional generator $W_{G,i}(s)$ and storage device $W_{S,i}(s)$ with design variables $f_c = 0.016$Hz, $n = 1$, $m_{G,i} = 33\%$, $m_{S,i} = 100\%$ is depicted in Fig. 3.2.

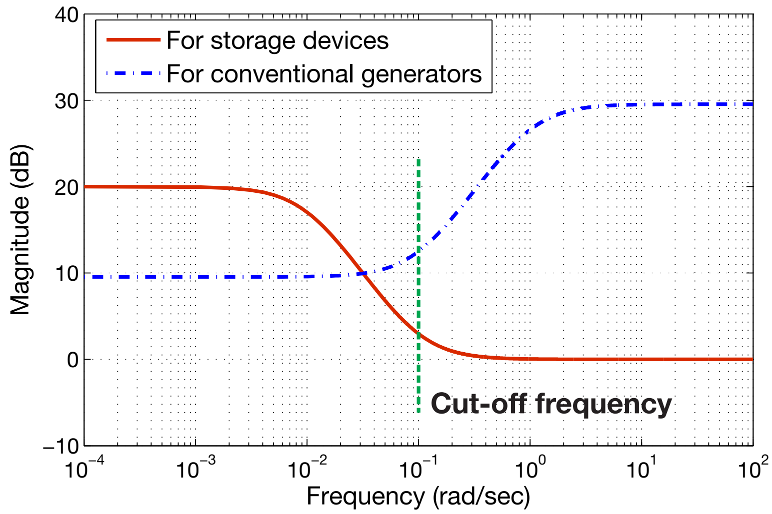


Figure 3.2: Example of $W_{Gi}(s), W_{Si}(s)$ with design variables $f_c = 0.016$Hz, $n = 1$, $m_{Gi} = 33\%$, $m_{Si} = 100\%$.

Therefore, the weighting function $W_z(s)$ in (3.25) is given by

$$\begin{aligned} W_z(s) = diag\{\, & \eta_{G,1}, \cdots, \eta_{G,N_G}, \eta_{S,1}, \cdots, \eta_{S,N_S}, W_{G,1}(s), \\ & \cdots, W_{G,N_G}(s), W_{S,1}(s), \cdots, W_{S,N_S}(s)\,\}, \end{aligned} \tag{3.30}$$

where $\eta_{G,i}$ and $\eta_{S,i}$ are the constant weights for $\Delta\omega_i$ and $\Delta SOC_i$ in the performance vector $z$, respectively.

In addition, the weighting function $W_w(s)$ in (3.25) needs to reflect the expected frequency spectrum of the exogenous input. Hence, this could correspond to the frequency spectrum of the RES generation in AFC. More generally, $W_w(s)$ is chosen to represent the designer's focus of the exogenous signal.

The resulting matrix valued weighting functions are then realized and integrated into the state space model of the entire system. Let the realizations of $W_z(s), W_w(s)$ be $(A_z, B_z, C_z, D_z)$ and $(A_w, B_w, C_w, D_w)$, respectively. Together with (3.20)-(3.22), the augmented state space model for AFC design including dynamics of weighting functions is

$$
\begin{aligned}
\begin{bmatrix} \dot{x} \\ \dot{x}_z \\ \dot{x}_w \end{bmatrix} &= \begin{bmatrix} A & 0 & B_1C_w \\ B_zC_1 & A_z & 0 \\ 0 & 0 & A_w \end{bmatrix} \begin{bmatrix} x \\ x_z \\ x_w \end{bmatrix} + \begin{bmatrix} B_1D_w \\ 0 \\ B_w \end{bmatrix} \bar{w} + \begin{bmatrix} B_2 \\ B_zD_{12} \\ 0 \end{bmatrix} u \\
&\triangleq \bar{A}\bar{x} + \bar{B}_1\bar{w} + \bar{B}_2u \qquad (3.31)
\end{aligned}
$$

$$
\bar{z} = \left[\, D_zC_1 \;\; C_z \;\; 0 \,\right] \begin{bmatrix} x \\ x_z \\ x_w \end{bmatrix} + D_zD_{12}u \triangleq \bar{C}_1\bar{x} + \bar{D}_{12}u \qquad (3.32)
$$

$$
y = \left[\, C_2 \;\; 0 \;\; 0 \,\right] \begin{bmatrix} x \\ x_z \\ x_w \end{bmatrix} \triangleq \bar{C}_2\bar{x} \qquad (3.33)
$$

where $x_z, x_w$ are states associated with $W_z(s), W_w(s)$; $\bar{w}, \bar{z}$ are the weighted exogenous input and performance vector. The yielding weighted transfer function from $\bar{w}$ to $\bar{z}$ is given by

$$
T_{\bar{z}\bar{w}}(s) = (\bar{C}_1 + \bar{D}_{12}K\bar{C}_2)(sI - \bar{A} - \bar{B}_2K\bar{C}_2)^{-1}\bar{B}_1. \qquad (3.34)
$$

As mentioned in the literature review section, when solving the optimization problem (3.25), usually the controller $K(s)$ is of the same order as the system with full state feedback, i.e. a centralized high-order controller. In AFC, we design decentralized controllers each located at either a generator or a storage device, having access only to local measurements. Hence, the decentralized static output feedback is adopted to obtain suboptimal but decentralized and low order controllers. Once the controllers are designed only local information is used as control input. For the conventional generator, this is the local frequency and the rotor angle which could also be derived as the integral of the local frequency. It can be easily recognized that such a robust controller is of proportional-integral type, which plays a critical role in restoring the frequency. For the storage device, the measured values are the local frequency and the SOC of the storage device. Due to the time-scale matching objective, voltage angles are not included in the storage controller inputs. Otherwise, there will be a constant steady-state power inflow/outflow from the storage devices. In summary, the control law for the $i$th generator and $i$th storage device under AFC is mathematically defined by

$$\begin{aligned}\Delta P_{Gi}^{ref} &= -k_{1i}\Delta\omega_{Gi} - k_{2i}\Delta\theta_{Gi} \\ \Delta P_{Si}^{ref} &= -k_{3i}\Delta\omega_{Si} + k_{4i}\Delta SOC_{Si}\end{aligned}, \tag{3.35}$$

where the subscripts $Gi$ and $Si$ denote the local information of the $i$th generator and the $i$th storage device, respectively. Eq. (3.16) is used to estimate the local frequency $\Delta\omega_{Si}$ in the design stage when the $i$th storage is located at a load bus.

Hence, the measurement vector $y$ in (3.22) includes the local frequencies and voltage angles of the conventional generators, and the local frequency and the SOCs of the energy storage devices, i.e.

$$y=[\,\Delta\omega_{G,1}, \Delta\theta_{G,1}, \cdots, \Delta\omega_{G,N_G}, \Delta\theta_{G,N_G}, \Delta\omega_{S,1}, \Delta SOC_1, \cdots, \Delta\omega_{S,N_S}, \Delta SOC_{N_S}\,]^T. \tag{3.36}$$

It can be recognized that $D_{21} = 0$ according to the form of (3.22) as the RES disturbance $w$ is not included in the measurement vector $y$. In a compact matrix form, the control input $u$ is represented in terms of the measurement vector $y$ as $u = Ky$, where the constant matrix $K$ only has non-zero elements in the columns corresponding to the respective local variables.

## 3.6 Optimal Gain Calculation

Having now set up the optimization problem given by (3.25) with $T_{zw}(s)$ corresponding to the transfer function from RES disturbances $w$ in (3.19) to the performance vector $z$ given by (3.26) and the weighting functions as defined, the next step is to solve this problem constraining the resulting controllers to have the form (3.35). Since the available commercial $H_\infty$ solvers such as Matlab routine `hinfsyn` do not allow to specify the yielding $H_\infty$ controller to be static and decentralized, a customized solver has to be developed in order to obtain the $H_\infty$ control gains. Based on two theorems in [37, 38] and the bisection method, an improved iterative linear matrix inequality (ILMI) algorithm is developed and tailored to solve the involved $H_\infty$ problem to provide the parameters $k_{1i}, k_{2i}, k_{3i}, k_{4i}$ for the low order controllers in (3.35). The CVX software package [39] is used as a numerical tool.

**Theorem 2** (Bounded Real Lemma [37, 38])**.** *Consider the linear time invariant continuous time (LTI-CT) system with the following state space representation and assume that $(A, B_2, C_2)$ is stabilizable and detectable.*

$$\begin{aligned}\dot{x} &= Ax + B_1 w + B_2 u \\ z &= C_1 x + D_{11} w + D_{12} u \\ y &= C_2 x + D_{21} w\end{aligned}$$

*The following three statements are equivalent:*

1. *There exists a static output feedback $u = Ky$ such that the closed-loop system is asymptotically stable and $\|T_{zw}\|_\infty < \gamma$;*

2. *There exists a positive definite solution $P$ to the LMI:*

$$\begin{bmatrix} A_{CL}^T P + P A_{CL} & P B_{CL} & C_{CL}^T \\ B_{CL}^T P & -\gamma I & D_{CL}^T \\ C_{CL} & D_{CL} & -\gamma I \end{bmatrix} \succ 0,$$

   *where $A_{CL} = A + B_2 K C_2$, $B_{CL} = B_1 + B_2 K D_{21}$, $C_{CL} = C_1 + D_{12} K C_2$, $D_{CL} = D_{11} + D_{12} K D_{21}$;*

3. *There exists a $\tilde{P} \succ 0$ in the form of*

$$\tilde{P} \triangleq \begin{bmatrix} P & 0 & 0 \\ 0 & I & 0 \\ 0 & 0 & I \end{bmatrix}$$

*such that* $\tilde{P}\bar{B}K\bar{C} + (\tilde{P}\bar{B}K\bar{C})^T + \bar{A}^T\tilde{P} + \tilde{P}\bar{A} \prec 0$*, where*

$$\bar{A} = \begin{bmatrix} A, & B_1, & 0 \\ 0, & -\gamma I/2, & D_{11}/2 \\ C_1, & D_{11}/2, & -\gamma I/2 \end{bmatrix}, \bar{B} = \begin{bmatrix} B_2 \\ 0 \\ D_{12} \end{bmatrix}, \bar{C} = \begin{bmatrix} C_2^T \\ D_{21}^T \\ 0 \end{bmatrix}^T.$$

The proof of the equivalence between 1) and 2) is given in [22, 23]. The equivalence between 2) and 3) can be verified by plugging coefficient matrices into the respective LMIs. Theorem 2 transforms the original $H_\infty$ problem in the frequency domain into a nonlinear matrix inequality problem that can be further transformed to a convex programming problem.

*Remark* 1. We introduce the following variation to the third statement in Theorem 2: There exists a $\bar{P} \succ 0$ in the form of

$$\bar{P} \triangleq \begin{bmatrix} P & 0 & 0 \\ 0 & qI & 0 \\ 0 & 0 & qI \end{bmatrix}$$

such that $\bar{P}\bar{B}K\bar{C} + (\bar{P}\bar{B}K\bar{C})^T + \bar{A}^T\bar{P} + \bar{P}\bar{A} \prec 0$.

Compared to the third statement in Theorem 2, Remark 1 enlarges the feasible set in terms of the unknown variable $P$, improving the convergence performance of Algorithm 1 described below.

The second theorem which is used to solve the problem is the stabilization lemma via static output feedback. This theorem essentially facilitates an iterative approach to solve the stabilization problem with static output feedback which is nonlinear and non-convex.

**Theorem 3** (Stabilization Lemma via Static Output Feedback [38])**.** *Consider the LTI-CT system* $\dot{x} = Ax + Bu$*,* $y = Cx$*. The following two statements are equivalent:*

*1. There exist $P \succ 0$ and $K$ such that*

$$(A + BKC)^T P + P(A + BKC) \prec 0;$$

*2. There exist $P \succ 0$, $X \succ 0$ and $K$ such that*

$$\begin{bmatrix} \begin{array}{c} A^T P + PA - XBB^T P \\ -PBB^T X + XBB^T X \end{array} & (B^T P + KC)^T \\ \\ (B^T P + KC) & -I \end{bmatrix} \prec 0.$$

*Remark* 2. We add an extra constraint $P \in \Psi$ on the positive definite matrix $P$ to Theorem 3 with $\Psi$ being a convex cone. The proof including this additional constraint is essentially the same as the proof of Theorem 3 in [38]. Theorem 3 plus the additional constraint links the static output feedback stabilization problem to a linear matrix inequality problem for a fixed positive definite matrix $X$.

Based on the two theorems and Remark 1 and Remark 2, the existing ILMI algorithm given in [38] is improved as outlined below and employed to solve the involved $H_\infty$ problem with decentralized static output feedback. The notations are consistent with the standard $H_\infty$ problem formulation and Theorem 2.

**Algorithm 1** (Improved ILMI Algorithm)**.**

1. Initialize the upper and lower bounds of $\|T_{zw}\|_\infty$ as $\gamma_{max}$ and $\gamma_{min}$, where $\gamma_{max}$ is a sufficiently large number and $\gamma_{min}$ is typically set to be 0.

2. If $\gamma_{max} - \gamma_{min} < \epsilon$, where $\epsilon$ is a preset tolerance, then $\gamma_{max}$ is the minimum value of $\|T_{zw}\|_\infty$. Stop. Otherwise, set $\gamma = (\gamma_{max} + \gamma_{min})/2$.

3. Select a constant matrix $Q \succ 0$ and solve $\bar{P}$ from the following algebraic Riccati

equation:

$$\bar{A}^T\bar{P} + \bar{P}\bar{A}^T - \bar{P}\bar{B}\bar{B}^T\bar{P} + Q = 0.$$

Set $i = 1$ and initialize $X_1$ by setting $X_1 = \bar{P}$.

4. Solve the following optimization problem $OP1$ in terms of decision variables $\bar{P}_i, K_i, \alpha_i$ using CVX:

$$\min_{\bar{P}_i, K_i, \alpha_i} \quad \alpha_i$$

$$\text{s.t.} \begin{bmatrix} \bar{A}^T\bar{P}_i + \bar{P}_i\bar{A} - X_i\bar{B}\bar{B}^T\bar{P}_i \\ -\bar{P}_i\bar{B}\bar{B}^T X_i + X_i\bar{B}\bar{B}^T X_i - \alpha_i I & (\bar{B}^T\bar{P}_i + K_i\bar{C})^T \\ (\bar{B}^T\bar{P}_i + K_i\bar{C}) & -I \end{bmatrix} \preceq 0 \tag{3.37}$$

$$\bar{P}_i = \begin{bmatrix} P_i & 0 & 0 \\ 0 & q_i I & 0 \\ 0 & 0 & q_i I \end{bmatrix} \succeq 0 \tag{3.38}$$

$$K_i \in \Omega \tag{3.39}$$

$$-\beta \leq [K_i]_{jk} \leq \beta \quad \forall j, k \tag{3.40}$$

$$\bar{P}_i \preceq \beta I \tag{3.41}$$

where $\beta$ is a large positive constant and $\Omega$ is a special set according to the decentralized control structure defined in (3.35). Note that $X_i$ is a parameter of $OP1$. Denote $\alpha_i^*$ as the minimum value of $\alpha_i$. Pick one pair $(\bar{P}_i^*, K_i^*)$ that achieves the minimum of $\alpha_i$.

5. If $\alpha_i^* < 0$, then $K_i^*$ is a stabilizing gain with $\|T_{zw}\|_\infty < \gamma$. Set $\gamma_{max} = \gamma$ and go to 2). Otherwise, go to 6).

6. If $\|X_i - \bar{P}_i^*\| < \delta$ or $i$ exceeds a preset iteration limit, where $\delta$ is a prescribed tolerance, set $\gamma_{min} = \gamma$ and go to 2); else, set $i = i + 1$ and $X_i = \bar{P}_{i-1}^*$, then go to 4).

*Remark* 3. Constraint (3.37) in $OP1$ corresponds to an improved relaxation formulation of the second theorem resulting in a convex problem. The original relaxation formulation of the existing ILMI algorithm in [38] is related to a generalized eigenvalue minimization problem, which is non-convex. Constraint (3.38) is included based on Remark 1 and the additional constraint (3.39) ensures the decentralized control design as defined in (3.35). The extra constraints (3.40)-(3.41) guarantee the solvability of $OP1$ (see Remark 4 below). Algorithm 1 reduces the number of optimization problems from two to one in each iteration compared to the algorithm presented in [38].

*Remark* 4. We now show that the optimization problem $OP1$ in Algorithm 1 is solvable. $OP1$ is equivalent to:

$$\min_{\bar{P}_i, K_i} \lambda_{max}[f_i(\bar{P}_i, K_i)] \quad \text{s.t.} (\bar{P}_i, K_i) \in \Sigma$$

where $\lambda_{max}(\cdot)$ denotes the maximum eigenvalue of a square matrix, $\Sigma$ is the compact set defined by (3.38)-(3.41), and

$$\begin{aligned} f_i(\bar{P}_i, K_i) = {} & \bar{A}^T \bar{P}_i + \bar{P}_i \bar{A} - X_i \bar{B} \bar{B}^T \bar{P}_i - \bar{P}_i \bar{B} \bar{B}^T X_i + X_i \bar{B} \bar{B}^T X_i \\ & + (\bar{B}^T \bar{P}_i + K_i \bar{C})^T (\bar{B}^T \bar{P}_i + K_i \bar{C}). \end{aligned} \tag{3.42}$$

$\lambda_{max}[f_i(\bar{P}_i, K_i)]$ is a continuous function because of the continuity of eigenvalue functions. According to the extreme value theorem, we know that a real-valued continuous function $f$ over a compact set $V$ must attain its minimum value at least once in $V$. Therefore, $OP1$ is solvable.

*Remark* 5. The optimization problem $OP1$ is of the semi-definite programming (SDP) type and can be efficiently handled by convex optimization solvers. It should be noted that the performance of such an ILMI algorithm is dependent on the initial condition. Therefore, a different initial matrix $Q$ may be selected if necessary.

## 3.7 Practical Implementation Issues

The possible issues associated with each step in practical implementation of the AFC approach are analyzed in this section. The steps of the AFC design are summarized below.

1. Derive the system model;
2. Identify the conventional generators and energy storage devices that are willing to participate in the AFC framework;
3. Determine the participation factors for all the participating generators and storages according to their willingness to provide frequency regulation and their physical capabilities;
4. Calculate the frequency dependent weighting functions based on the participation factors and the desired cut-off frequency;
5. Calculate the controller gains by solving the resulting minimization problem.

Among the steps above, the most difficult and challenging step is to obtain a system model with reasonable accuracy, especially when dealing with very large scale power systems. In case that the system model is inaccurate, additional trial-and-error based fine tuning procedures for the yielding robust controllers are needed in order to achieve the desired control performance. However, this is out of scope of this dissertation. The practice in power system analysis with respect to the application of robust control in frequency regulation assumes that the system model is trustworthy, such as in [24, 25].

In terms of steps 2) and 3), no critical issues are involved in implementing them. These steps fit well into the current deregulated electricity market, specifically the ancillary services market. The participation factors can be determined according to the bids submitted by generators and storages. The concept of participation factors is also adopted in the aforementioned previous work [24, 25]. One possible issue associated with step 4) is the choice of a proper cut-off frequency $f_c$, which is a design variable to reflect the trade-off between the usage of conventional generators and the usage of storage devices in balancing the RES variations. A lower value of $f_c$ in the controller design stage indicates that an increased usage of the storage participating in frequency regulation is desired. Finally, step 5) can be easily carried out based on the description in Section 3.6.

If AFC is integrated into the electricity markets, the frequency of re-performing the controller design steps above depends on the specific ancillary services market. For example, the current PJM ancillary services market clears its regulation market on an hourly basis [40, 41]. PJM would have to redo the AFC design process every hour if they would adopt the proposed AFC approach. Two separate bidding pools need to be set up in order to accommodate the two types of resources – the generator pool for slow responding resources and the storage pool for fast responding resources. Based on the bids from generators and storages together with the anticipated regulation requirement of the system, the participation factors in (3.29) can be calculated and therefore the frequency dependent weighting functions in (3.27)-(3.28) are determined given a prescribed cut-off frequency. Once the controller gains are computed, they are sent to the corresponding resources to adjust their governor/power electronics controller settings. The entire process of AFC design in a market environment can be implemented using computer programs and automatic control equipments.

## 3.8 Case Studies

In this section, we apply the proposed AFC approach to two widely used test systems in power system dynamic studies – the Western Electricity Coordinating Council (WECC) 9-bus system and the IEEE New England 39-bus system.

### 3.8.1 WECC 9-Bus System

The WECC 9-bus test system shown in Fig. 3.3 is used to illustrate the performance of the AFC level control of the proposed two-level control approach. The RES generator is installed at Bus 9 and the energy storage device is placed at Bus 8, which is a load bus. The parameters of the test system that are taken from [2, 42] are given in the Appendix A.

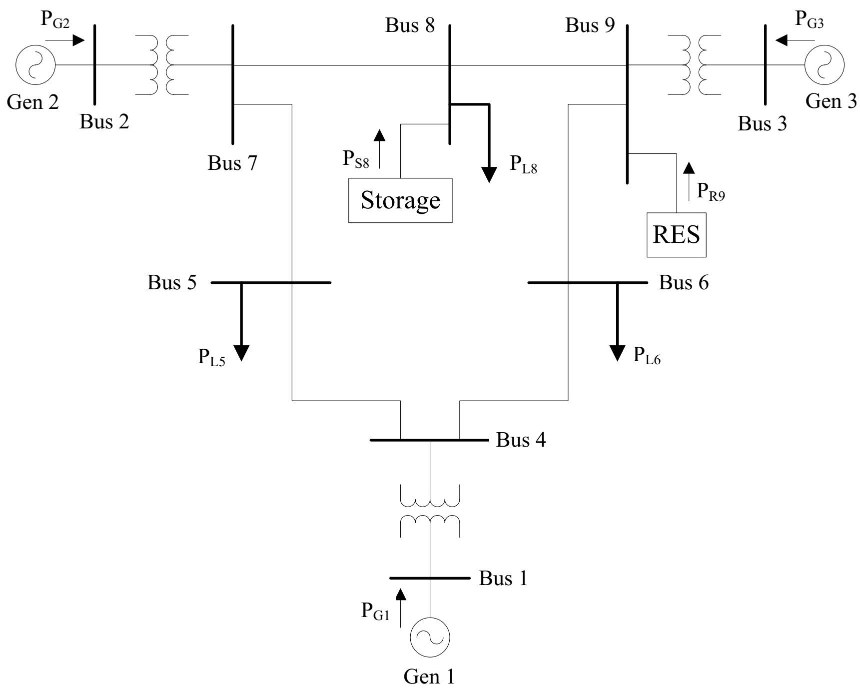


Figure 3.3: WECC 9-bus test system.

The system power base is 100 MVA. The capacity of the storage device is 2 MWh with 50 MW maximum power input/output capability, reflecting the fact that the energy storage application in frequency regulation is a high power application. The RES variations (Fig. 3.4) are within about $\pm 5\%$ [42] around the average value of 600 MW and the RES generator capacity is 800 MW. In case that the amount of the high frequency components in RES variations is greater than the power rating of the storage device, conventional generators will kick in to help to balance the fast RES fluctuations leading to the consequence that the time-scale matching objective may not be achieved as designed. The load is assumed to be constant with a total of $1,000$ MW for the considered time frame. The foregoing numeric values associated with RES and load are chosen such that a scenario with very high penetration of renewable generation is considered in the simulation.

The base case corresponds to the situation where all the three generators are equipped

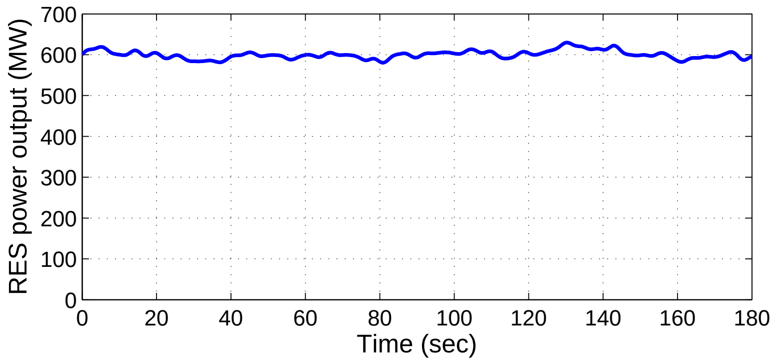


Figure 3.4: RES variations.

with governors with droop coefficient $R$ and the secondary AGC control is in place with the frequency sensor located at Bus 1. The parameters of the proportional-integral AGC controller are tuned by the trial and error method. The resulting AGC control signal is set to be equally assigned to each conventional generator and the storage device. The base case is termed as CFC, i.e. conventional frequency control. Under the proposed AFC, new decentralized controllers are designed for all the three generators and the storage device. The design variables are chosen as follows: $f_c = 0.016$Hz, $n = 1$, $m_{G,1} = m_{G,2} = m_{G,3} = 33\%$, $m_{S,1} = 100\%$. The corresponding frequency dependent weighting functions for generator and storage power output are shown in Fig. 3.2. For illustration purposes, the weighting function $W_w(s)$ in (3.25) for the exogenous input is chosen to be a low pass filter with cut-off frequency at 1 Hz, roughly reflecting the fact that the majority of frequency components in RES variations such as wind and solar generation is below 1 Hz. Thus, the yielding AFC controllers after $H_\infty$ minimization are obtained:

$$\Delta P_{G1}^{ref} = -22.1391\Delta\omega_1 - 0.0852\Delta\theta_1$$
$$\Delta P_{G2}^{ref} = -7.7482\Delta\omega_2 - 0.0870\Delta\theta_2$$
$$\Delta P_{G3}^{ref} = -1.7399\Delta\omega_3 - 0.0857\Delta\theta_3$$
$$\Delta P_{S1}^{ref} = -806.8710\Delta\omega_8 + 1.3995\Delta SOC_1.$$

### Time-Scale Matching Objective

The Bode magnitude diagram of the transfer functions from the RES disturbance $w$ to the real power output of the three generators and the storage device is depicted in Fig. 3.5. As can be seen from Fig. 3.5, the time-scale matching objective in the AFC design is successfully achieved, i.e. all the three generators are mainly responsible to balance the low frequency components of the RES variations below 0.1 rad/sec ($\sim$ 0.016 Hz) while the storage device takes care of the high frequency components above 0.1 rad/sec. In contrast, the generators in the base case tend to pick up the RES disturbances with the frequency spectrum up to 3 rad/sec. Moreover, the storage device in the base case acts like a conventional generator as it is simply requested to follow the AGC signal. It is noted that the curves corresponding to the generator power output under AFC overlap with each other because the participation factors are chosen to be identical for all the three generators.

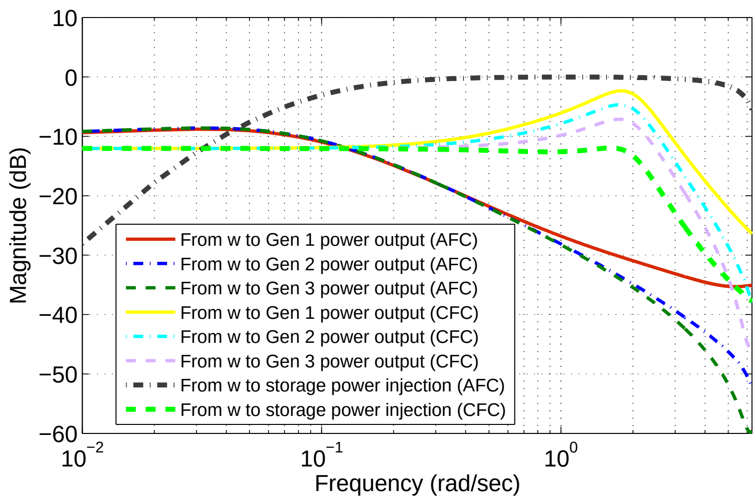


Figure 3.5: Real power output in the frequency domain.

### Frequency Response

Fig. 3.6 shows the comparison of frequency deviations at Bus 3 between AFC and CFC in the presence of the aforementioned RES variations. Similar frequency deviation curves are observed at the other two generator buses. The frequency deviations under AFC are further reduced and narrowed within a tighter band than the base case.

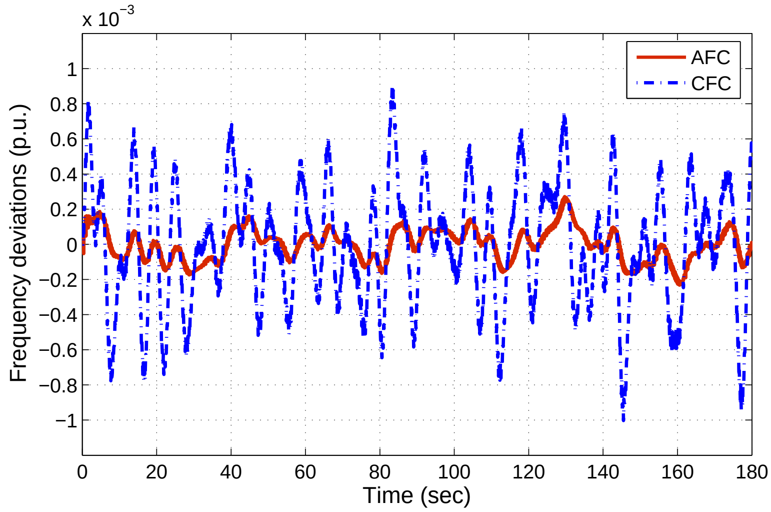


Figure 3.6: Frequency deviations at Bus 3.

### Generator Response

The power output deviations of Generator 3 from its operating point are plotted in Fig. 3.7. Similar power output deviation curves are observed for the other two generators. Compared to the base case, the power output of the three generators under AFC is smoothed out and high frequency fluctuations in the power output are greatly attenuated. The reason is that the burden on conventional generators to follow the RES variations is shared by the energy storage device according to the time-scale matching objective.

### Storage Response

Fig. 3.8 shows the power injection deviations and the SOC deviations of the storage device under AFC. The storage device is sensitive to the high frequency component of the RES variations and therefore ramps up and down very heavily and frequently. On the other hand, the SOC deviations are well maintained within the ±2% range by the AFC storage controller.

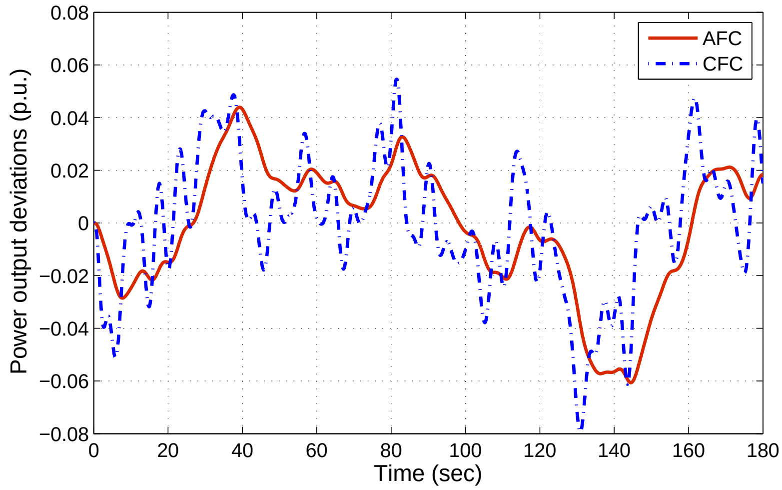


Figure 3.7: Power output deviations of Generator 3 from its operating point.

With the SOC close to its predefined level, the storage device is able to participate in other power or energy applications maximizing its economic value. However, if an increased usage of the storage participating in frequency control is desired, the corresponding weighting functions can be adjusted accordingly.

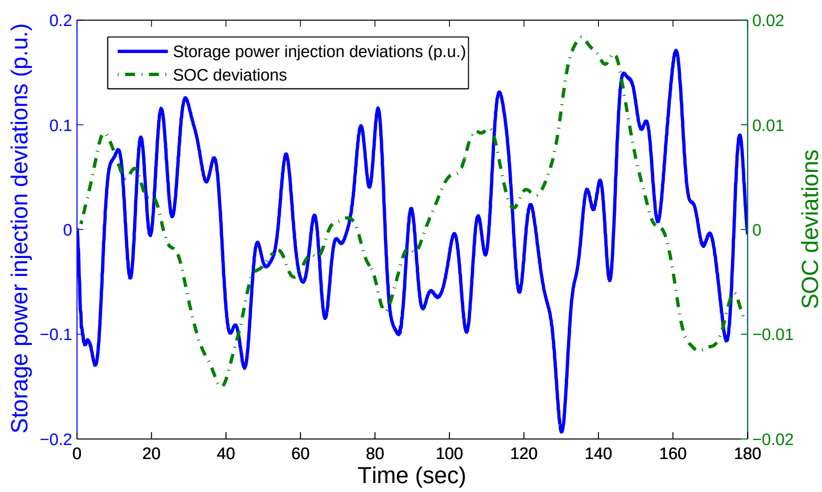


Figure 3.8: Time domain storage response under AFC.

In addition, the comparison of SOC between AFC and CFC in the frequency domain is plotted in Fig. 3.9, showing the magnitudes of the transfer functions from the RES disturbance $w$ to SOC deviations under AFC and CFC over the entire frequency spectrum. According to Fig. 3.9, the peak magnitude of the closed loop transfer function from disturbance $w$ to SOC deviations under AFC is approximately $-20$ dB, which implies that the root-mean-square (RMS) SOC deviations are guaranteed to be bounded in the $\pm 3\%$ range for any bounded disturbance input with RMS smaller than 0.3 p.u. in the test system. In contrast, there is no upper bound on the peak magnitude of the same transfer function under CFC. The SOC under CFC is prone to exceed its limit with the increase of the low frequency components in RES variations.

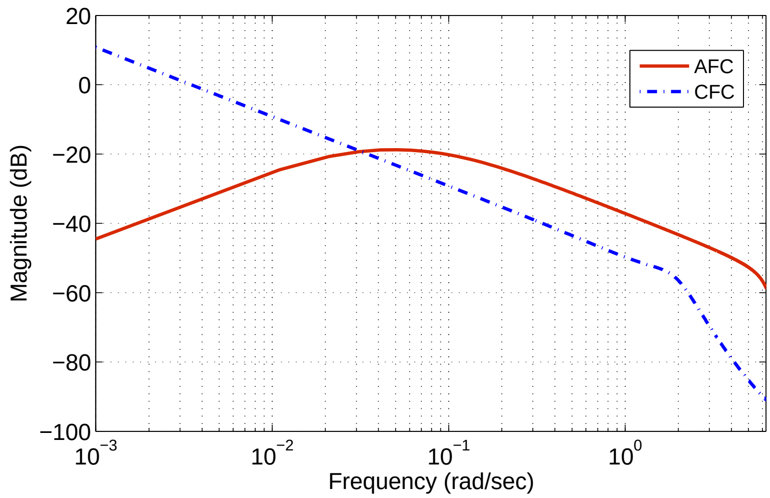


Figure 3.9: Bode magnitude diagram of the transfer function from $w$ to $\Delta SOC$.

### 3.8.2 IEEE New England 39-Bus System

The IEEE New England 39-bus test system shown in Fig. 3.10 is used to further illustrate the performance of the proposed AFC approach. The original test system is modified by connecting a storage device to Bus 27 and a wind generator to Bus 26. The parameters of the test system that are taken from [5, 42] are given in the Appendix B.

The system power base is 100 MVA. As for the storage device, the capacity is set to 5 MWh (0.05 p.u.h) and the maximum input/output power is symmetric and set to 100 MW

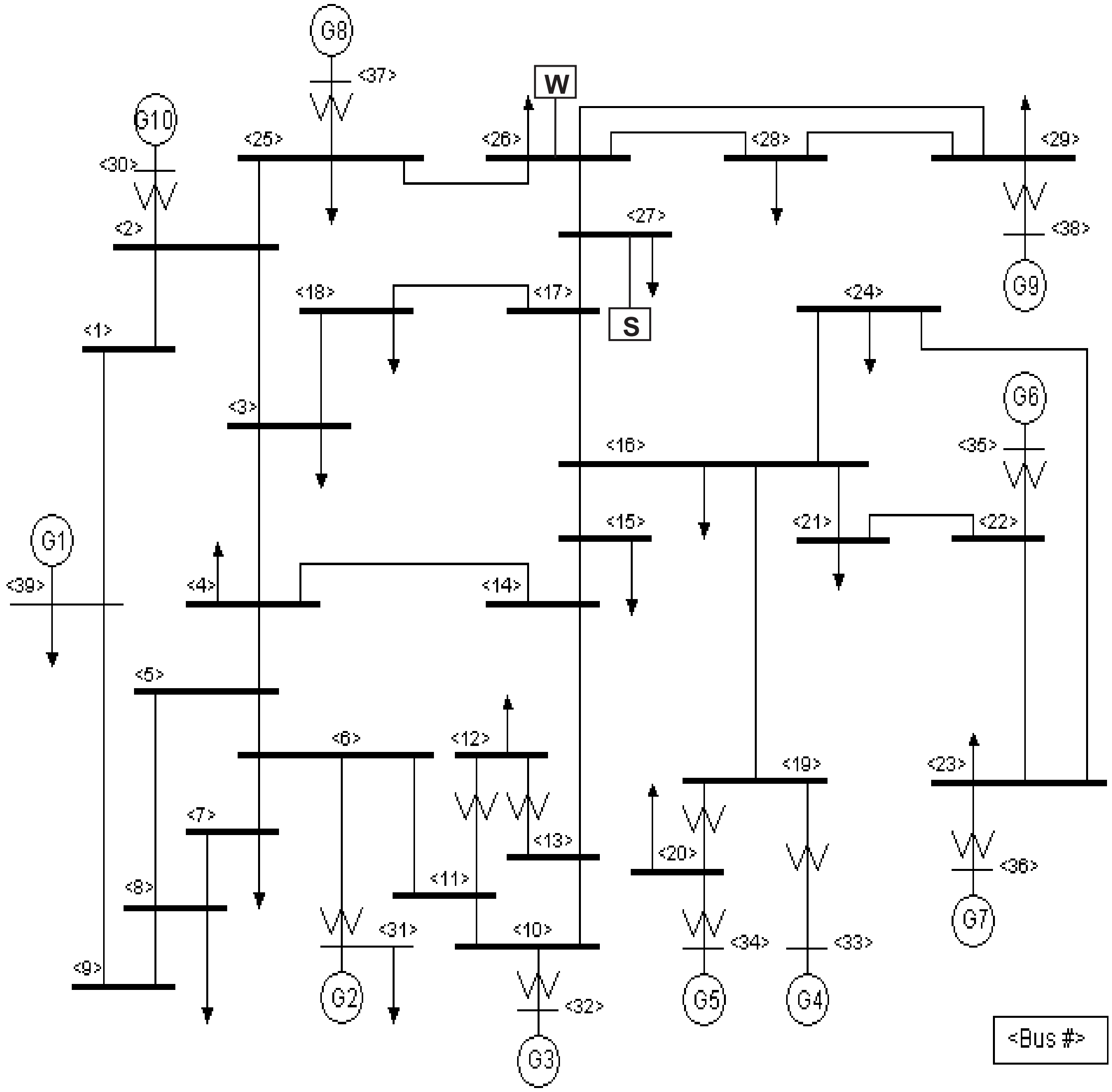


Figure 3.10: IEEE New England 39-bus test system [5].

(1 p.u.). In terms of the wind generator, the rated capacity is assumed to be $1,000$ MVA (10 p.u.), which takes up about 12.5% of the total generation capacity of the system. The wind power variations (Fig. 3.11) are within about $\pm 15\%$ around the average value of 800 MW. The load is assumed to be constant for the considered time frame.

The base case denoted by CFC corresponds to the situation where all the ten generators are equipped with governors with droop coefficient $R$ and the secondary control is in place

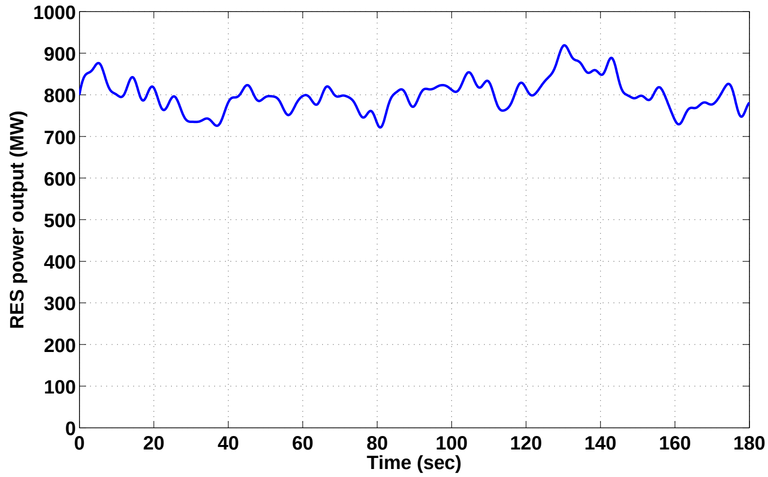


Figure 3.11: Wind power variations.

with the frequency sensor located at Bus 31 (the slack bus specified in [5]). The parameters of the proportional-integral AGC controller are tuned by the trial and error method. The AGC control signal is set to be equally assigned to each conventional generator and the storage device in CFC. In contrast, new decentralized controllers are designed for all the ten generators and the storage device under AFC. The design variables are chosen as follows: $f_c = 0.0016$Hz, $n = 1$, $m_{G,i} = 10\% \ \forall \ i \in G$, $m_{S,1} = 100\%$. The selected cut-off frequency $f_c$ here is smaller than that in the simulation of the WECC 9-bus system because generators with higher power ratings typically have larger inertia constants leading to relatively slower responses. The corresponding frequency dependent weighting functions for generator and storage power output are shown in Fig. 3.12. The weighting function $W_w(s)$ for the exogenous input is chosen to be a low pass filter with cut-off frequency at 1 Hz.

By following the solution procedure of the decentralized static output feedback based $H_\infty$ minimization in Section 3.6, the yielding AFC controller gains are calculated:

$$\Delta P_{G1}^{ref} = -45.82\Delta\omega_{39} - 0.02187\Delta\theta_{39}$$

$$\Delta P_{G2}^{ref} = -28.26\Delta\omega_{31} - 0.02347\Delta\theta_{31}$$

$$\Delta P_{G3}^{ref} = -26.65\Delta\omega_{32} - 0.02346\Delta\theta_{32}$$

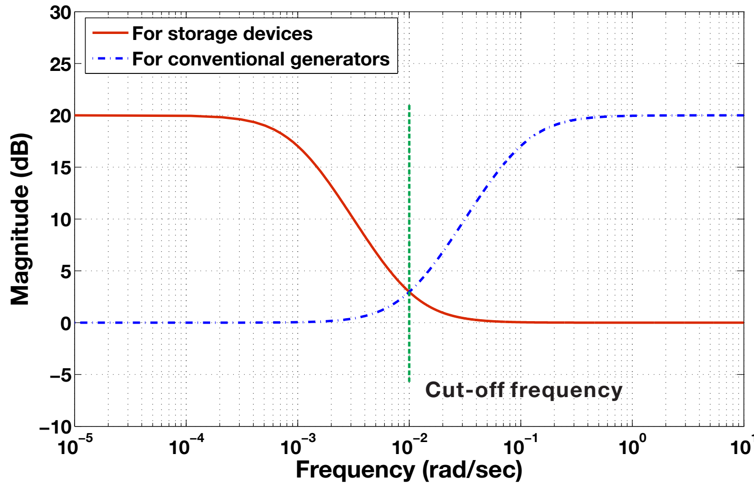


Figure 3.12: Frequency dependent weighting functions with design variables $f_c = 0.0016$Hz, $n = 1$, $m_{Gi} = 10\% \ \forall \ i \in G$, $m_{S1} = 100\%$.

$$\Delta P_{G4}^{ref} = -19.78\Delta\omega_{33} - 0.02347\Delta\theta_{33}$$

$$\Delta P_{G5}^{ref} = -20.80\Delta\omega_{34} - 0.02315\Delta\theta_{34}$$

$$\Delta P_{G6}^{ref} = -22.47\Delta\omega_{35} - 0.02348\Delta\theta_{35}$$

$$\Delta P_{G7}^{ref} = -24.57\Delta\omega_{36} - 0.02338\Delta\theta_{36}$$

$$\Delta P_{G8}^{ref} = -23.11\Delta\omega_{37} - 0.02373\Delta\theta_{37}$$

$$\Delta P_{G9}^{ref} = -47.38\Delta\omega_{38} - 0.02351\Delta\theta_{38}$$

$$\Delta P_{G10}^{ref} = -22.69\Delta\omega_{30} - 0.02372\Delta\theta_{30}$$

$$\Delta P_{S1}^{ref} = -7579.20\Delta\omega_{27} + 0.09227\Delta SOC_1.$$

### Time-Scale Matching Objective

The Bode magnitude diagram of the transfer functions from the wind power disturbance $w$ to the real power output of the ten generators and the storage device under AFC is depicted in Fig. 3.13. As can be seen from Fig. 3.13, the time-scale matching objective in the AFC design is successfully achieved, i.e. all the ten generators are mainly responsible to balance the low frequency components of the wind power variations below 0.01 rad/sec ($\sim$ 0.0016

Hz) while the storage device takes care of the high frequency components above 0.01 rad/sec. The curves corresponding to the generator power output under AFC overlap with each other because the participation factors are chosen to be identical for all the ten generators. In contrast, the bode magnitude diagram of the same set of transfer functions under CFC is shown in Fig. 3.14. The generators in the base case tend to pick up disturbances with the frequency spectrum up to 0.2 rad/sec and the storage device acts like a conventional generator as it is simply requested to follow the AGC signal.

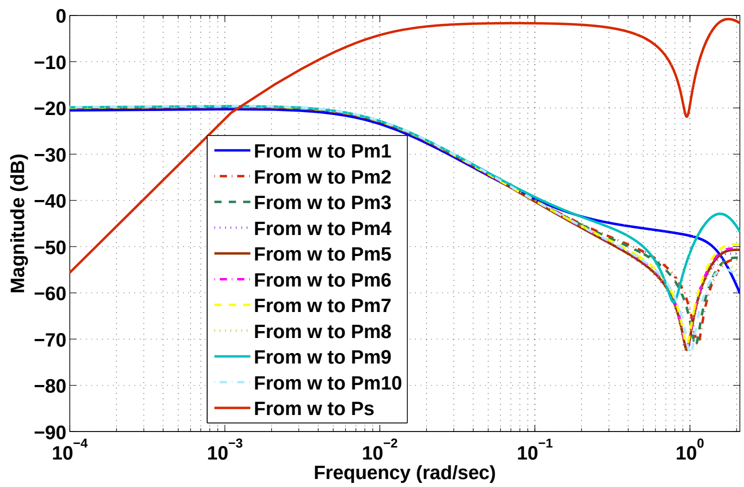


Figure 3.13: Real power output under AFC in the frequency domain.

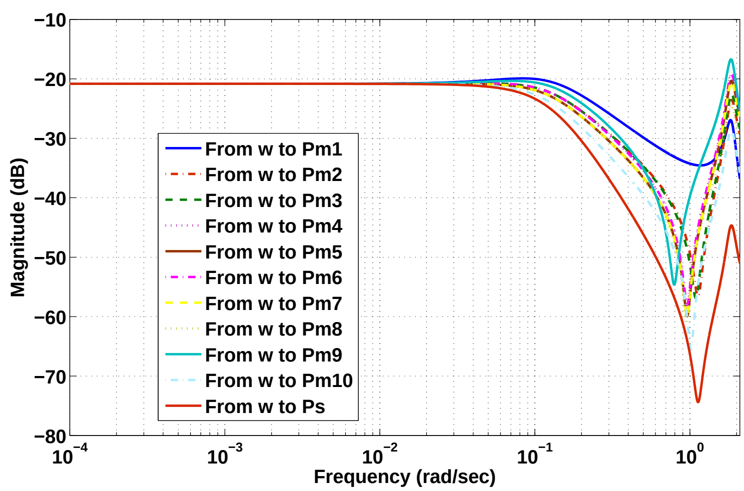


Figure 3.14: Real power output under CFC in the frequency domain.

### Frequency Response

Fig. 3.15 shows the comparison of frequency deviations at Bus 37 (Generator 8) between AFC and CFC in the presence of the aforementioned wind power variations. Similar frequency deviation curves are observed at the other nine generator buses. The frequency deviations under AFC are further reduced and narrowed within a tighter band than the base case.

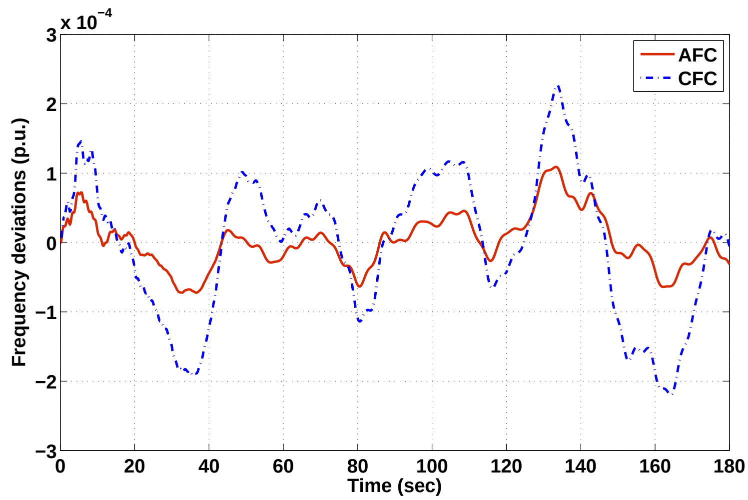


Figure 3.15: Frequency deviations at Bus 37.

### Generator Response

The power output deviations of Generator 8 from its operating point are plotted in Fig. 3.16. Similar power output deviation curves are observed for the other nine generators. Compared to the base case, the power output of the ten generators under AFC is smoothed out and high frequency fluctuations in the power output are greatly attenuated. To better understand the reduced burden on generator ramping, real power output from Generator 8 in the frequency domain is shown in 3.17. It is evident that the generator under AFC is mainly in charge of wind power variations below 0.01 rad/sec compared to its responsibility of up to 0.2 rad/sec under CFC.

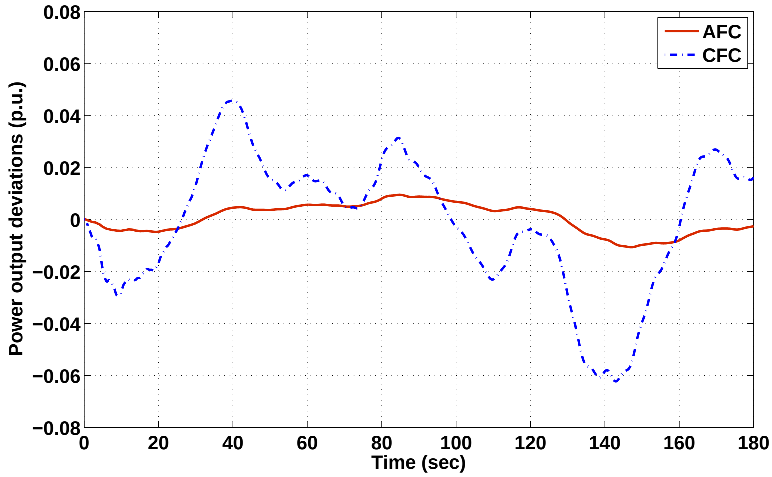


Figure 3.16: Power output deviations of Generator 8 from its operating point.

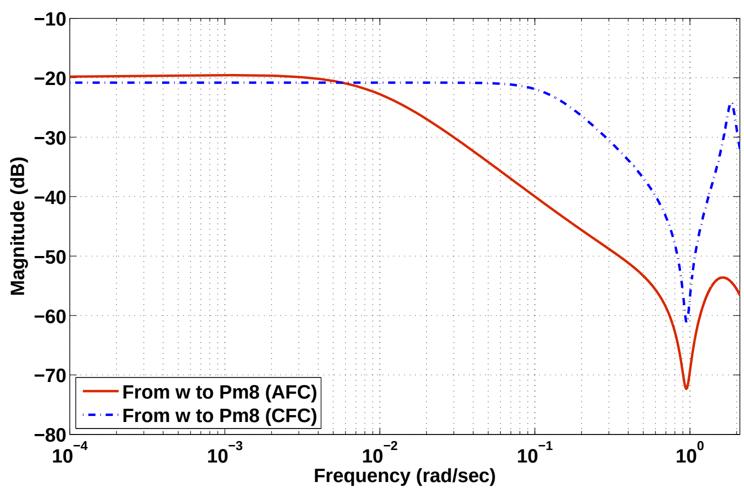


Figure 3.17: Power output from Generator 8 in the frequency domain.

### Storage Response

Fig. 3.18 shows the power injection deviations and the SOC deviations of the storage device under AFC. The storage device ramps up and down very heavily and frequently to compensate the high frequency component of the wind power variations whereas the SOC deviations are well maintained within the ±5% range by the AFC storage controller.

In addition, the comparison of SOC between AFC and CFC in the frequency domain

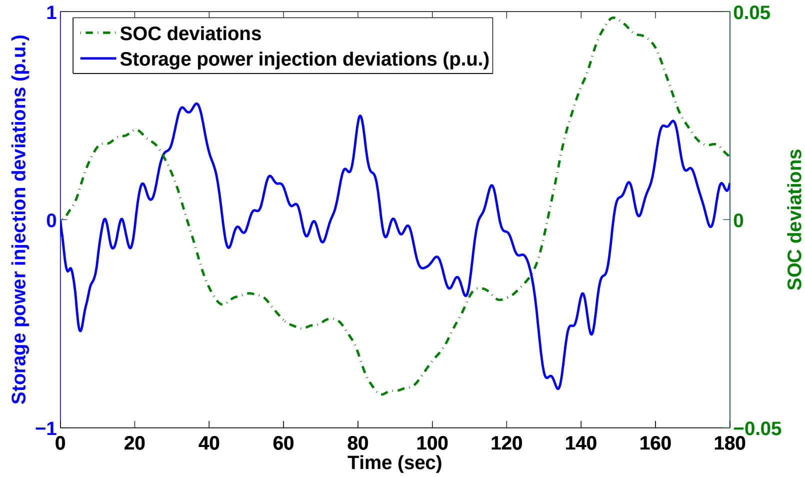


Figure 3.18: Time domain storage response under AFC.

is plotted in Fig. 3.19, showing the magnitudes of the transfer functions from the RES disturbance $w$ to SOC deviations under AFC and CFC over the entire frequency spectrum. The magnitude of the closed loop transfer function from disturbance $w$ to SOC deviations under AFC is bounded while there is no upper bound on the peak magnitude of the same transfer function under CFC. The possibility for the storage device under CFC to hit the SOC limit grows with the increase of low frequency components in wind power variations.

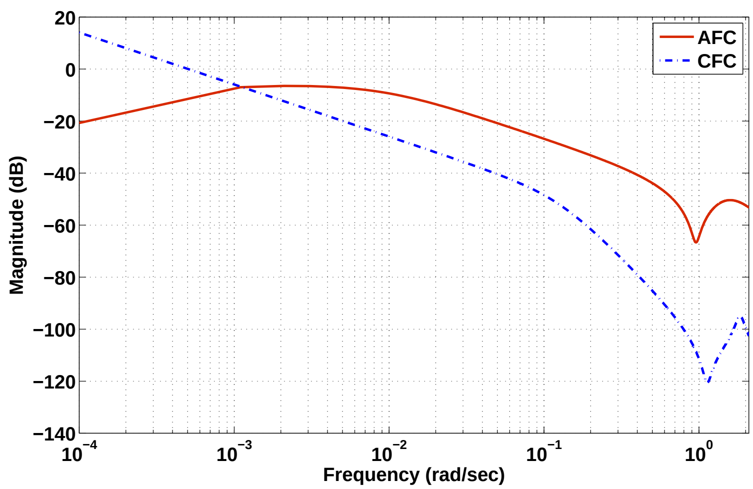


Figure 3.19: Bode magnitude diagram of the transfer function from $w$ to $\Delta SOC$.

### Performance of the Frequency Estimation Model

Fig. 3.20 shows the comparison between the estimated frequency and the actual frequency at Bus 27 in the AFC case. The actual frequency in the simulation is calculated by numerically differentiating the voltage angle signal. The fact that the two curves in Fig. 3.20 almost overlap with each other indicates the good performance of the frequency estimation model for non-generator buses derived in Section 3.3.

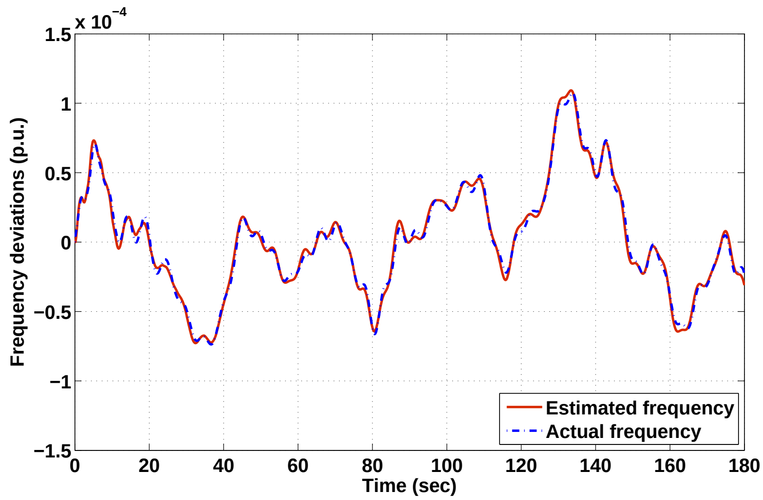


Figure 3.20: Comparison between estimated frequency and actual frequency at Bus 27.

### Importance of the Structure-Preserving Approach

Fig. 3.21 shows the frequencies at all the ten generator buses in the base case using the structure-preserving model. It is apparent that the traditional model for power system frequency control analysis where a uniformed frequency is assumed for each control area is inaccurate as the frequencies at different generator buses actually differ from each other.

## 3.9 Summary

Based on the decentralized static output feedback, a new $H_\infty$-based and structure-preserving approach to redesign the frequency control framework in power systems with significant

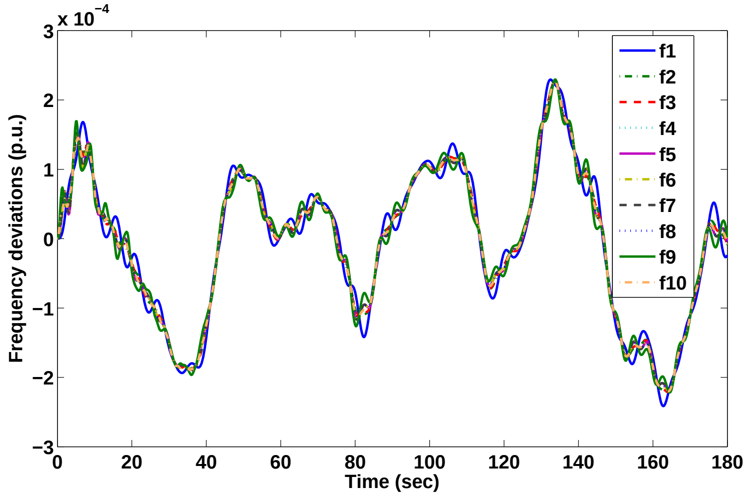


Figure 3.21: Frequencies at all the ten generator buses in the CFC case.

amounts of RESs is proposed in this chapter. A proof of concept is given for the AFC design using the WECC 9-bus test system and the IEEE New England 39-bus test system. Under the proposed AFC framework, conventional generators and energy storage devices are coordinated to take the responsibility of power balancing according to the spectrum of the RES variations, i.e. high frequency RES variations are balanced by the storage devices while low frequency RES deviations are balanced by the conventional generators reducing the required ramping of the conventional generators. Consequently, the AFC design enables the incorporation of energy storage devices in frequency control taking into account their limitations with regards to provided energy. In addition, the proposed AFC approach provides a means to design and coordinate decentralized PI controllers for multiple conventional generators which enables the return to the nominal frequency.

In terms of modeling and control, a mathematical model is developed to estimate the local frequency at non-generator buses to facilitate the proposed decentralized control scheme and an existing ILMI algorithm is improved to solve the involved $H_\infty$ problem. More importantly, the AFC applies the decentralized static output feedback technique to achieve the time-scale matching objective, resulting in task-specific but easily-implementable controllers.

# Chapter 4

# Stochastic Optimal Dispatch

This level aims to deal with the second and the third issues mentioned in Chapter 1, i.e. the current frequency control scheme does not take into account the increased uncertainty caused by RESs at the tertiary level and in addition, it is not suitable for the integration of energy storage devices as not only the power output but also the provided energy is limited. Based on the concept of stochastic model predictive control (SMPC), the level of stochastic optimal dispatch solves a two-stage stochastic version of the traditional security constrained economic dispatch (SCED) problem in power systems. As economic dispatch is the core part of real time electricity markets, the solution process of this level must be done within the time frame of 5 to 15 minutes depending on the specific market. The proposed SMPC based stochastic optimal dispatch optimizes over a look-ahead horizon with knowledge of the system model and various constraints while explicitly taking into account the uncertainties as scenarios in order to dispatch power resources including both energy storage and conventional generation in the most economic and safe manner. The uncertainties here correspond to the power output of RES generators as well as the demand at load buses. The objective is to minimize the expectation of the sum of the generation and ramping costs for conventional generators and the costs associated with storage conversion losses while satisfying all the system constraints. The time-scale matching principle is achieved by using the quadratic ramping cost terms associated with conventional generation in the objective function. Due to the large size of the resulting SMPC optimization problem, optimization decomposition techniques are employed to decompose the overall problem into subproblems which can be solved in parallel thereby reducing the computation time. In addition, scenario reduction techniques are adopted to reduce the number of scenarios, further relieving the computational burden.

The goal of this chapter is to provide an approach which efficiently solves the proposed SMPC based SCED problem. The focuses of this chapter are therefore twofold: 1) problem formulation for the SMPC based SCED problem, and 2) investigation of the influences of different decomposition methods as well as different decomposition schemes on the convergence speed. Energy storage devices with operational constraints are incorporated in the proposed stochastic SCED formulation acting as an energy buffer to counterbalance the fluctuations in the power output of RES generators. With respect to the optimization decomposition methods, both the primal decomposition and the dual decomposition will be investigated. In terms of the way how the overall problem is decomposed, both the scenario based and the temporal based decompositions will be looked into in order to achieve a trade-off between convergence speed and the number of subproblems.

## 4.1 Background and Literature Review

The two key characteristics which make a large scale integration of renewable resources challenging are: (1) their variable and intermittent power output and (2) the difficulty to accurately predict that output [6, 7]. To resolve this challenge, a rethinking of how decisions are currently made in electric power systems is required; deterministic decision making needs to be replaced by stochastic decision making which explicitly takes into account the increased uncertainty in the system [43]. Multiple papers such as [44–46] have demonstrated the advantage of stochastic optimization over deterministic optimization with respect to cost reduction in unit commitment, economic dispatch, and electric vehicle charging management. The counterpart of the proposed stochastic optimal dispatch in today's deterministic decision making power industry is economic dispatch. The traditional economic dispatch optimizes only for the current time interval and does not take into account predicted future conditions of the grid. The uncertainties in this case correspond to the power output of the non-dispatchable generation resources. A dispatchable generator should ramp up in advance if a sudden drop in wind generation is foreseen. For this reason, model predictive control (MPC) based economic dispatch was proposed by researchers, such as the work in [47–49]. However, the stochastic variables in those papers are either assumed to be perfectly predicted or represented by their corresponding expected values.

Recently, the stochastic model predictive control (SMPC) method where the uncertain variables are treated as random processes is applied to the economic dispatch problem under uncertainties, such as in [45, 50–52]. In stochastic optimization, the objective is to minimize the expected value for a given objective function taking into account a range of possible scenarios for the random processes and the probabilities for these scenarios to occur. If stochastic optimization is combined with model predictive control, then, the size of the optimization problem very rapidly grows to a scale which becomes hard to solve and to manage. Optimization decomposition and parallelization based solution methods are therefore in high demand to reduce the computation time. In [45, 50], the involved SMPC problems are solved without parallelization, i.e. either directly by general commercial optimization solvers or via dynamic programming. As a result, it will not be possible to solve the problem for a larger system without the usage of methods which improve the computational efficiency. In addition, the power network constraints are neglected causing risks of overloading the power transmission lines. In [51], the Lagrangian relaxation decomposition is adopted to tackle the SMPC problem. However, such a method requires careful tuning of parameters as well as a scheme for multiplier update. Alternatively, the authors of [52] applied the Schur-complement decomposition method to decompose the Jacobian matrix associated with the nonlinear equation system generated by the interior point method. The underlying assumption is that a customized solver of the interior point method is developed and available. Besides, neither [51] nor [52] include energy storage devices in their problem formulation.

## 4.2 SMPC Basics and Problem Formulation

In this section, we first briefly describe the concept of stochastic model predictive control together with its general formulation and then the specific problem formulation for the SMPC based SCED problem will be given.

Stochastic model predictive control is an advanced control technology that integrates the advantage of explicit inclusion of uncertainties in stochastic programming and the capability of anticipating the future behavior of the target system when making control decisions in model predictive control. A two-stage problem is typically considered in practical applications. The SMPC controller merely implements the first-stage control action of a two-stage problem at each time step. The second-stage decision in theory of stochastic programming is a collection of recourse actions that need to be taken in response to each random outcome for the considered uncertainties. However, these recourse decisions are never implemented under the SMPC setup because a new two-stage SMPC problem incorporating the new information regarding uncertainties and system states will be formulated and solved at the next time step according to the spirit of model predictive control. The reason for this is that there are always errors in predictions and mathematical models, e.g. the prediction of the wind power output is inaccurate, or losses of the storage devices are not exactly modeled.

The general mathematical formulation for a two-stage stochastic model predictive control problem at each time step (denoted by time step $t$) is given by

$$\min_{u^s} \sum_{s \in \mathcal{N}} \pi^s \left[ \sum_{k \in \mathcal{T}} l_k(x^s(t+k), u^s(t+k)) + l_K(x^s(t+K)) \right] \tag{4.1}$$

$$
\begin{aligned}
s.t. \quad & x^s(t+k+1) = Ax^s(t+k) + Bu^s(t+k) && \forall s \in \mathcal{N}, k \in \mathcal{T} && (4.2a)\\
& x^{min} \leq x^s(t+k+1) \leq x^{max} && \forall s \in \mathcal{N}, k \in \mathcal{T} && (4.2b)\\
& u^{min} \leq \quad u^s(t+k) \quad \leq u^{max} && \forall s \in \mathcal{N}, k \in \mathcal{T} && (4.2c)\\
& h(x^s(t+k), u^s(t+k), d^s(t+k)) \leq 0 && \forall s \in \mathcal{N}, k \in \mathcal{T} && (4.2d)\\
& u^s(t) = u^{s+1}(t) && \forall s \in \{1, \ldots, N-1\} && (4.2e)
\end{aligned}
$$

where the parameters and variables are given as:

$$
\begin{aligned}
\mathcal{N} &: \text{set of all scenarios, } \mathcal{N} \triangleq \{1, \cdots, N\},\\
\mathcal{T} &: \text{set of the receding horizon, } \mathcal{T} \triangleq \{0, \cdots, K-1\},\\
K &: \text{optimization horizon,}\\
\pi^s &: \text{probability associated with Scenario } s,\\
x^s(t+k) &: \text{system states for scenario } s \text{ at time step } t+k,\\
u^s(t+k) &: \text{control input for scenario } s \text{ at time step } t+k,\\
d^s(t+k) &: \text{disturbances for scenario } s \text{ at time step } t+k,\\
l_k(\cdot) &: \text{cost function for scenario } s \text{ at time step } t+k,\\
l_K(\cdot) &: \text{cost function for scenario } s \text{ at final step } t+K.
\end{aligned}
$$

This formulation captures inter-temporal constraints in (4.2a) and upper and lower limits on state and control variables in (4.2b) and (4.2c). Constraint (4.2d) accounts for intra-temporal constraints. The last constraint (4.2e) is known as the so-called nonanticipativity constraint in the stochastic programming community, stating that the first stage decisions should not be dependent on future observations of the random disturbances.

In terms of the general SMPC formulation, the complete procedure of implementing SMPC is the following:

- At time step $t$, the optimization problem (4.1)-(4.2) is solved in order to find the values for the first-stage and second-stage control decisions;
- The first-stage control decision $u^s(t)$ is applied to the physical system;
- The state of the system at the following time step is determined by measurements, e.g. actual energy level of storage devices, actual power supply level of dispatchable generators, etc.;
- The horizon is moved by one, i.e. $t$ becomes $t+1$ and the optimization is redone at this next time step for the shifted horizon.

The specific problem we consider in this chapter is the two-stage SMPC based SCED problem in a setting that consists of dispatchable generators, variable renewable energy sources, energy storage devices, and demands. For simplicity, we let the current time step $t = 0$ in the rest of this chapter. The SMPC based SCED problem formulation is given by

$$\begin{aligned}\min_{\Delta P_G^s, P_{Si}^s, P_{So}^s} \sum_{s\in\mathcal{N}} \pi^s \Bigg[ &\sum_{k\in\mathcal{T}} \sum_{i\in\Omega_G} C_{G_i}\left(P_{G_i}^s(k), \Delta P_{G_i}^s(k)\right) \\ &+ \sum_{k\in\mathcal{T}} \sum_{i\in\Omega_S} C_{S_i}\left(P_{Si_i}^s(k), P_{So_i}^s(k)\right) + \sum_{i\in\Omega_G} C_{G_i}\left(P_{G_i}^s(K)\right)\Bigg] \end{aligned} \tag{4.3}$$

$s.t. \forall s \in \mathcal{N}, k \in \mathcal{T}:$

$$E_{S_i}^s(k+1) = \eta_i E_{S_i}^s(k) + \alpha_i T \cdot P_{Si_i}^s(k) - \frac{1}{\alpha_i} T \cdot P_{So_i}^s(k), \quad \forall i \in \Omega_S \tag{4.4a}$$

$$P_{G_i}^s(k+1) = P_{G_i}^s(k) + \Delta P_{G_i}^s(k), \quad \forall i \in \Omega_G \tag{4.4b}$$

$$E_{S_i}^{min} \leq E_{S_i}^s(k+1) \leq E_{S_i}^{max}, \quad \forall i \in \Omega_S \tag{4.4c}$$

$$0 \leq P_{Si_i}^s(k) \leq P_{S_i}^{max}, \quad \forall i \in \Omega_S \tag{4.4d}$$

$$0 \leq P_{So_i}^s(k) \leq P_{S_i}^{max}, \quad \forall i \in \Omega_S \tag{4.4e}$$

$$P_{G_i}^{min} \leq P_{G_i}^s(k+1) \leq P_{G_i}^{max}, \quad \forall i \in \Omega_G \tag{4.4f}$$

$$\Delta P_{G_i}^{min} \leq \Delta P_{G_i}^s(k) \leq \Delta P_{G_i}^{max}, \quad \forall i \in \Omega_G \tag{4.4g}$$

$$\sum_{i\in\Omega_G} (P_{G_i}^s(k) + \Delta P_{G_i}^s(k)) + \sum_{i\in\Omega_R} P_{R_i}^s(k) - \sum_{i\in\Omega_D} P_{D_i}^s(k) - \sum_{i\in\Omega_S} (P_{Si_i}^s(k) - P_{So_i}^s(k)) = 0 \tag{4.4h}$$

$$-P_{ij}^{max} \leq DF_{ij} \cdot P^s(k) \leq P_{ij}^{max}, \quad \forall ij \in \Omega_L \tag{4.4i}$$

$\forall s \in \{2, \ldots, N\}:$

$$\Delta P_{G_i}^1(0) = \Delta P_{G_i}^s(0), \quad \forall i \in \Omega_G \tag{4.4j}$$

$$P_{Si_i}^1(0) = P_{Si_i}^s(0), \quad \forall i \in \Omega_S \tag{4.4k}$$

$$P_{So_i}^1(0) = P_{So_i}^s(0), \quad \forall i \in \Omega_S \tag{4.4l}$$

where the parameters and variables are given as[1]:

$\mathcal{N}$ : set of all scenarios, $\mathcal{N} \triangleq \{1, \cdots, N\}$,

$\mathcal{T}$ : set of the receding horizon, $\mathcal{T} \triangleq \{0, \cdots, K-1\}$,

$K$ : optimization horizon,

$\pi^s$ : probability associated with Scenario $s$,

$\Omega_G$ : buses to which a generator is connected

$\Omega_S$ : buses to which a storage is connected,

$\Omega_R$ : buses to which a non-dispatchable renewable generator is connected,

$\Omega_D$ : buses to which demand is connected,

$\Omega_L$ : set of lines in the system,

$E^s_{S_i}$ : energy level for storage at bus $i$ for scenario $s$,

$P^s_{Si_i}$ : charging of storage at bus $i$ for scenario $s$,

$P^s_{So_i}$ : discharging of storage at bus $i$ for scenario $s$,

$\eta_i$ : standby loss coefficient of storage at bus $i$,

$\alpha_i$ : conversion loss coefficient of storage at bus $i$,

$T$ : time between two time steps,

$P^s_{G_i}$ : output of generator at bus $i$ for scenario $s$,

$\Delta P^s_{G_i}$ : change in power output of generator at bus $i$ for scenario $s$,

$P^s_{R_i}$ : output of non-dispatchable renewable generator at bus $i$ for scenario $s$,

$P^s_{D_i}$ : demand at bus $i$ for scenario $s$,

$C_{G_i}(\cdot)$ : quadratic cost function for generator at bus $i$, including power generation cost and ramping cost,

$C_{S_i}(\cdot)$ : linear cost function associated with conversion losses for storage device at bus $i$,

$DF_{ij}$ : row for line $ij$ in the distribution factor matrix,

$P^s$ : vector of power injections at buses in scenario $s$.

The goal is to supply the demand in the most economic and safe manner by dispatching the available power resources, achieving optimal coordination between generators and storage

[1]for simplicity the indication of the time step, i.e. $(k)$ is omitted;

devices with respect to real power balancing. The uncertainties in the output from the non-dispatchable generation resources and in the demand consumption are captured in the set of considered scenarios with corresponding probabilities. Constraints on line flows are taken into account using a DC power flow model. The system states include the energy level in the storage and the power supply level of the dispatchable generators, the control variables correspond to the dispatchable generator ramp settings and the charging/discharging power of the energy storage, and the disturbances include demand and non-dispatchable generation.

The energy level $E^s_{S_i}(0)$ is not a variable but a fixed value, namely the current energy level of the storage at bus $i$ at the beginning of the optimization horizon, whereas $P^s_{G_i}(0)$ is the fixed generation output of the generator at bus $i$ during the time step right before the optimization horizon, which is treated as the initial state of the generator. Consequently, the power output of generator at bus $i$ in time step $k$ is represented by the state variable $P^s_{G_i}(k+1)$. This notation might not be intuitive but it makes the generator model consistent with the state space modeling convention.

The objective function is the expectation of the sum of the electric power generation cost, generator ramping cost, and the cost associated with storage conversion losses considering the range of scenarios $\mathcal{N}$ and probabilities $\pi$ of these scenarios, which is a convex function in our case. The cost term for the final time step $K$ is separated from the cost terms for other time steps in the objective function because there are no control inputs associated with time step $K$ in such a finite horizon problem but there is a cost associated with this step. The inter-temporal dependencies of the energy levels and of the generator power outputs are modeled by (4.4a) and (4.4b). Limitations on energy levels, power outputs from generators and storage devices, and ramp rates of generators are taken into account by (4.4c)–(4.4g). The overall power balance is kept in (4.4h) and line flow constraints are taken into account in (4.4i) where the distribution factor matrix $DF$ is calculated based on the DC power flow model. Equations (4.4j)–(4.4l) correspond to the nonanticipativity for generation ramp and storage charging/discharging settings.

## 4.3 Scenario Reduction

In order to keep the complexity of the two-stage SMPC based SCED problem manageable, scenario reduction techniques are needed to reduce the number of scenarios. The Kantorovich metric based scenario reduction method that was first developed and introduced in [53, 54] is adopted in this dissertation. The Kantorovich method is a universal scenario reduction method as there are no requirements posted on the properties of the considered stochastic process such as the time dependance structure or the dimension of the process. In addition, the Kantorovich method is independent of the structure of the scenarios, e.g. tree-structured or fan-structured. Compared to the traditional scenario reduction methods such as k-means clustering, one advantage of the Kantorovich method is that there is no need to select/generate the representative scenario for each yielding cluster.

The key ingredient in the Kantorovich method is the Kantorovich distance, which quantitatively measures the "distance" between two probability distributions. Let $\mathcal{P}$ and $\mathcal{Q}$ be discrete probability distributions of two $n$-dimensional stochastic processes of horizon length $K$ with finite scenarios $\{\xi^1, \ldots, \xi^N\}$ and $\{\tilde{\xi}^1, \ldots, \tilde{\xi}^M\}$, and probability weights $\{p_1, \ldots, p_N\}$ and $\{q_1, \ldots, q_M\}$, respectively. The Kantorovich distance denoted by $D_K(\cdot, \cdot)$ between $\mathcal{P}$ and $\mathcal{Q}$ is defined by the optimal value of the following linear program.

$$
\begin{aligned}
D_K(\mathcal{P}, \mathcal{Q}) \triangleq \min_{\tau_{ij}} & \sum_{i=1}^{N} \sum_{j=1}^{M} \tau_{ij} \cdot c(\xi^i, \tilde{\xi}^j) && (4.5)\\
\text{s.t. } & \tau_{ij} \geq 0, \ \forall i, j && (4.5a)\\
& \sum_{i=1}^{N} \tau_{ij} = q_j, \ \forall j && (4.5b)\\
& \sum_{j=1}^{M} \tau_{ij} = p_i, \ \forall i && (4.5c)
\end{aligned}
$$

where $c(\xi^i, \tilde{\xi}^j) \triangleq \|\xi^i - \tilde{\xi}^j\|$ which measures the distance between two scenarios on the entire time horizon and $\|\cdot\|$ denotes some matrix norm on $\mathbb{R}^{n \times K}$.

Let an index set $\mathcal{J} \subset \{1, \ldots, N\}$ and consider $\mathcal{Q}$ be a reduced probability distribution of

$\mathcal{P}$, i.e. $\mathcal{Q}$ has scenarios $\xi^j$ with probabilities $q_j$ where $j \in \{1, \ldots, N\} \backslash \mathcal{J}$. In other words, $\mathcal{Q}$ is obtained from $\mathcal{P}$ by deleting all scenarios $\xi^j, j \in \mathcal{J}$ and by assigning new probability weights to each preserved scenarios $\xi^j, j \notin \mathcal{J}$. According to the *optimal weights theorem* in [53], the minimum Kantorovich distance $D_K(\mathcal{P}, \mathcal{Q})$ is attained by the following optimal redistribution rule for probability weights:

$$q_j \triangleq p_j + \sum_{i \in \mathcal{J}_j} p_i, \forall j \notin \mathcal{J}, \tag{4.6}$$

where $\mathcal{J}_j \triangleq \arg\min_{i \in \mathcal{J}} c(\xi^i, \xi^j)$ for each $j \notin \mathcal{J}$. Moreover, the minimum Kantorovich distance has the following explicit representation:

$$D_K^*(\mathcal{P}, \mathcal{Q}) = \sum_{i \in \mathcal{J}} p_i \min_{j \notin \mathcal{J}} c(\xi^i, \xi^j). \tag{4.7}$$

The interpretation of (4.6) is that the new probability of a preserved scenario in the reduced distribution is the sum of its original probability and all the probabilities of the deleted scenarios that are "closest" to it in terms of scenario distance measure $c(\cdot, \cdot)$.

Thus, the Kantorovich metric based optimal scenario reduction problem with a given cardinality $m$ of the index set $\mathcal{J}$ is given by:

$$\min_{\mathcal{J}} \quad \sum_{i \in \mathcal{J}} p_i \min_{j \notin \mathcal{J}} c(\xi^i, \xi^j) \tag{4.8}$$

$$\text{s.t.} \quad \mathcal{J} \subset \{1, \ldots, N\} \tag{4.8a}$$

$$card(\mathcal{J}) = m \tag{4.8b}$$

It is evident that the number of preserved scenarios after scenario reduction is $N - m$. However, it can be shown that the problem (4.8) actually corresponds to a set covering problem that is NP-hard. A common heuristic algorithm called backward reduction for the Kantorovich metric based optimal scenario reduction problem was therefore proposed in [54] to achieve a suboptimal solution but with much less computational effort. The main idea of backward reduction is to iteratively eliminate one scenario until the requested cardinality of $\mathcal{J}$ is reached based on the fact that the special case of deleting one scenario of (4.8) can be relatively easy to solve. The backward Kantorovich reduction algorithm is given below.

**Algorithm 2** (Backward Kantorovich Scenario Reduction [54])**.**

1. Set $\mathcal{J}^{[0]} = \emptyset$ and let the index set associated with the original scenarios be $\mathcal{N} \triangleq \{1, \ldots, N\}$.

2. Set $i = 0$. Compute the $N \times N$ distance matrix of scenario pairs as $C = \{c_{i,j} = c(\xi^i, \xi^j),\ \forall\, i, j \in \mathcal{N}\}$.

3. For each $l \in \mathcal{N} \backslash \mathcal{J}^{[i]}$, compute $z_l^{[i]} = \min_{j \neq l, j \in \mathcal{N} \backslash \mathcal{J}^{[i]}} c_{l,j}$.

4. Find $l_*^{[i]} \in \arg\min_{l \in \mathcal{N} \backslash \mathcal{J}^{[i]}} p_l^{[i]} \cdot z_l^{[i]}$. Set $\mathcal{J}^{[i+1]} = \mathcal{J}^{[i]} \cup \{l_*^{[i]}\}$.

5. Find $j_*^{[i]} \in \arg\min_{j \neq l_*^i, j \in \mathcal{N} \backslash \mathcal{J}^{[i]}} c_{l_*^i, j}$. Set $p_{j_*^{[i]}}^{[i+1]} = p_{j_*^{[i]}}^{[i]} + p_{l_*^{[i]}}^{[i]}$.

6. Set $i = i + 1$. If $i < m$ where $m$ is the predetermined cardinality of $\mathcal{J}$, go to Step 3. Else, stop and the index set associated with the reduced scenarios is $\mathcal{N} \backslash \mathcal{J}^{[i]}$ with probabilities $p_j^{[i]}$ where $j \in \mathcal{N} \backslash \mathcal{J}^{[i]}$.

## 4.4 Classical Solution Methods

The structure of the considered two-stage SMPC based SCED problem which is essentially an SMPC problem lends itself to employ optimization decomposition techniques to decompose the overall problem into subproblems which are solved in a parallel but coordinated manner. The expectation is that the reduced size of the subproblems and the fact that they can be solved in parallel allows for an improvement in computational efficiency for the considered stochastic model predictive control problem.

In this section, we provide an overview over the two fundamental classes of decomposition methods that serve as the classical solution methods for solving SMPC problems and, more generally, stochastic programs. These decomposition methods are then applied to the considered two-stage SMPC based SCED problem. In particular, two well-known decomposition methods in stochastic programming – *Benders decomposition* and *progressive hedging algorithm* are emphasized in this section. In addition, we follow the classical assumption that the optimization problems we are considering are convex.

### 4.4.1 Primal Decomposition

Consider the following optimization problem in the form of

$$\min_{x_1,\dots,x_M,y} \quad \sum_{m=1}^{M} f_m(x_m, y) \tag{4.9}$$

$$\text{s.t.} \quad g_m(x_m, y) \leq 0, \;\; m = 1, \dots, M \tag{4.9a}$$

$$h(y) \leq 0 \tag{4.9b}$$

where $M$ is the total number of subproblems and the decision variables $x_1, \dots, x_M, y$ are all vectors and $y$ is known as the *complicating variable* because the overall problem becomes trivially decomposable if it is fixed and $y$ complicates the overall problem. Following this idea, we can formulate the subproblems of (4.9) where each subproblem is separable from each other and can be solved independently and in parallel.

$$\text{Subproblem } m : \phi_m(\bar{y}^{(j)}) = \min_{x_m} \; f_m(x_m, \bar{y}^{(j)}) \tag{4.10}$$

$$\text{s.t. } g_m(x_m, \bar{y}^{(j)}) \leq 0 \tag{4.10a}$$

where $\phi_m(y)$ denotes the optimal value of (4.10) and the superscript $j$ stands for the iteration index and the overhead bar indicates fixed values. Then the original problem (4.9) is equivalent to the following problem which is called the master problem.

$$\text{Master problem}: \min_{y^{(j+1)}} \sum_{m=1}^{M} \phi_m(y^{(j+1)}) \tag{4.11}$$

$$\text{s.t. } h(y^{(j+1)}) \leq 0 \tag{4.11a}$$

The master problem provides an update for the complicating variable $y$ for the next iteration and it can be solved by traditional methods such as subgradient or cutting-plane methods [55–57]. This decomposition method is termed *primal decomposition* because we directly decompose the original primal problem and part of the primal variables – complicating variables are manipulated by the master problem. The general primal decomposition algorithm is described below.

**Algorithm 3** (General Primal Decomposition Algorithm)**.**

1. Set $j = 1$. Find feasible complicating variables $y^{(j)}$ such that $h(y^{(j)}) \leq 0$.

2. Solve each subproblem defined in (4.10) in parallel.

3. If stopping criteria are fulfilled, stop. Else, continue.

4. Solve the master problem defined in (4.11) to update complicating variables $y^{(j+1)}$.

5. Set $j = j + 1$. Go to Step 2.

**Benders Decomposition**

Benders decomposition (BD) is named after the Dutch mathematician Jacques F. Benders due to his work of [58], which was originally developed for mixed integer linear programming and was later generalized to nonlinear programming by other researchers in [59, 60]. Theoretically, Benders decomposition is in the class of primal decomposition with the cutting-plane method. In terms of the general problem in the form of (4.9), the subproblems and the master problem in BD are formulated as:

$$\text{Subproblem } m : \phi_m(\bar{y}^{(j)}) = \min_{x_m} \; f_m(x_m, y) \tag{4.12}$$

$$\text{s.t. } g_m(x_m, y) \leq 0 \tag{4.12a}$$

$$y = \bar{y}^{(j)} \cdots\cdots\cdots\cdots \lambda_m^{(j)} \tag{4.12b}$$

$$\text{Master problem} : \min_{\gamma^{(j+1)}, y^{(j+1)}} \; \gamma^{(j+1)} \tag{4.13}$$

$$\text{s.t. } \gamma^{(j+1)} \geq \sum_{m=1}^{M} \phi_m(\bar{y}^{(\nu)})$$

$$- \sum_{m=1}^{M} \lambda_m^{(\nu)T} (y^{(j+1)} - \bar{y}^{(\nu)}) \; \forall \; \nu = 1, \ldots, j \tag{4.13a}$$

$$h(y^{(j+1)}) \leq 0 \tag{4.13b}$$

where $\lambda_m^{(j)}$ is the Lagrangian multiplier vector associated with (4.12b) at the $j$th iteration. The newly introduced variable $\gamma^{(j+1)}$ is used to approximate the original objective function $\sum_{m=1}^{M} \phi_m(y^{(j+1)})$ in (4.11) by multiple so-called Benders cuts in the form of (4.13a). This is also why we mentioned earlier that BD is essentially a primal decomposition with the cutting-plane method. It is noted that the size of the master problem grows as the iteration process progresses, which is one disadvantage of BD in certain cases where the problem takes many iterations to converge.

There might be cases where the solution of the master problem results in an infeasible subproblem. In such a situation, nonnegative slack variables are added to the infeasible subproblem and its objective function is modified accordingly by including a large penalty term for the slack variables. The detailed Benders decomposition algorithm is given below.

**Algorithm 4** (Benders Decomposition Algorithm)**.**

1. Set $j = 1$, $\gamma^{(j)} = -\infty$. Find feasible complicating variables $y^{(j)}$ such that $h(y^{(j)}) \leq 0$.

2. Solve each subproblem defined in (4.12) in parallel.

3. Resolve the infeasibility issue for certain subproblems by adding slack variables.

4. If $|\sum_{m=1}^{M}\phi_m(y^{(j)})-\gamma^{(j)}|/|\gamma^{(j)}|\leq\varepsilon$ where $\varepsilon$ is the error tolerance, stop. Else, continue.

5. Solve the master problem defined in (4.13) to update complicating variables $y^{(j+1)}$.

6. Set $j=j+1$. Go to Step 2.

In terms of two-stage stochastic optimization, the basic idea of BD is to decompose the overall problem into subproblems by fixing the first stage variables and then to add the resulting sensitivity information in the form known as Benders cuts with respect to the first stage variables to a master problem. Such a process iterates until convergence is reached. The complicating variables here correspond to the first stage decision variables. The sensitivity information is essentially represented by the Lagrangian multipliers of the subproblems. The subproblems give an upper bound of the original problem in each iteration whereas the master problem yields a lower bound.

In order to utilize Benders decomposition for the considered two-stage SMPC based SCED problem, the original problem formulation (4.3)-(4.4) needs to be modified by only keeping one copy of the variables for each equation of (4.4j)–(4.4l) among all the subproblems.

By applying BD to the modified SMPC based SCED problem, subproblems for $s\in\mathcal{N}$ are mathematically formulated as

$$\min_{\Delta P_G^s, P_{Si}^s, P_{So}^s} \pi^s \Bigg[\sum_{k\in\tilde{\mathcal{T}}}\sum_{i\in\Omega_G} C_{G_i}\left(P_{G_i}^s(k),\Delta P_{G_i}^s(k)\right) + \sum_{k\in\tilde{\mathcal{T}}}\sum_{i\in\Omega_S} C_{S_i}\left(P_{Si_i}^s(k),P_{So_i}^s(k)\right) + \sum_{i\in\Omega_G} C_{G_i}\left(P_{G_i}^s(K)\right)\Bigg] \tag{4.14}$$

$$s.t. \quad (4.4a)-(4.4i)$$

$$\Delta P_{G_i}(0)=\Delta\overline{P}_{G_i}^{(j)}(0),\quad \forall i\in\Omega_G \tag{4.15a}$$

$$P_{Si_i}(0)=\overline{P}_{Si_i}^{(j)}(0),\quad \forall i\in\Omega_S \tag{4.15b}$$

$$P_{So_i}(0)=\overline{P}_{So_i}^{(j)}(0),\quad \forall i\in\Omega_S \tag{4.15c}$$

where $\tilde{\mathcal{T}} = \mathcal{T}\backslash\{0\}$ and the values of the first stage variables $\Delta P_{G_i}(0)$, $P_{Si_i}(0)$ and $P_{So_i}(0)$ are provided by the master problem at the $(j-1)$th iteration. The master problem formulation at the $j$th iteration is given by

$$\begin{aligned}
\min_{\Delta P_G^{(j+1)}(0), P_{Si}^{(j+1)}(0), P_{So}^{(j+1)}(0)} \; & \sum_{i\in\Omega_G} C_{G_i}\left(P_{G_i}^{(j+1)}(0), \Delta P_{G_i}^{(j+1)}(0)\right) \\
& + \sum_{i\in\Omega_S} C_{S_i}\left(P_{Si_i}^{(j+1)}(0), P_{So_i}^{(j+1)}(0)\right) + \gamma^{(j+1)} \qquad (4.16)
\end{aligned}$$

$$\begin{aligned}
s.t. \quad & (4.4d), (4.4e), (4.4g) - (4.4i), \quad \forall k = 0 \\
& \gamma^{(j+1)} \geq \overline{\theta}^{(\nu)} - \sum_{i\in\Omega_G} \overline{\mu}_{G,i}^{(\nu)} \left(\Delta P_{G_i}^{(j+1)}(0) - \Delta\overline{P}_{G_i}^{(\nu)}(0)\right) \\
& \qquad - \sum_{i\in\Omega_S} \overline{\mu}_{Si,i}^{(\nu)} \left(P_{Si_i}^{(j+1)}(0) - \overline{P}_{Si_i}^{(\nu)}(0)\right) \\
& \qquad - \sum_{i\in\Omega_S} \overline{\mu}_{So,i}^{(\nu)} \left(P_{So_i}^{(j+1)}(0) - \overline{P}_{So_i}^{(\nu)}(0)\right) \\
& \qquad \forall\, \nu = 1, \cdots, j \qquad (4.17a)
\end{aligned}$$

The Benders cuts are represented in (4.17a) and $\nu$ is the iteration index. $\overline{\mu}_{G,i}^{(\nu)}$, $\overline{\mu}_{Si,i}^{(\nu)}$ and $\overline{\mu}_{So,i}^{(\nu)}$ are Lagrangian multipliers associated with (4.15a)-(4.15c) at the $\nu$th iteration. $\overline{\theta}^{(\nu)}$ is the sum of objective function values of all the $N$ subproblems at the $\nu$th iteration and the variable $\gamma^{(j+1)}$ is used to approximate the subproblem objective functions as a single function solely dependent on the first stage variables. The flowchart of the iterative update for the considered SMPC problem using BD is visualized in Fig. 4.1.

### 4.4.2 Dual Decomposition

The primal decomposition described previously is mainly used to tackle problems with complicating variables. The other class of decomposition methods – *dual decomposition* that we will introduce in this subsection deals with problems with so-called *complicating constraints*. In fact, a problem with complicating variables can be easily reformulated as a problem with complicating constraints by duplicating the complicating variables for each subproblem and

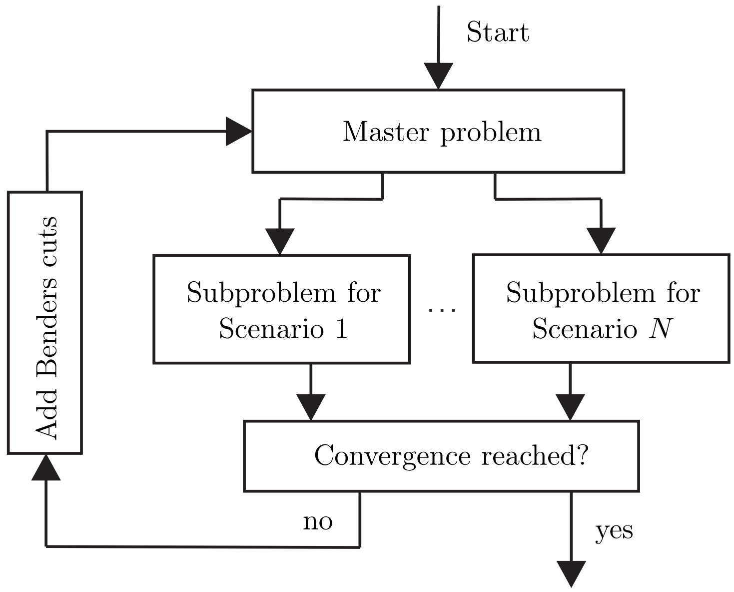


Figure 4.1: Flow chart of the iterative update using BD.

enforcing the equality among all the copies. These equality constraints are actually complicating constraints. Let us consider the following optimization problem in the form of

$$\min_{x_1,\ldots,x_M} \quad \sum_{m=1}^{M} f_m(x_m) \tag{4.18}$$

$$\text{s.t.} \quad g_m(x_m) \leq 0, \;\; m = 1, \ldots, M \tag{4.18a}$$

$$\sum_{m=1}^{M} h_m(x_m) \leq 0 \cdots\cdots\cdots\cdots \lambda \tag{4.18b}$$

where $M$ is the number of subproblems and (4.18b) is known as *complicating constraint* because if it is relaxed the overall problem becomes trivially separable. We can achieve this relaxation by dualizing the original problem (4.18) with respect to (4.18b). Thus, the subproblems of (4.18) using dual decomposition are

$$\text{Subproblem } m : \phi_m(\bar{\lambda}^{(j)}) = \min_{x_m} \; f_m(x_m) + \bar{\lambda}^{(j)^T} h_m(x_m) \tag{4.19}$$

$$\text{s.t. } g_m(x_m) \leq 0 \tag{4.19a}$$

where $\phi_m(\lambda)$ denotes the optimal value of (4.19) and the superscript $j$ stands for the iteration index and the overhead bar indicates fixed values. $\bar{\lambda}^{(j)}$ is the Lagrangian multipliers vector associated with (4.18b) at the $j$th iteration and is fixed in subproblems. Under the convexity assumption, the original problem (4.18) is equivalent to the following dual problem which is called the master problem.

$$\text{Master problem} : \max_{\lambda^{(j+1)}} \sum_{m=1}^{M} \phi_m(\lambda^{(j+1)}) \tag{4.20}$$

$$\text{s.t. } \lambda^{(j+1)} \geq 0 \tag{4.20a}$$

The master problem provides an update for the dual variable $\lambda$ for the next iteration and similar to the situation in the primal decomposition it can be solved by traditional methods such as subgradient or cutting-plane methods. This class of decomposition methods is termed *dual decomposition* because we decompose the dual problem into subproblems and the dual variables corresponding to complicating constraints that are used to achieve problem separability are manipulated by the master problem. The general dual decomposition algorithm is described below.

**Algorithm 5** (General Dual Decomposition Algorithm)**.**

1. Set $j = 1$. Initialize dual variables vector $\lambda^{(j)}$.

2. Solve each subproblem defined in (4.19) in parallel.

3. Solve the master problem defined in (4.20) to update dual variables $\lambda^{(j+1)}$.

4. If stopping criteria are fulfilled, stop. Else, set $j = j + 1$ and go to Step 2.

#### Lagrangian Relaxation Decomposition

The Lagrangian relaxation decomposition (LRD) method is typically referred to as the dual decomposition with the subgradient multiplier update method. In terms of the general problem in the form of (4.18), the subproblems in LRD are exactly the same as (4.19). The master problem in (4.20) is solved using the subgradient method which is stated below to update Lagrangian multipliers vector $\lambda^{(j+1)}$. Under the subgradient method, the multipliers are updated according to the following rule [61].

$$\lambda^{(j+1)} = \lambda^{(j)} + \kappa^{(j)} \cdot \frac{\sum_{m=1}^{M} h_m(x_m^{(j)})}{\| \sum_{m=1}^{M} h_m(x_m^{(j)}) \|} \tag{4.21}$$

where $\kappa^{(j)}$ is the step size at the $j$th iteration and it should satisfy the conditions $\lim_{j\to\infty} \kappa^{(j)} = 0$ and $\sum_{j=1}^{\infty} \kappa^{(j)} = \infty$. In addition, $\lambda^{(j+1)}$ should be kept nonnegative at all times. The vector $\sum_{m=1}^{M} h_m(x_m^{(j)})$ is indeed a subgradient of the dual function at $\lambda^{(j)}$. A typical selection of the step size sequence is $\kappa^{(j)} = \frac{1}{a+b\cdot j}$ where $a$ and $b$ are positive constants [61]. Although the subgradient method is easy to implement, it tends to exhibit slow and oscillating converging behaviors due to the non-differentiability of the dual function. The detailed Lagrangian relaxation decomposition algorithm is described below.

**Algorithm 6** (Lagrangian Relaxation Decomposition Algorithm)**.**

Replace Step 3 in Algorithm 5 by: Use (4.21) to update multipliers $\lambda^{(j+1)}$.

By applying LRD to the considered problem (4.3)-(4.4), the yielding subproblems for $s \in \{2, \ldots, N\}$ are given as

$$\begin{aligned} \min_{\Delta P_G^s, P_{Si}^s, P_{So}^s} \quad & \pi^s \Bigg[ \sum_{k\in\mathcal{T}} \sum_{i\in\Omega_G} C_{G_i}\left(P_{G_i}^s(k), \Delta P_{G_i}^s(k)\right) \\ & + \sum_{k\in\mathcal{T}} \sum_{i\in\Omega_S} C_{S_i}\left(P_{Si_i}^s(k), P_{So_i}^s(k)\right) + \sum_{i\in\Omega_G} C_{G_i}\left(P_{G_i}^s(K)\right) \Bigg] \\ & - \sum_{i\in\Omega_G} \bar{\lambda}_{G,i}^s \cdot \Delta P_{G_i}^s(0) - \sum_{i\in\Omega_S} \bar{\lambda}_{Si,i}^s \cdot P_{Si_i}^s(0) - \sum_{i\in\Omega_S} \bar{\lambda}_{So,i}^s \cdot P_{So_i}^s(0) \end{aligned} \tag{4.22}$$

$$s.t. (4.4a) - (4.4i)$$

where $\bar{\lambda}_{G,i}^s, \bar{\lambda}_{Si,i}^s, \bar{\lambda}_{So,i}^s$ are Lagrangian multipliers associated with (4.4j)-(4.4l). The first subproblem corresponding to $s = 1$ is a little special and is given below due to the way in which the nonanticipativity constraints are formulated in the original problem.

$$\begin{aligned}\min_{\Delta P_G^1, P_{Si}^1, P_{So}^1} \quad & \pi^1 \Bigg[ \sum_{k\in\mathcal{T}} \sum_{i\in\Omega_G} C_{G_i}\left(P_{G_i}^1(k), \Delta P_{G_i}^1(k)\right) \\ & + \sum_{k\in\mathcal{T}} \sum_{i\in\Omega_S} C_{S_i}\left(P_{Si_i}^1(k), P_{So_i}^1(k)\right) + \sum_{i\in\Omega_G} C_{G_i}\left(P_{G_i}^1(K)\right)\Bigg] \\ & + \sum_{s=2}^{N} \left( \sum_{i\in\Omega_G} \bar{\lambda}_{G,i}^s \cdot \Delta P_{G_i}^1(0) + \sum_{i\in\Omega_S} \bar{\lambda}_{Si,i}^s \cdot P_{Si_i}^1(0) + \sum_{i\in\Omega_S} \bar{\lambda}_{So,i}^s \cdot P_{So_i}^1(0) \right) \quad (4.23) \\ & s.t. (4.4a) - (4.4i)\end{aligned}$$

Following Algorithm 6, the flowchart of the iterative update for the considered SMPC problem using LRD is shown in Fig. 4.2.

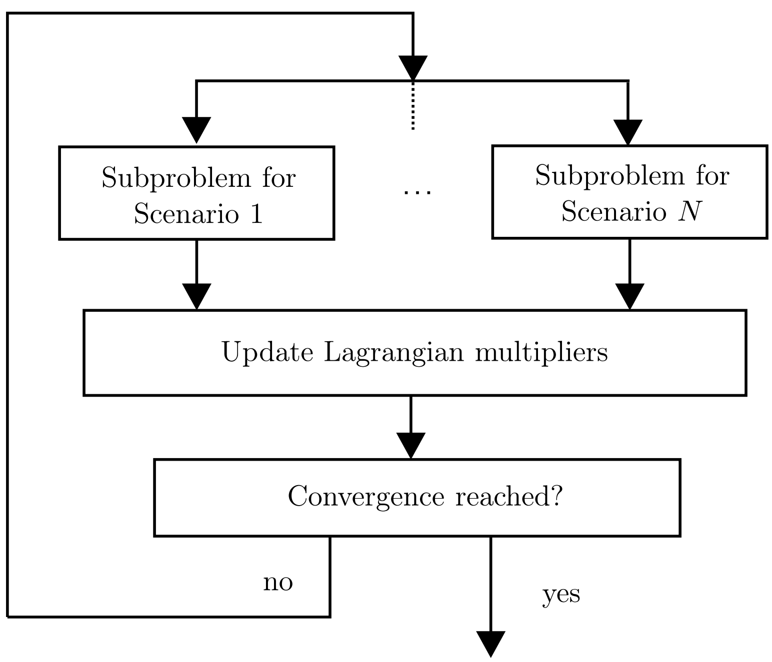


Figure 4.2: Flow chart of the iterative update using LRD.

### Augmented Lagrangian Decomposition

The augmented Lagrangian decomposition (ALD) is developed based on the Lagrangian relaxation decomposition to improve convergence by introducing an additional quadratic term associated with the complicating constraints to the Lagrangian function. For simplicity, we consider the following case where there are merely equality complicating constraints in the problem. For the detailed algorithm derivation of the general case, please refer to [61].

$$\min_{x_1,\ldots,x_M} \quad \sum_{m=1}^{M} f_m(x_m) \tag{4.24}$$

$$\text{s.t.} \quad g_m(x_m) \leq 0, \;\; m = 1, \ldots, M \tag{4.24a}$$

$$\sum_{m=1}^{M} h_m(x_m) = 0 \cdots\cdots\cdots\cdots \lambda \tag{4.24b}$$

The augmented Lagrangian function with respect to complicating constraints is defined as

$$L_A \triangleq \sum_{m=1}^{M} f_m(x_m) + \lambda^T \sum_{m=1}^{M} h_m(x_m) + \frac{1}{2}\rho \| \sum_{m=1}^{M} h_m(x_m) \|^2 \tag{4.25}$$

where $\rho$ is a large penalty associated with the additional quadratic term and goes to infinity in theory with the progress of the iteration process. Due to this quadratic term, the dual function is no longer trivially separable. Two common approaches can be employed to achieve subproblem separability – one is to linearize the quadratic term and fix a minimum number of variables in the linearized augmented Lagrangian [62] and the other is to directly fix a minimum number of variables in the augmented Lagrangian. For illustration purposes, the subproblems in ALD using the foregoing second separation approach are given below.

$$\text{Subproblem } m : \phi_m(\bar{\lambda}^{(j)}) = \min_{x_m} \; f_m(x_m) + \bar{\lambda}^{(j)^T} h_m(x_m)$$

$$+ \frac{1}{2}\rho^{(j)} \| h(\bar{x}_1, \ldots, x_m, \ldots, \bar{x}_M) \|^2 \tag{4.26}$$

$$\text{s.t. } g_m(x_m) \leq 0 \tag{4.26a}$$

Here, we use $h(x_1, \ldots, x_M)$ to denote the original complicating constraint (4.24b) for conciseness. In terms of the multiplier update, the so-called multiplier method with the following update rule is typically adopted [63, 64].

$$\lambda^{(j+1)} = \lambda^{(j)} + \rho^{(j)} h(x_1^{(j)}, \ldots, x_M^{(j)}) \tag{4.27}$$

To see the reasoning behind, we take partial derivative of the augmented Lagrangian with respect to the entire variable set $x = [x_1^T, \ldots, x_M^T]^T$, yielding

$$\nabla_x L_A^{(j)} = \nabla_x \left( \sum_{m=1}^{M} f_m(x_m^{(j)}) \right) + \nabla_x^T h(x^{(j)}) \cdot \lambda^{(j)} + \nabla_x^T h(x^{(j)}) \cdot \rho^{(j)} \cdot h(x^{(j)}). \tag{4.28}$$

On the other hand, the partial derivative of $L_A$ with respect to $x$ at the optimal point $x^*$ given the fact that $\lim_{j \to \infty} \rho^{(j)} = \infty$ is

$$\lim_{j \to \infty} \nabla_x L_A^{(j)} = \nabla_x \left( \sum_{m=1}^{M} f_m(x_m^*) \right) + \nabla_x^T h(x^*) \cdot \lambda^*. \tag{4.29}$$

By comparing (4.28) and (4.29), we conclude that

$$\lim_{j \to \infty} \left( \lambda^{(j)} + \rho^{(j)} \cdot h(x^{(j)}) \right) = \lambda^*. \tag{4.30}$$

In terms of the update of the penalty term $\rho$, it is increasing with the progress of the iteration steps but it has to be chosen in such a way that no ill-conditioning takes place due to too large penalties [64]. Therefore, careful tuning of parameters is critical to the success in applying ALD to attain optimality of an optimization problem. The detailed augmented Lagrangian decomposition algorithm is described below.

**Algorithm 7** (Augmented Lagrangian Decomposition Algorithm)**.**

> Replace Step 3 in Algorithm 5 by: Use (4.27) to update multipliers $\lambda^{(j+1)}$ and properly update the penalty term $\rho^{(j+1)}$.

The application of ALD to the considered SMPC problem is very similar to the case for

LRD but merely with an additional quadratic term. Hence, we will not provide the detailed subproblem formulations for the SMPC problem using ALD. Instead, in the following, we will briefly describe a well-known decomposition algorithm in the stochastic programming community which is essentially an augmented Lagrangian decomposition method – the *progressive hedging algorithm*.

The progressive hedging algorithm was first introduced in [65] and is well applicable to the two-stage stochastic optimization problems. In terms of the considered two-stage SMPC based SCED problem, the progressive hedging algorithm is nothing but Algorithm 7 (augmented Lagrangian decomposition algorithm) applied to the original problem (4.3)-(4.4) with a slight modification of the formulation for the nonanticipativity constraints at each iteration. The original nonanticipativity constraints (4.4j)–(4.4l) at the $j$th iteration are replaced by

$$
\begin{aligned}
&\forall\ s \in \mathcal{N} \\
&\Delta P_{G_i}^{s(j)}(0) = \Delta \bar{P}_{G_i}^{(j)}(0), \quad \forall i \in \Omega_G && \text{(4.30a)} \\
&\quad P_{Si_i}^{s(j)}(0) = \bar{P}_{Si_i}^{(j)}(0), \quad \forall i \in \Omega_S && \text{(4.30b)} \\
&\quad P_{So_i}^{s(j)}(0) = \bar{P}_{So_i}^{(j)}(0), \quad \forall i \in \Omega_S && \text{(4.30c)}
\end{aligned}
$$

with the following right hand side values

$$
\begin{aligned}
\Delta \bar{P}_{G_i}^{(j)}(0) &= \sum_{s=1}^{N} \pi^s \Delta \bar{P}_{G_i}^{s(j-1)}(0), \quad \forall i \in \Omega_G \\
\bar{P}_{Si_i}^{(j)}(0) &= \sum_{s=1}^{N} \pi^s \bar{P}_{Si_i}^{s(j-1)}(0), \quad \forall i \in \Omega_S \\
\bar{P}_{So_i}^{(j)}(0) &= \sum_{s=1}^{N} \pi^s \bar{P}_{So_i}^{s(j-1)}(0), \quad \forall i \in \Omega_S
\end{aligned}
$$

where the overhead bars indicate fixed values. The interpretation is that the first stage variables at the current iteration try to agree to their corresponding probability weighed values of all the scenarios obtained from the previous iteration. Compared to the direct application of ALD to the original problem, the progressive hedging algorithm achieves a trivially separable augmented Lagrangian function so that subproblems are directly decoupled.

## 4.5 OCD based Solution Approach

Although the classical solution methods discussed in the previous section are considered effective and efficient, there are weaknesses associated with them. For example, the bottleneck of Benders decomposition lies in the master problem in the sense that on the one hand decomposition cannot progress until the master problem is solved during each iteration and on the other hand the size of the master problem increases as the iterative process goes. The downside of progress hedging or more generally the augmented Lagrangian decomposition or even Lagrangian relaxation decomposition is the difficulty in well tuning the penalty parameters associated with the quadratic augmented term in the Lagrangian dual function and/or properly updating Lagrangian dual variables in each iteration.

To overcome the foregoing shortcomings, we instead propose the application of the so-called *optimality condition decomposition* (OCD) (first introduced in [66]) to the SMPC based SCED problem. Neither parameter tuning nor master problem are needed in the OCD algorithm and multiplier update is done automatically. In this section, we first describe the concept of the unlimited point method [67] which is used to eliminate inequalities in the first order optimality conditions as the Newton-Raphson method is typically bundled with the OCD implementation.Then we provide an overview over the OCD which is employed to solve the resulting first order optimality conditions in parallel. Possible communication issues related to OCD are then discussed. The advantages provided by OCD over the other primal/dual decomposition techniques are given as well. In addition, several measures such as generalized minimal residual and line search algorithms that are used to improve the convergence performance of OCD are briefly described.

### 4.5.1 Unlimited Point Method

The unlimited point method is used to accomplish the step of transforming inequality constraints into equality ones, which is required by the Newton-Raphson based OCD method. Consider the following general optimization problem:

$$\min_{x} \quad f(x) \tag{4.31}$$

$$\text{s.t.} \quad h(x) = 0 \tag{4.31a}$$

$$g(x) \leq 0 \tag{4.31b}$$

According to the unlimited point method, the modified Karush-Kuhn-Tucker (KKT) conditions are given by

$$KKT = \left[\nabla_x^T \mathcal{L}, \quad h^T, \quad (g + \epsilon^2)^T, \quad (\text{diag}\{\mu\} \cdot \epsilon)^T\right]^T \tag{4.32}$$

where $\mathcal{L}$ is the modified Lagrangian function

$$\mathcal{L} = f(x) + \lambda^T \cdot h(x) + (\mu^2)^T \cdot g(x) \tag{4.33}$$

and $\lambda, \mu^2$ are the Lagrangian multipliers and $\epsilon^2$ is the vector of squared slack variables for inequalities. Due to the fact that there are no limits imposed on slack variables or Lagrange multipliers, the method is named as "unlimited point method". For the complete algorithm, readers are referred to [67]. Compared to the interior point method which could be used alternatively, the main difference is that the unlimited point method does not require variables to stay within a feasible region during iterations and is considered easily-implementable.

### 4.5.2 Optimality Condition Decomposition (OCD)

The optimality condition decomposition (OCD) is an extension to Lagrangian relaxation decomposition [61]. Assuming that state and control variables are all included in a single variable vector $z$ which is composed of $M$ subsets of variables $z_m,\ m = 1, \ldots, M$ of which each will be assigned to a specific subproblem $m$, the general overall optimization problem formulation is given by

$$\min_{z_1,\cdots,z_M} \quad f(z_1, \cdots, z_M) \tag{4.34}$$

$$\text{s.t.} \quad g_m(z_m) \leq 0, \qquad m = 1, \cdots, M \tag{4.34a}$$

$$h_m(z_1, \cdots, z_M) \leq 0, \quad m = 1, \cdots, M \tag{4.34b}$$

Constraints (4.34a) correspond to non-coupling constraints which can directly be included in subproblem $m$. However, the complicating constraints (4.34b) are functions of decision variables from multiple variable sets and these variables involved in complicating constraints are called coupling variables. Each of these complicating constraints is assigned to a subproblem $m$ (as indicated by the index $m$ in (4.34b)) whose variables appear in that constraint. However, this constraint also needs to be taken into account in the other subproblems whose variables appear in that constraint. This is done by adding them as relaxed constraint to the objective function weighted by a Lagrange multiplier $\lambda_m$.

Hence, the $m$th subproblem using OCD is formulated as:

$$\begin{aligned} \min_{z_m} \quad & f(\bar{z}_1, \cdots, \bar{z}_{m-1}, z_m, \bar{z}_{m+1}, \cdots, \bar{z}_M) \\ & + \sum_{p=1, p\neq m}^{M} \bar{\lambda}_p^T h_p(\bar{z}_1, \cdots, \bar{z}_{m-1}, z_m, \bar{z}_{m+1}, \cdots, \bar{z}_M) \end{aligned} \tag{4.35}$$

$$\text{s.t.} \quad g_m(z_m) \leq 0 \tag{4.35a}$$

$$h_m(\bar{z}_1, \cdots, \bar{z}_{m-1}, z_m, \bar{z}_{m+1}, \cdots, \bar{z}_M) \leq 0 \tag{4.35b}$$

where $\bar{z}_p, \bar{\lambda}_p$ are determined by the $p$th subproblem and fixed in the $m$th subproblem. By including (4.35b) in the $m$th subproblem as a hard constraint, the corresponding Lagrangian multiplier vector $\lambda_m$ is obtained by solving the subproblem. This provides an automatic update for the multipliers in the objective function in the next iteration.

Once the subproblems have been formulated, the following iterative procedure is carried out to obtain the solution to the overall optimization problem:

**Algorithm 8** (Optimality Condition Decomposition Algorithm)**.**

1. Initialize all variables $\bar{z}_m$ and Lagrangian multipliers $\bar{\lambda}_m,\ m = 1, \ldots, M$.

2. Carry out one or multiple Newton Raphson steps on the first order optimality conditions for subproblems defined by (4.35) and (4.36).

3. Update $\bar{z}_m, \bar{\lambda}_m$ for all $M$ subproblems by the values obtained in Step 2.

4. If stopping criteria are fulfilled, stop. Else, go to Step 2.

As can be seen from Algorithm 8, necessary data communication among subproblems is required in each iteration. The influence caused by communication networks such as communication bandwidth and latency (delays) constraints on the performance of the OCD algorithm depends on the specific application. Generally speaking, the communication latency in the parallel computing setup is small and can be neglected in the development of parallel algorithms as the computation nodes (processors) are typically placed in very close proximity to each other and connected by high speed data links. In contrast, communication delays could be significant in the application area of distributed control where the distributed controllers that need to communicate with each other might be geographically scattered hundreds of miles apart. On the other hand, the total amount of data that need to be exchanged in each iteration of the OCD algorithm for both cases is identical and proportional to the number of coupling variables and complicating constraints. Communication bandwidth limits are usually not concerned in OCD given the fact that there are not many coupling variables and complicating constraints for most practical problems with decomposable structures [61, 66].

The advantages provided by OCD over the other primal/dual decomposition techniques are that: 1) no master problem is needed and all the subproblems are peer problems; 2) the update for the Lagrangian multipliers is implicitly given by each subproblem; 3) there is no need for parameter tuning; 4) the subproblems can be solved either until optimality or just one single Newton-Raphson iteration is applied to the first order optimality conditions, i.e. KKT conditions [61].

If a single Newton Raphson step is applied, an iteration of the distributed approach corresponds to calculating the update $\tilde{\Delta}$ for the variables according to

$$\tilde{\Delta} = -\tilde{J}^{-1} \cdot KKT \tag{4.36}$$

where $\tilde{J}$ is the block-diagonal Jacobian matrix of the combined first order optimality conditions over all subproblems and each block corresponds to the Jacobian matrix of the first order optimality conditions for a specific subproblem. A Newton-Raphson step applied to the overall optimization problem is thereby given by

$$\Delta = -J^{-1} \cdot KKT \tag{4.37}$$

where $J$ corresponds to the Jacobian matrix of the KKT conditions for the overall optimization problem. If the order of the associated variables and constraints is the same in $J$ and $\tilde{J}$, the difference between the two matrices is that $J$ has some off block-diagonal elements which are non-zero. Hence, computational efficiency in OCD is basically gained by being able to parallelize (4.36) due to the block diagonal structure of $\tilde{J}$.

Like any other KKT based methods, conclusions from duality theory hold for the OCD algorithm. If the OCD algorithm converges, the yielding solution is the global optimum for convex problems whereas for general non-convex problems only local optimum can be found. The convergence condition for OCD will be discussed in the next subsection.

### 4.5.3 Generalized Minimal Residual Method

The condition for the iterative procedure of the optimality condition decomposition to converge is given by

$$\rho(I - \tilde{J}_*^{-1} \cdot J_*) < 1 \tag{4.38}$$

where $\rho(A)$ is the spectral radius of matrix $A$ and $\tilde{J}_*$ and $J_*$ are the Jacobian matrices at the optimal solution. If (4.38) is not fulfilled, then, a pre-conditioned Generalized Minimal Residual (GMRES) method with $\tilde{J}$ being the pre-conditioner matrix can be used to make it converge. Derivation, explanation and pseudo codes for that method can be found, e.g. in [68, 69].

Hence, within each iteration described in Algorithm 8 an additional limited number of iterations for the GMRES method are carried out. The entering conditions of the GMRES iterations adopted in this dissertation is based on [66]. With regards to the computational aspect, the most important fact is that these iterations will require using $\tilde{J}^{-1}$. However, given that the Newton-Raphson step in Algorithm 8 corresponds to (4.36), the resulting LU factorization determined to solve (4.36) can be stored and reused in the GMRES steps. This tremendously speeds up the computation process of each GMRES step.

### 4.5.4 Globally Convergent Modifications

To ensure global convergence of the algorithm, certain modifications have to be made to the Newton-Raphson based decomposition solution approach as the Newton-Raphson method is only proved to be locally q-quadratically convergent [70]. Two classical approaches, namely the trust region approach and the line search approach, are discussed in this subsection in terms of their compatibility with the decomposition scheme. In either of the two approaches, a merit function $\psi(\cdot)$ is constructed in order to measure the progress contributed by the current move. Such a function for the considered problem can be defined as

$$\psi(y) = \frac{1}{2} KKT^T(y) \cdot KKT(y) \tag{4.39}$$

where $y$ is the vector of all variables including decision variables, Lagrangian multipliers and slack variables. A good step results in a sufficient decrease in the merit function value.

**Trust Region Approach**

The trust region approach models the merit function as a quadratic function with respect to the search step within a small region around the current point. The goal is to find the best search step within that region where the approximate model is considered trustworthy. The resulting optimization problem is given by [70]

$$\min_{p} \quad \psi(y_c) + (J^T KKT)^T p + \frac{1}{2} p^T (J^T J) p \tag{4.40}$$

$$\text{s.t.} \quad \|p\|_2 \leq \delta_c \tag{4.41}$$

where $y_c$ is the current point and $p$ is the search step. $J$ is the same Jacobian of the overall problem as in (4.37). $\delta_c$ defines the trust region size which is updated at every iteration. Due to the term $J^T J$ in (4.40) which mixes all the information of subproblems, the trust region approach is not compatible with the decomposition scheme.

**Line Search Approach**

Another classical approach to attempt global convergence is the line search approach. The basic idea is to backtrack along the search direction generated by the Newton-Raphson iteration until an acceptable reduction in (4.39) is achieved. Quadratic or cubic models are used to approximate the merit function (4.39) based on merit function values evaluated at several points. For the detailed derivation and description of the line search algorithm, readers are referred to [71]. Unlike the trust region approach, only merit function evaluations that can be done distributedly are required in the line search method, implying that the line search can be implemented in a distributed manner with limited coordination among subproblems. Therefore, the line search approach is adopted to gain global convergence of the OCD based decomposition framework described in this section.

### 4.5.5 Application of OCD in SMPC based SCED Problem

We use OCD to achieve a scenario-based decomposition for the considered SMPC based SCED problem. We take advantage of the fact that if the nonanticipativity constraints (4.4j)–(4.4l) are neglected, the problem becomes decomposable into subproblems where each subproblem corresponds to a specific scenario for the disturbances, i.e. variable generation and load. Consequently, (4.4j)–(4.4l) are the coupling constraints in this scenario-based decomposition. Each coupling constraint is assigned to a specific subproblem to be taken into account as hard constraint and as soft constraint in the objective function in the subproblem whose variables are part of that particular coupling constraint. The decision variables in a subproblem are all the variables for the scenario associated with that subproblem.

The subproblem $SP_s$ for scenarios $s \in \{2, \ldots, N\}$ is therefore given by

$$\min_{\Delta P_G^s, P_{Si}^s, P_{So}^s} \pi^s \Bigg[ \sum_{k \in \mathcal{T}} \sum_{i \in \Omega_G} C_{G_i} \left( P_{G_i}^s(k), \Delta P_{G_i}^s(k) \right) + \sum_{k \in \mathcal{T}} \sum_{i \in \Omega_S} C_{S_i} \left( P_{Si_i}^s(k), P_{So_i}^s(k) \right) + \sum_{i \in \Omega_G} C_{G_i} \left( P_{G_i}^s(K) \right) \Bigg] \tag{4.42}$$

$$s.t. \quad (4.4a) - (4.4i)$$

$$\Delta \bar{P}_{G_i}^1(0) = \Delta P_{G_i}^s(0), \quad \forall i \in \Omega_G \tag{4.43a}$$

$$\bar{P}_{Si_i}^1(0) = P_{Si_i}^s(0), \quad \forall i \in \Omega_S \tag{4.43b}$$

$$\bar{P}_{So_i}^1(0) = P_{So_i}^s(0), \quad \forall i \in \Omega_S \tag{4.43c}$$

whereas for scenario $s = 1$, the hard constraints (4.43a)–(4.43c) are omitted but additional soft constraints are added in the objective function. The bar over a variable indicates that this is a fixed value given from another subproblem at a previous iteration. The formulation of the subproblem corresponding to $s = 1$ is given by

$$\begin{aligned}
\min_{\Delta P_G^1, P_{Si}^1, P_{So}^1} \quad & \pi^1 \Bigg[ \sum_{k \in \mathcal{T}} \sum_{i \in \Omega_G} C_{G_i} \left( P_{G_i}^1(k), \Delta P_{G_i}^1(k) \right) \\
& + \sum_{k \in \mathcal{T}} \sum_{i \in \Omega_S} C_{S_i} \left( P_{Si_i}^1(k), P_{So_i}^1(k) \right) + \sum_{i \in \Omega_G} C_{G_i} \left( P_{G_i}^1(K) \right) \Bigg] \\
& + \sum_{s=2}^{N} \left( \sum_{i \in \Omega_G} \bar{\lambda}_{G,i}^s \cdot \Delta P_{G_i}^1(0) + \sum_{i \in \Omega_S} \bar{\lambda}_{Si,i}^s \cdot P_{Si_i}^1(0) + \sum_{i \in \Omega_S} \bar{\lambda}_{So,i}^s \cdot P_{So_i}^1(0) \right) \\
& - \sum_{s=2}^{N} \left( \sum_{i \in \Omega_G} \bar{\lambda}_{G,i}^s \cdot \Delta \bar{P}_{G_i}^s(0) + \sum_{i \in \Omega_S} \bar{\lambda}_{Si,i}^s \cdot \bar{P}_{Si_i}^s(0) + \sum_{i \in \Omega_S} \bar{\lambda}_{So,i}^s \cdot \bar{P}_{So_i}^s(0) \right) \quad (4.44)
\end{aligned}$$

$$s.t. (4.4a) - (4.4i)$$

It is noted that $\Delta \bar{P}_{G_i}^s(0), \bar{P}_{Si_i}^s(0), \bar{P}_{So_i}^s(0)$ are actually not needed as they form a term that is constant in the objective function of (4.44).

The flow chart of the iterative update for the considered SMPC problem using OCD is depicted in Fig. 4.3. As indicated in Fig. 4.3, NR-steps are carried out first and then based on an entering condition for the GMRES algorithm additional GMRES steps are carried out which requires information exchange among the relevant subproblems of different scenarios due to the coupling imposed by the nonanticipativity constraints. In addition, line search with limited information exchange is conducted for each subproblem based on the search direction obtained by the NR-step together with necessary GMRES iterations. The foregoing iterative procedure continues until final convergence or maximum number of iterations is reached. A major iteration includes steps from “NR-step” to “Update variables”.

## 4.6 OCD based Two-Stage Decomposition

With the hope of further improving the computational efficiency for the SMPC based SCED problem, we propose an OCD based two-stage decomposition approach. The conceptual sketch of the two-stage decomposition is depicted in Fig. 4.4. The first stage corresponds

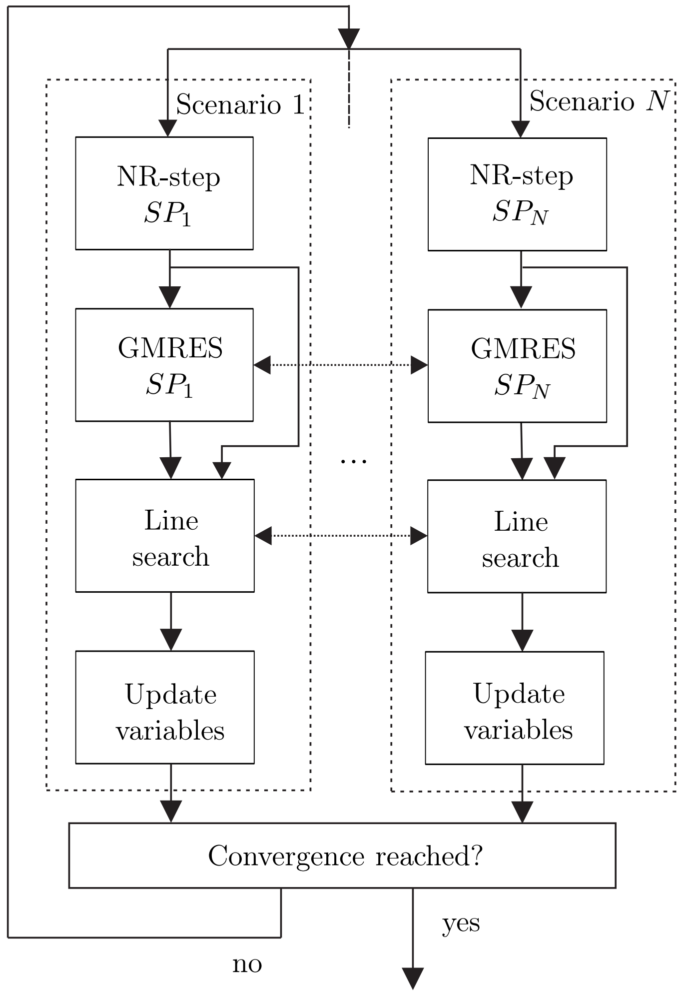


Figure 4.3: Flow chart of the iterative update using OCD.

to the scenario-based decomposition in the previous section. Each of the resulting subproblems ($SP_s$) of that stage is further decomposed into even smaller subsubproblems ($SSP_{s,Q_s}$) corresponding to subsets of time steps in the optimization horizon for the second stage decomposition. The coupling of these subsubproblems in the second stage is present due to the inter-temporal energy storage equations and the limited ramp rates of dispatchable generation resources. Hence, the second stage decomposition is termed as temporal-based decomposition. Figure 4.5 provides a more detailed visualization of how we propose to decompose the overall optimization problem into subproblems and indicates the resulting coupling constraints between the subproblems.

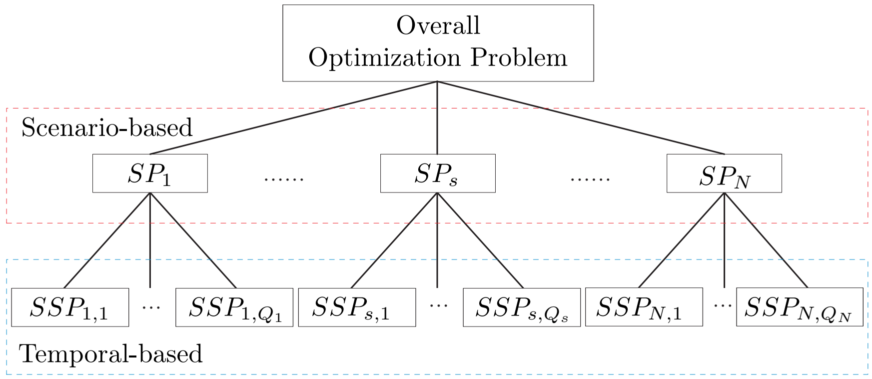


Figure 4.4: Conceptual sketch of the two-stage decomposition.

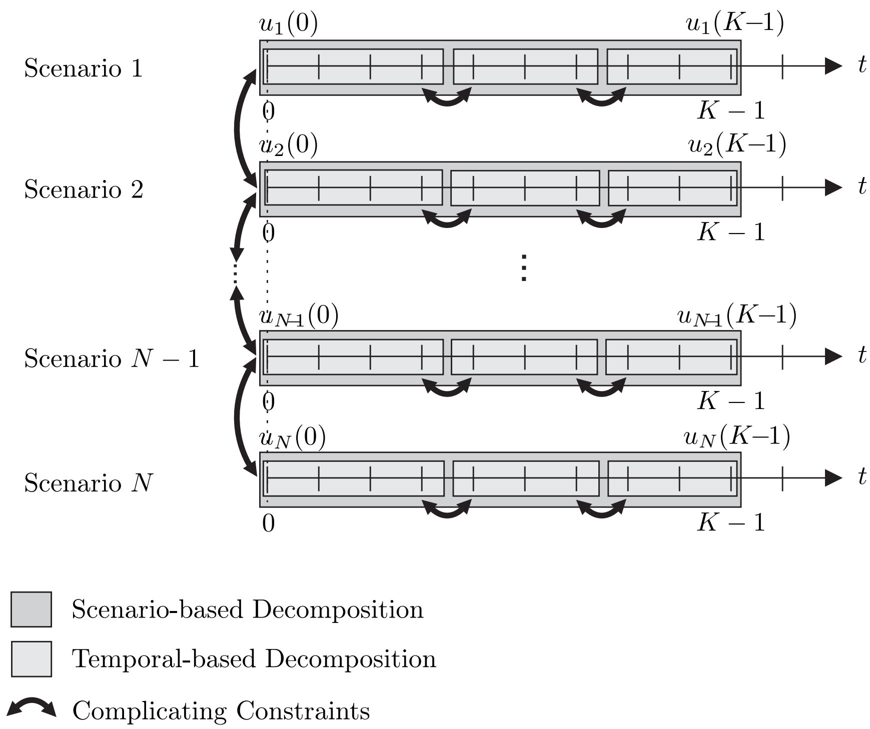


Figure 4.5: Two-stage decomposition: a detailed view.

As visualized in Fig. 4.5, a subsubproblem $s, q$ for scenario $s$ corresponds to the optimization of specific time steps within the optimization horizon. The number of time steps included in each subsubproblem may range from just one to all $K + 1$ steps (in the latter the subsubproblem $s, q$ is the same as subproblem $s$).

### 4.6.1 Temporal-based Decomposition

We again use the OCD algorithm to achieve the temporal-based decomposition. The complicating constraints in this stage of decomposition correspond to the inter-temporal constraints for the energy level (4.4a) and the generation outputs (4.4b). Depending on the choice of whether to assign the complicating constraints to the lower indexed subsubproblem or the higher indexed one, two different subsubproblem formulations are conceivable for the temporal-based decomposition.

#### Subsubproblem Formulation A

Formulation A corresponds to the choice of assigning the inter-temporal complicating constraints to the lower indexed subsubproblems. Subsubproblem $SSP_{s,q}$ for $q \in \{2, \ldots, Q_s - 1\}$ where $Q_s$ is the number of subsubproblems in scenario $s \in \mathcal{N}$ is therefore given by

$$\begin{aligned}
\min \quad & \pi^s \left[ \sum_{k \in \mathcal{T}_{s,q}} \sum_{i \in \Omega_G} C_{G_i} \left( P^s_{G_i}(k), \Delta P^s_{G_i}(k) \right) + \sum_{k \in \mathcal{T}_{s,q}} \sum_{i \in \Omega_S} C_{S_i} \left( P^s_{Si_i}(k), \Delta P^s_{So_i}(k) \right) \right] \\
& + \sum_{i \in \Omega_G} \overline{\nu}^{s,q-1}_{G,i} \left( P^s_{G_i}(k^q_1) - \overline{P}^s_{G_i}(k^{q-1}_F) - \Delta \overline{P}^s_{G_i}(k^{q-1}_F) \right) \\
& + \sum_{i \in \Omega_S} \overline{\nu}^{s,q-1}_{S,i} \left( E^s_{S_i}(k^q_1) - \eta_i \overline{E}^s_{S_i}(k^{q-1}_F) - \alpha_i T \overline{P}^s_{Si_i}(k^{q-1}_F) + \frac{1}{\alpha_i} T \overline{P}^s_{So_i}(k^{q-1}_F) \right)
\end{aligned} \tag{4.45}$$

$$\text{s.t.} \quad \overline{P}^s_{G_i}(k^{q+1}_1) = P^s_{G_i}(k^q_F) + \Delta P^s_{G_i}(k^q_F), \ \forall i \in \Omega_G \tag{4.46a}$$

$$\overline{E}^s_{S_i}(k^{q+1}_1) = \eta_i E^s_{S_i}(k^q_F) + \alpha_i T P^s_{Si_i}(k^q_F) - \frac{1}{\alpha_i} T P^s_{So_i}(k^q_F), \ \forall i \in \Omega_S \tag{4.46b}$$

$$\forall k \in \mathcal{T}_{s,q} : (4.4c) - (4.4i)$$

$$\forall k = [k^q_1, \ldots, k^q_F - 1] : (4.4a) - (4.4b)$$

where $\mathcal{T}_{s,q} = \{k^q_1, \ldots, k^q_F\}$ is a subset of $\mathcal{T} \cup \{K\}$ with the time steps included in subsubproblem $SSP_{s,q}$, i.e. the combination of $\mathcal{T}_{s,q}, q \in \{1, \ldots, Q_s\}$ is equal to $\mathcal{T} \cup \{K\}$. For subsubproblem $SSP_{s,Q_s}$, no hard constraints (4.46a) and (4.46b) for any complicating constraints are included and for $SSP_{s,1}$ no relaxed constraints for the complicating constraints are added in the objective function (4.45) but temporal-based complicating constraints appear only as hard constraints in the constraint set; as opposed to the other subsubproblems, subsubproblems $SSP_{s,1}$ include time step $k = 0$ which means that nonanticipativity constraints become part of these subsubproblems. As described in Section 4.5.5, these complicating constraints appear in the objective function as well as in the constraint set or just as relaxed constraints in the objective function or only as hard constraints in the constraint set.

**Subsubproblem Formulation B**

Formulation B corresponds to the choice of assigning the inter-temporal complicating constraints to the higher indexed subsubproblems. Using the same notations in Formulation A, subsubproblem $SSP_{s,q}$ for $q \in \{2, \ldots, Q_s - 1\}$ and $s \in \mathcal{N}$ is given by

$$\begin{aligned}\min \quad & \pi^s \left[ \sum_{k \in \mathcal{T}_{s,q}} \sum_{i \in \Omega_G} C_{G_i} \left( P^s_{G_i}(k), \Delta P^s_{G_i}(k) \right) + \sum_{k \in \mathcal{T}_{s,q}} \sum_{i \in \Omega_S} C_{S_i} \left( P^s_{Si_i}(k), \Delta P^s_{So_i}(k) \right) \right] \\ & + \sum_{i \in \Omega_G} \overline{\nu}^{s,q+1}_{G,i} \left( \overline{P}^s_{G_i}(k_1^{q+1}) - P^s_{G_i}(k_F^q) - \Delta P^s_{G_i}(k_F^q) \right) \\ & + \sum_{i \in \Omega_S} \overline{\nu}^{s,q+1}_{S,i} \left( \overline{E}^s_{S_i}(k_1^{q+1}) - \eta_i E^s_{S_i}(k_F^q) - \alpha_i T P^s_{Si_i}(k_F^q) + \frac{1}{\alpha_i} T P^s_{So_i}(k_F^q) \right) \end{aligned} \tag{4.47}$$

$$s.t. \quad P^s_{G_i}(k_1^q) = \overline{P}^s_{G_i}(k_F^{q-1}) + \Delta \overline{P}^s_{G_i}(k_F^{q-1}), \ \forall i \in \Omega_G \tag{4.48a}$$

$$E^s_{S_i}(k_1^q) = \eta_i \overline{E}^s_{S_i}(k_F^{q-1}) + \alpha_i T \overline{P}^s_{Si_i}(k_F^{q-1}) - \frac{1}{\alpha_i} T \overline{P}^s_{So_i}(k_F^{q-1}), \quad \forall i \in \Omega_S \tag{4.48b}$$

$$\forall k \in \mathcal{T}_{s,q} : (4.4c) - (4.4i)$$

$$\forall k = [k_1^q, \ldots, k_F^q - 1] : (4.4a) - (4.4b)$$

For subsubproblem $SSP_{s,1}$, no hard constraints (4.48a) and (4.48b) are included but the relaxed inter-temporal complicating constraints appear in the objective function (4.47). For subsubproblem $SSP_{s,Q_s}$, no relaxed constraints for the complicating constraints are added in the objective function whereas the corresponding inter-temporal complicating constraints appear as hard constraints in the constraint set. Regarding the subsubproblems including time step $k = 0$, the same modification rule as in Formulation A is applied.

By carefully examining the two subsubproblem formulations, it is simple to infer that Formulation A is to outperform Formulation B in terms of convergence speed. The reason is that fewer variables are fixed in the constraints of subsubproblems in Formulation A compared to the situation in Formulation B. In other words, the coupling strength among subsubproblems in Formulation A is less than the coupling strength in Formulation B. Hence, we will adopt Formulation A for the subsubproblem formulations in the proposed two-stage decomposition.

The flow chart of the iterative update for the two-stage decomposition scheme for the considered SMPC problem is shown in Fig. 4.6, which is similar to the case of OCD based scenario decomposition in the previous section. The major difference is that there are now multiple parallel processes for each scenario compared to Fig. 4.3 where there is just one process for one scenario. With more parallel processes in the two-stage decomposition, the hope is to reduce the computation time for solving the overall problem by being able to use more computational resources simultaneously.

### 4.6.2 Singularity Issues

There exist situations where the resulting Jacobian matrices are singular at the optimal solution for both the scenario- and temporal-based decompositions. This needs to be resolved in order to ensure convergence of the algorithm.

#### Scenario-based Decomposition

The Jacobian matrices for the scenario-based decomposition become singular when any of the variables in the nonanticipativity constraints (4.4j)–(4.4l) hit either the lower or upper limits at the optimal solution, leading to the situation where the number of binding constraints is greater than the number of variables. An easy fix is to remove constraints (4.4c)–(4.4i) corresponding to $k = 0$ for all the subproblems $s \in \mathcal{N} \backslash \{N\}$.

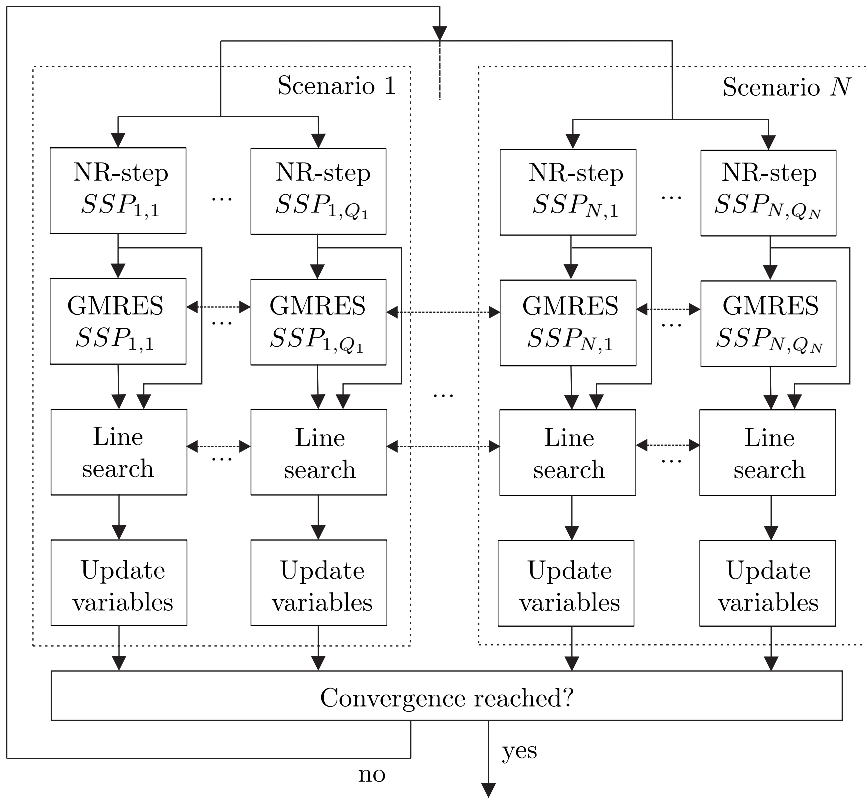


Figure 4.6: Flow chart of the iterative update using two-stage OCD.

### Temporal-based Decomposition with Formulation A

The Jacobian matrices in this case become singular as long as $\exists\ i \in \Omega_G : P^s_{G_i}(k^q_F), \Delta P^s_{G_i}(k^q_F)$ are both at their limits or/and $\exists\ i \in \Omega_S : E^s_{S_i}(k^q_F), P^s_{Si_i}(k^q_F), P^s_{So_i}(k^q_F)$ all hit their bounds at the optimal solution. The rationale behind this is again the fact that the Jacobian becomes singular when the number of variables is less than the number of binding constraints.

### Temporal-based Decomposition with Formulation B

Via the same reasoning, the Jacobian matrices in this case become singular when $\exists\ i \in \Omega_G : P^s_{G_i}(k^q_1)$ is at its limit or/and $\exists\ i \in \Omega_S : E^s_{S_i}(k^q_1)$ hits the bound at the optimal solution.

### Solution for Temporal-based Decomposition

Due to the difficulty in predicting whether or not any of the aforementioned conditions are fulfilled without knowing the optimal solution, special measures have to be taken to overcome the singular issue for temporal-based decomposition. The solution is as follows. Assume that the Jacobian $\tilde{J}_{s,q}$ associated with subsubproblem $SSP_{s,q}$ is singular at iteration step $j$. We first do the LU factorization for $\tilde{J}_{s,q}$, which is given by

$$P_{s,q} \cdot \tilde{J}_{s,q} \cdot Q_{s,q} = L_{s,q} \cdot U_{s,q} \tag{4.49}$$

where $P_{s,q}, Q_{s,q}$ are permutation matrices; $L_{s,q}$ is a unit lower triangular matrix; $U_{s,q}$ is an upper triangular matrix. By inspecting the absolute values of the diagonal elements in $U_{s,q}$, singular $\tilde{J}_{s,q}$ is easily detected. Then we generate a nonsingular matrix $\bar{J}_{s,q}$ to replace $\tilde{J}_{s,q}$ by perturbing $U_{s,q}$ as

$$P_{s,q} \cdot \bar{J}_{s,q} \cdot Q_{s,q} = L_{s,q} \cdot (U_{s,q} + \tau I) \tag{4.50}$$

where $I$ is the identity matrix and $\tau$ is a small number such that $\bar{J}_{s,q}$ is nonsingular. According to our experience, the default value for $\tau$ is set to be $10^{-5}$. $\bar{J}_{s,q}$ also plays the role of preconditioner for the corresponding GMRES iterations. In some cases, the singularity issues can be completely removed for certain subsubproblems by perturbing the way of dividing the time blocks in the look-ahead horizon, i.e. by perturbing the $k_1^q$ or $k_F^q$ of the relevant subsubproblems.

## 4.7 Improved Two-Stage Decomposition

There exists one disadvantage in the OCD method, which lies in the involved GMRES steps. The computational complexity in terms of each GMRES step in OCD is of positive correlation with the size of the overall problem before decomposition. In addition, the number of GMRES steps required in each major iteration grows with the increase of the number of subproblems under OCD. Therefore, we propose a mixed two-stage decomposition for the considered SMPC problem, consisting of a Benders decomposition for the first-stage scenario-based decomposition and an optimality condition decomposition for the second-stage temporal-based decomposition. We term this mixed two-stage decomposition scheme simply as mixed decomposition (MD). The improvement gained from the proposed MD compared to the two-stage OCD approach in Section 4.6 is that the computational complexity associated with the GMRES steps in OCD is now limited by limiting the size of the problem for which we apply OCD. Each optimization problem in which OCD is applied under MD is an MPC problem corresponding to each scenario. In other words, we only apply OCD to each independent subproblem decomposed by BD. The proposed mixed decomposition scheme should work very well especially when the number of iterations for the BD loop is relatively small so that the bottleneck effect of the BD algorithm mentioned in the beginning of Section 4.5 can be neglected.

In terms of the subsubproblem formulations, subsubproblems $SSP_{s,q}$ for $q \in \{2, \ldots, Q_s\}$ and $s \in \mathcal{N}$ under MD for the considered SMPC based SCED problem are identical to those in the OCD based two-stage decomposition given by (4.45)-(4.46). In contrast, subsubproblems $SSP_{s,1}$ for $s \in \mathcal{N}$ in MD and two-stage OCD are different due to the different formulations in the scenario-based decomposition between BD and OCD. The subsubproblem $SSP_{s,1}$ for $s \in \mathcal{N}$ in MD is given by

$$\min \quad \pi^s \left[ \sum_{k \in \tilde{\mathcal{T}}_{s,1}} \left( \sum_{i \in \Omega_G} C_{G_i} \left( P^s_{G_i}(k), \Delta P^s_{G_i}(k) \right) + \sum_{i \in \Omega_S} C_{S_i} \left( P^s_{Si_i}(k), \Delta P^s_{So_i}(k) \right) \right) \right] \quad (4.51)$$

$$
\begin{aligned}
s.t. \quad \overline{P}^{s}_{G_i}(k^2_1) =& P^{s}_{G_i}(k^1_F) + \Delta P^{s}_{G_i}(k^1_F), \ \forall i \in \Omega_G && \text{(4.52a)}\\
\overline{E}^{s}_{S_i}(k^2_1) =& \eta_i E^{s}_{S_i}(k^1_F) + \alpha_i T P^{s}_{Si_i}(k^1_F) - \frac{1}{\alpha_i} T P^{s}_{So_i}(k^1_F), \ \forall i \in \Omega_S && \text{(4.52b)}\\
\Delta P_{G_i}(0) =& \Delta \overline{P}^{(j)}_{G_i}(0), \quad \forall i \in \Omega_G && \text{(4.52c)}\\
P_{Si_i}(0) =& \overline{P}^{(j)}_{Si_i}(0), \quad \forall i \in \Omega_S && \text{(4.52d)}\\
P_{So_i}(0) =& \overline{P}^{(j)}_{So_i}(0), \quad \forall i \in \Omega_S && \text{(4.52e)}\\
& \forall k \in \tilde{\mathcal{T}}_{s,1} : (4.4c) - (4.4i)\\
& \forall k = [k^1_1, \ldots, k^1_F - 1] : (4.4a) - (4.4b)
\end{aligned}
$$

where $\tilde{\mathcal{T}}_{s,1} = \mathcal{T}_{s,1} \backslash \{0\}$ and subscript $j$ is the current iteration for the BD loop.

On the other hand, the master problem for the first-stage BD is exactly the same as the problem in (4.16)-(4.17). The flow chart of the iterative update for the improved two-stage decomposition scheme for the considered SMPC problem is given in Fig. 4.7. As can be seen from Fig. 4.7, the number of parallel processes is the same as that number in the OCD based two-stage decomposition given the same partitioning of the time horizon. However, the information exchange associated with both the GMRES steps and the line search steps is now restricted within each scenario, greatly reducing the computational burden on calculating the correction in search direction of each iteration. The only drawback of MD is the existence of a master problem whose size increases with the progress of the iteration process. Under the condition where there are only few iterations in the BD loop, the proposed MD scheme has a clear advantage over the two-stage OCD in terms of computational efficiency.

## 4.8 Case Studies

In this section, the WECC 9-bus test system in Fig. 3.3 and the IEEE New England 39-bus test system in Fig. 3.10 are used to investigate the performance of the three proposed decomposition schemes – the OCD based scenario decomposition (Section 4.5), the OCD based two-stage decomposition (Section 4.6) and the mixed decomposition (Section 4.7) for

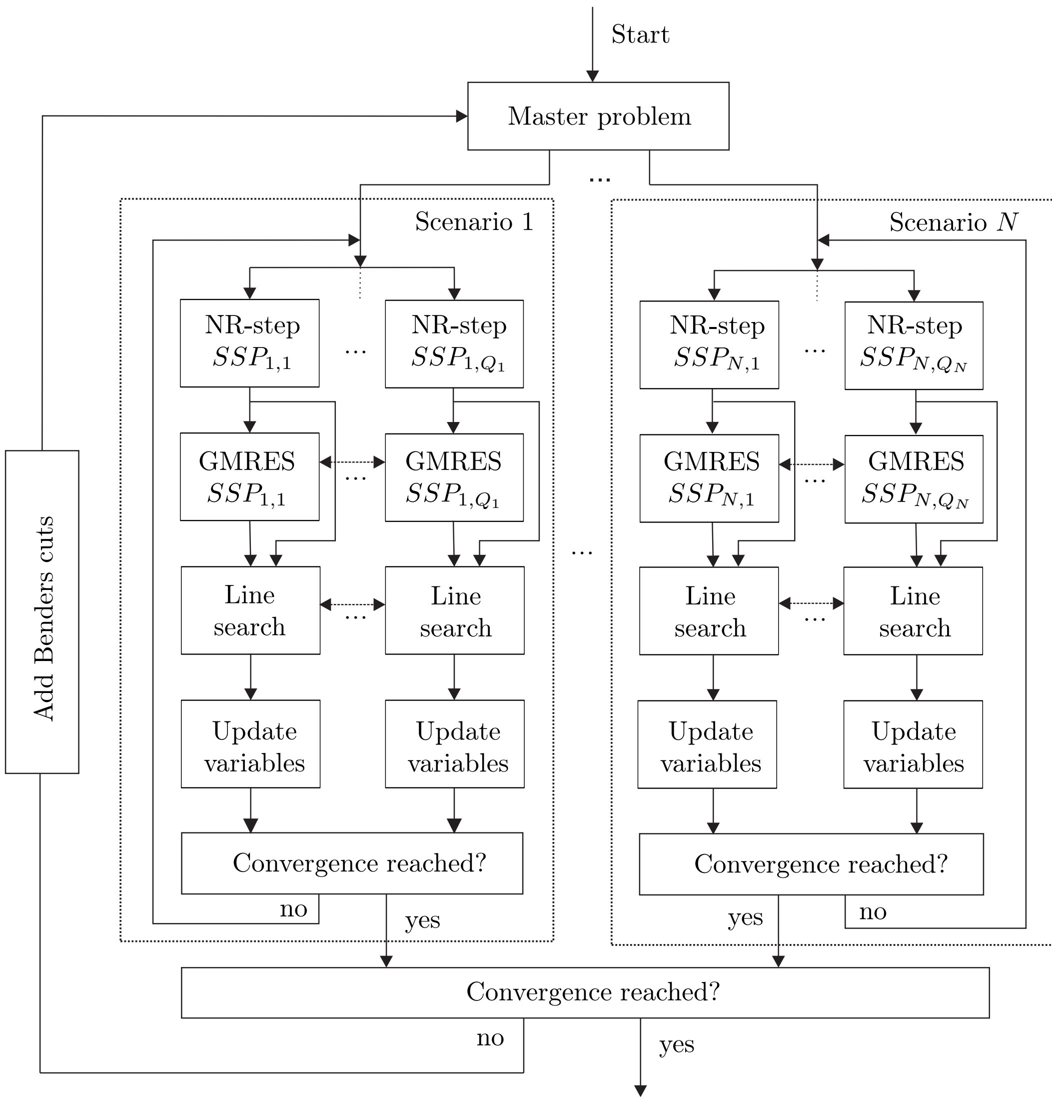


Figure 4.7: Flow chart of the iterative update using MD.

the SMPC based SCED problem in the stochastic optimal dispatch level in terms of speed and convergence. In addition, Benders decomposition as a classical solution method for two-stage stochastic optimization problems is compared with the three proposed methods in the simulation. The reason why we only pick Benders decomposition rather than the other classical solution methods is because the work in [61, 72] suggested that both OCD and BD tend to have much better convergence performance than both the Lagrangian relaxation decomposition and the augmented Lagrangian decomposition. However, the comparison between OCD and BD in terms of convergence performance is yet unclear.

The problem we focus on in the simulation is a single two-stage SMPC problem with the overall problem formulation given by (4.3)-(4.4) to investigate the convergence performance of various decomposition methods. All the test cases are implemented in Matlab R2013a and run on a personal computer with a 2.80GHz CPU and a 16GB RAM.

### 4.8.1 WECC 9-Bus System

The basic system setup is stated in Section 3.8.1. The parameters of the energy storage device are modified to reflect the fact that the storage application in the stochastic optimal dispatch level is a high energy application. The capacity of the storage device is set to 100 MWh (1 p.u.h) and the maximum input/output power is symmetric and set to 100 MW (1 p.u.). The standby loss coefficient $\eta$ is 99% and the round trip efficiency $\alpha^2$ is 81%. The storage device is also assumed to be required to operate within the range of 0.1% to 100% in terms of state-of-charge (SOC). No ramp rate limits are imposed on the storage device as the associated power electronic inverter can typically respond to power requests almost instantaneously. In addition, parameters for conventional generators including minimum/maximum power output and ramp rate limits are given in the Appendix A. The flow limits for all the transmission lines are set to 2.5 p.u.

Due to the emphasis on testing the feasibility and efficiency of the three proposed approaches to solve the SMPC problem, fifty scenarios corresponding to fifty realizations of the wind power generation for a look-ahead horizon of 4 hours (48 time steps with 5-min interval) are generated by randomly perturbing a 4-hour time series of historical wind power data within a reasonable error bound. For the same reason, the probability of each scenario in the simulation is assumed to be identical, i.e. 0.02 for each scenario. The load profile is assumed to be deterministic over the horizon for simplicity purpose. The yielding two-stage SMPC problem is considerable in size including $21,600$ decision variables, $12,196$ equality constraints and $84,636$ inequality constraints.

The following five test cases are considered in the simulation. In the first case which serves as the benchmark, the overall SMPC problem is directly solved by using the Newton-Raphson method. The first case is therefore termed as BF, i.e. brute force method. The subproblems in Case BD are also solved using the Newton-Raphson method. Each scenario in the two-stage OCD case is identically decomposed into three time blocks while each scenario in the mixed decomposition case is identically decomposed into six time blocks. For example, the time blocks within each scenario in the two-stage OCD start with time steps $k = 0, 16, 32$, respectively. The forgoing specific numbers of time blocks actually correspond to the best trade-off between convergence speed and the size of subsubproblems for cases where the temporal-based decomposition is implemented, which will be numerically investigated in the following. The equally divided time blocks ensure a load balance among all subsubproblems with respect to computational burdens. In summary, there are 150 subsubproblems for the two-stage OCD case whereas the mixed decomposition case has 300 subsubproblems. There are 50 subproblems in all scenario-based decomposition cases.

- Case “BF”: The overall SMPC problem is directly solved w/o line search.
- Case “BD”: Benders decomposition is applied.
- Case “OCD”: The OCD based scenario decomposition w/ line search is applied.
- Case “2OCD”: The OCD based two-stage decomposition w/ line search is applied.
- Case “MD”: The mixed decomposition is applied.

### Main Results

Table 4.1 shows the numerical results including the number of iterations, wall-clock time (actual time difference measured from the start of a computer program until the end), and estimated running time in a parallel computing environment using the five different methods. “-” means not applicable. The wall-clock time in Table 4.1 is the actual time observed for each case to run in the sequential computing environment. The estimated time in a parallel computing environment is calculated by dividing the corresponding wall-clock time by the number of subproblems (subsubproblems). The assumption here is that the overhead of communication either between subproblems or between subproblems and the master problem is relatively small in terms of the amount of actual computing jobs and that the master problem in BD is much easier to solve than subproblems. As with numbers of iterations, each major iteration refers to the outmost iteration loop and each minor iteration in the BD based methods corresponds to the inner loop for iteratively solving each of the scenario-based subproblems.

Table 4.1: Numerical results for the WECC 9-bus system

| Cases | Total # of Major Iter. | Total # of Minor Iter. | Total # of GMRES Iter. | Wall Time in sec. | Est. Time in sec. for Par. Computing |
|---|---|---|---|---|---|
| BF | 84 | - | - | 62.52 | 62.52 |
| BD | 4 | $8,637$ | - | 185.14 | 3.70 |
| OCD | 79 | - | 342 | 69.55 | 1.39 |
| 2OCD | 78 | - | $5,813$ | 664.48 | 4.43 |
| MD | 4 | $11,587$ | $72,661$ | 375.07 | 1.25 |

In terms of the estimated time for the parallel implementation, the proposed MD performs best with about 50 times faster than the base case without any decomposition. The second best method is the proposed OCD based scenario decomposition with speedup of about 45 times. In addition, MD is almost 3 times faster compared to the classical BD method. The reason why the two-stage OCD does not perform well with respect to the scenario-based OCD is because way too many GMRES steps are required in the two-stage OCD.

In order to verify the accuracy of the decomposed solutions, the evolution of the objective function values under the direct solution method (Case BF) and the four decomposition solution methods is shown in Fig. 4.8. The final objective function values for the four decomposition cases are exactly the same as the final objective function value obtained from the direct method. The reason for this converging behavior of the decomposed methods is because the considered problem defined by (4.3)-(4.4) is a convex optimization problem.

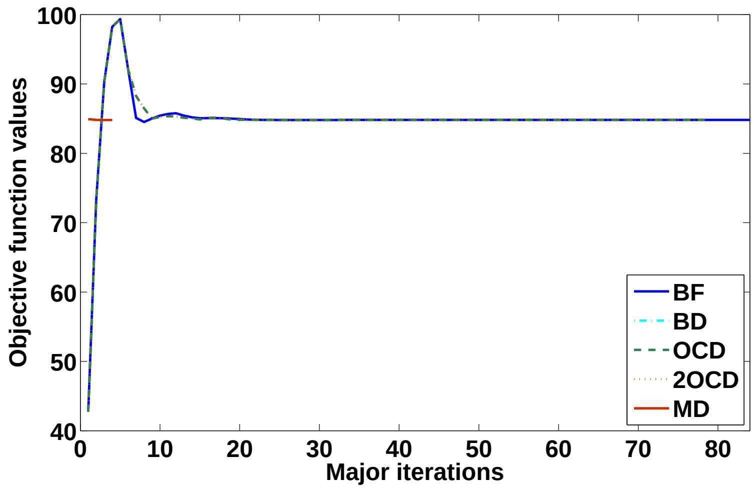


Figure 4.8: Evolution of objective function values for the WECC 9-bus system.

### Trade-Off between Convergence Speed and Subsubproblem Size

For cases where the temporal-based decomposition is implemented, a trade-off between convergence speed and subsubproblem size needs to be achieved. Table 4.2 lists the convergence results for the two-stage OCD method with numbers of time blocks of each scenario ranging from 2 to 6. The more the number of time blocks is, the smaller the size of subsubproblems becomes. As can be seen from Table 4.2, the optimal number of time blocks within each scenario for the two-stage OCD is three.

Table 4.2: Results for the two-stage OCD with different numbers of time blocks

| Number of Time Blocks | Total # of Major Iter. | Total # of GMRES Iter. | Wall Time in sec. | Est. Time in sec. for Par. Computing |
|---|---|---|---|---|
| 2 | 92 | 5,000 | 453.44 | 4.53 |
| 3 | 78 | 5,813 | 664.48 | 4.43 |
| 4 | 84 | 8,544 | 1,165.20 | 5.83 |
| 6 | 77 | 11,423 | 2,496.20 | 8.32 |

Similarly, Table 4.3 shows the numerical results using MD with different numbers of time blocks in each scenario ranging from 2 to 8. As indicated in Table 4.3, the optimal number of time blocks within each scenario for MD is six.

Table 4.3: Results for MD with different numbers of time blocks

| Number of Time Blocks | Total # of Major Iter. | Total # of Minor Iter. | Total # of GMRES Iter. | Wall Time in sec. | Est. Time in sec. for Par. Computing |
|---|---|---|---|---|---|
| 2 | 4 | 8,754 | 37,174 | 228.33 | 2.28 |
| 3 | 4 | 8,709 | 45,147 | 260.11 | 1.73 |
| 4 | 4 | 10,268 | 59,922 | 295.76 | 1.48 |
| 6 | 4 | 11,587 | 72,661 | 375.07 | 1.25 |
| 8 | 4 | 18,003 | 155,814 | 731.70 | 1.83 |

**Importance of GMRES in OCD based Methods**

Fig. 4.9 shows the evolution of the preconditioned residual norm before and after GMRES steps, implying the important role of the GMRES in the OCD based approaches (Case OCD and Case 2OCD). The preconditioned residual norm before GMRES steps in each major iteration is defined as $\|\tilde{J}^{-1}(J \cdot \tilde{\Delta} + KKT)\|_2$. A refined search step $\bar{\Delta}$ via GMRES steps replaces the step $\tilde{\Delta}$ in calculating the post-GMRES preconditioned residual norm. It can be seen from Fig. 4.9 that the pre-GMRES preconditioned residual norm in Case 2OCD is larger than that in Case OCD. Therefore, the two-stage OCD is more difficult to converge and requires more GMRES iterations, which is consistent with the result in Table 4.1.

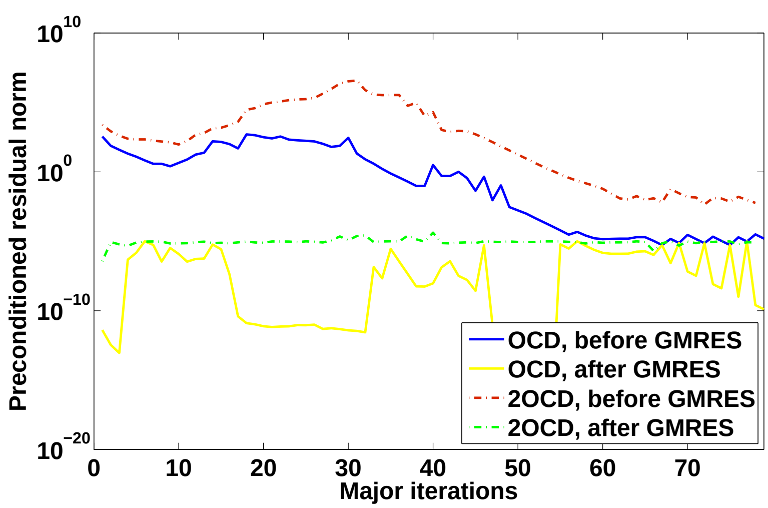


Figure 4.9: Evolution of the preconditioned residual norm before and after GMRES steps for OCD based methods.

### Importance of Line Search in OCD based Methods

The importance of line search in the OCD based methods is evaluated in terms of the evolution of the KKT norm (see Fig. 4.10). By examining the curves of the two pairs of with and without line search for the two OCD based cases (Case OCD and Case 2OCD), it is clear that the KKT norm increases rapidly for the cases without line search implementation as the iteration process goes, which in turn demonstrates that line search is one of the most critical measures for ensuring the convergence of the proposed OCD based methods. However, it can also be observed from Fig. 4.10 that the base case without line search still manages to converge. One possible explanation is that the search direction is always exact in the base case compared to the situation of the decomposition cases where only approximated search directions are available.

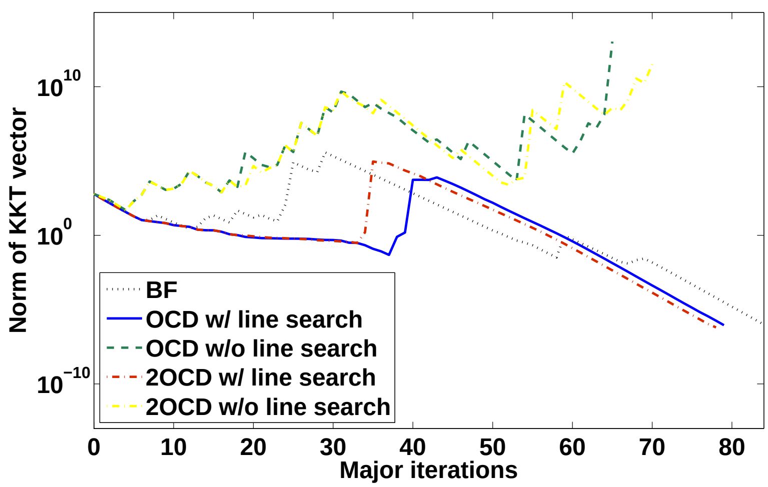


Figure 4.10: Evolution of the KKT norm for OCD based methods.

### Scaling Performance in terms of Number of Scenarios

The scaling performance of the top two proposed decomposition approaches (OCD and MD) is evaluated by measuring the wall-clock time with respect to the change in the number of scenarios in the stochastic SCED problem. The problems with reduced numbers of scenarios are obtained by using Algorithm 2 described in Section 4.3. The number of scenarios in OCD is equal to the number of parallelizable subproblems whereas the number of subsubproblems in MD is six times more than the number of scenarios. Fig. 4.11 shows the wall-clock time as a function of the number of scenarios using OCD and MD. Both the two approaches exhibit a near linear scaling property, which is desired in parallel computing.

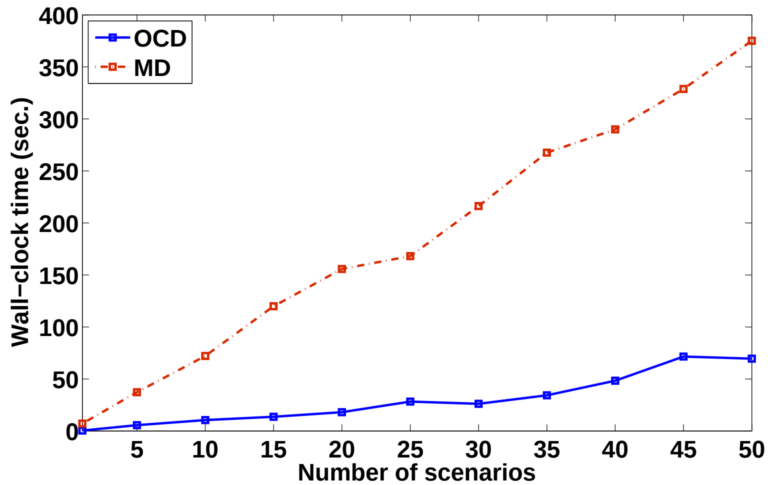


Figure 4.11: Scaling performance for OCD and MD.

### 4.8.2 IEEE New England 39-Bus System

The basic system setup of the IEEE New England 39-bus test system is stated in Section 3.8.2. The parameters and operational limits of the energy storage device are identical to the case in the WECC 9-bus system. The parameters for conventional generators including minimum/maximum power output and ramp rate limits are given in the Appendix B. The flow limits for all the transmission lines are set to 11 p.u.

Similar to the simulation for the WECC 9-bus system, fifty scenarios corresponding to fifty realizations of the wind power generation at Bus 26 for a look-ahead horizon of 4 hours (48 time steps with 5-min interval) are generated by randomly perturbing a 4-hour time series of historical wind power data within a reasonable error bound. Each scenario in the simulation is assigned an equal probability and the load profile is assumed to be deterministic over the horizon for illustration purposes. The yielding two-stage SMPC problem is considerable in size including $55,200$ decision variables, $29,339$ equality constraints and $324,438$ inequality constraints.

The same five test cases as in the WECC 9-bus system are considered in the simulation. For cases where the temporal-based decomposition is implemented, the optimal numbers of time blocks in each scenario in Case 2OCD and Case MD happen to be identical to those numbers in the 9-bus system test. Hence, there are 150 equally sized subsubproblems for Case 2OCD while Case MD has 300. There are 50 subproblems in the other two scenario-based decomposition cases.

- Case "BF": The overall SMPC problem is directly solved w/o line search.
- Case "BD": Benders decomposition is applied.
- Case "OCD": The OCD based scenario decomposition w/ line search is applied.
- Case "2OCD": The OCD based two-stage decomposition w/ line search is applied.
- Case "MD": The mixed decomposition is applied.

### Main Results

Table 4.4 shows the numerical results including the number of iterations, wall-clock time, and estimated running time in a parallel computing environment using the five different methods. The wall-clock time in Table 4.4 is the actual time measured for each case to run in the sequential computing environment. The estimated time in a parallel computing environment is calculated by dividing the corresponding wall-clock time by the number of subproblems (subsubproblems). Each major iteration refers to the outmost iteration loop and each minor iteration which is only applicable in the BD based methods corresponds to the inner loop for iteratively solving each of the scenario-based subproblems.

In terms of the estimated time for the parallel implementation, the proposed MD again performs best with over 170 times faster than the base case without any decomposition.

Table 4.4: Numerical results for the IEEE New England 39-bus system

| Cases | Total # of Major Iter. | Total # of Minor Iter. | Total # of GMRES Iter. | Wall Time in sec. | Est. Time in sec. for Par. Computing |
|---|---|---|---|---|---|
| BF | 262 | - | - | $1,864.32$ | $1,864.32$ |
| BD | 3 | $12,720$ | - | $2,856.07$ | 57.12 |
| OCD | 234 | - | $1,780$ | $1,901.33$ | 38.03 |
| 2OCD | 193 | - | $20,159$ | $8,079.91$ | 53.87 |
| MD | 3 | $14,848$ | $110,802$ | $3,228.37$ | 10.76 |

The second best method is the proposed OCD based scenario decomposition with speedup of about 49 times. In addition, MD is over 5 times faster compared to the classical BD method. Due to the computational burden on GMRES steps, the two-stage OCD fails to outperform the scenario-based OCD.

In order to verify the accuracy of the decomposed solutions, the evolution of the objective function values under the direct solution method (Case BF) and the four decomposition solution methods is shown in Fig. 4.12. The final objective function values for the four decomposition cases are exactly the same as the final objective function value obtained from the direct method. This is due to the fact that the considered problem defined by (4.3)-(4.4) is a convex problem.

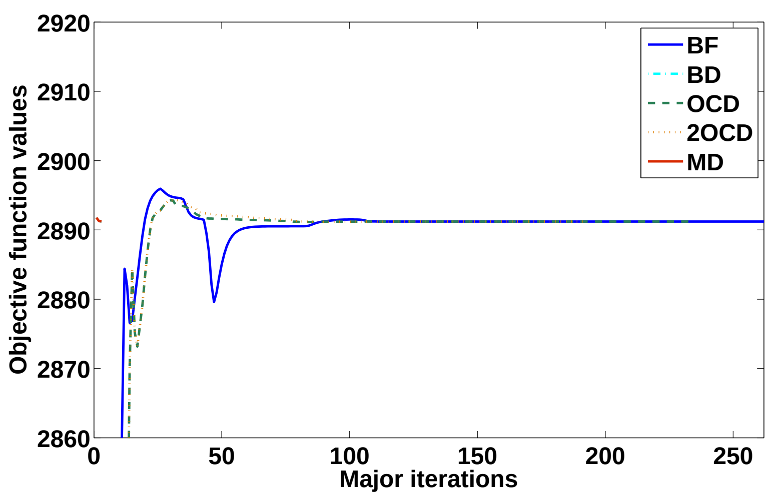


Figure 4.12: Evolution of objective function values for the IEEE New England 39-bus system.

### Trade-Off between Convergence Speed and Subsubproblem Size

For cases where the temporal-based decomposition is implemented, a trade-off between convergence speed and subsubproblem size needs to be achieved. Table 4.5 shows the numerical results for the two-stage OCD method with numbers of time blocks of each scenario ranging from 2 to 6. It can be determined that the optimal number of time blocks within each scenario for the two-stage OCD is three.

Table 4.5: Results for the two-stage OCD with different numbers of time blocks

| Number of Time Blocks | Total # of Major Iter. | Total # of GMRES Iter. | Wall Time in sec. | Est. Time in sec. for Par. Computing |
|---|---|---|---|---|
| 2 | 230 | 15,801 | 5,967.20 | 59.67 |
| 3 | 193 | 20,159 | 8,079.91 | 53.87 |
| 4 | 216 | 39,194 | 20,160.59 | 100.80 |
| 6 | 230 | 47,746 | 28,721.56 | 95.74 |

Similarly, the numerical results using MD with different numbers of time blocks in each scenario ranging from 2 to 8 are listed in Table 4.6. The estimated parallel computing time in the case with 6 time blocks is very close to the case with 8 time blocks. Given the result that the number of GMRES steps in the case with 6 time blocks is merely 40% of that number in the case with 8 time blocks but the increase in the number of minor iterations for the case with 6 time blocks is less than 15%, we conclude that the optimal number of time blocks within each scenario for MD is six.

Table 4.6: Results for MD with different numbers of time blocks

| Number of Time Blocks | Total # of Major Iter. | Total # of Minor Iter. | Total # of GMRES Iter. | Wall Time in sec. | Est. Time in sec. for Par. Computing |
|---|---|---|---|---|---|
| 2 | 3 | 12,757 | 70,642 | 2,734.98 | 27.35 |
| 3 | 3 | 12,665 | 85,029 | 2,754.69 | 18.36 |
| 4 | 3 | 14,326 | 103,802 | 3,083.87 | 15.42 |
| 6 | 3 | 14,848 | 110,802 | 3,228.37 | 10.76 |
| 8 | 3 | 12,948 | 283,050 | 4,252.78 | 10.63 |

### Importance of GMRES in OCD based Methods

Fig. 4.13 shows the evolution of the preconditioned residual norm before and after GMRES steps, implying the important role that the GMRES measure plays in the OCD based approaches (Case OCD and Case 2OCD). It can be seen from Fig. 4.13 that the pre-GMRES preconditioned residual norm in Case 2OCD is larger than that in Case OCD, verifying the slow converging behavior of the two-stage OCD we observed in Table 4.4.

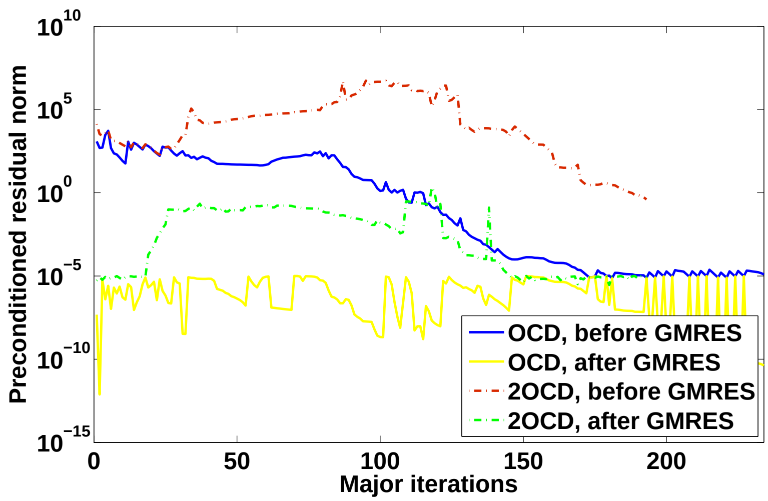


Figure 4.13: Evolution of the preconditioned residual norm before and after GMRES steps for OCD based methods.

### Importance of Line Search in OCD based Methods

The evolution of the KKT norm shown in Fig. 4.14 implies the importance of line search in the OCD based methods. By examining the curves of the two pairs of with and without line search for the two OCD based cases (Case OCD and Case 2OCD), it is evident that with the progress of the iteration process the KKT norm increases rapidly in the cases without line search implementation, which in turn demonstrates that line search is one of the most critical measures for ensuring the convergence of the proposed OCD based methods. It is interesting to observe from Fig. 4.14 that the base case without line search still manages to converge. The possible reason behind this is that the search direction is always exact in the base case compared to the situation of the decomposition cases where only approximated search directions are available.

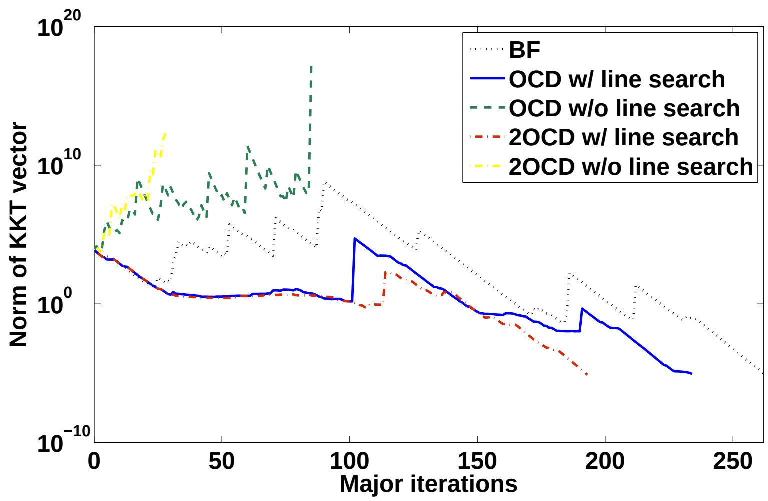


Figure 4.14: Evolution of the KKT norm for OCD based methods.

### Scaling Performance in terms of Number of Scenarios

The scaling performance of the top two proposed decomposition approaches (OCD and MD) is evaluated by measuring the wall-clock time with respect to the change in the number of scenarios in the SMPC based SCED problem. The problems with reduced numbers of scenarios are obtained by using Algorithm 2 (backward Kantorovich scenario reduction) described in Section 4.3. Fig. 4.15 shows the wall-clock time as a function of the number of scenarios using OCD and MD. The number of scenarios in OCD is equal to the number of parallelizable subproblems whereas the number of subsubproblems in MD is six times more than the number of scenarios. As can be seen in Fig. 4.15, both the two approaches exhibit a near linear scaling property, which is desired in parallel computing.

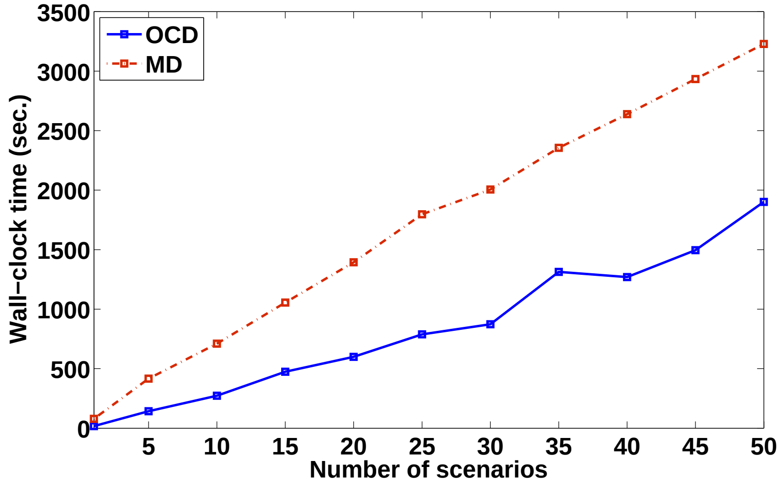


Figure 4.15: Scaling performance for OCD and MD.

## 4.9 Summary

This chapter proposes a stochastic model predictive control approach to control energy storage in power systems under increasing uncertainties introduced by variable generation resources and demand. In order to efficiently solve the resulting computationally demanding SMPC problem, three optimization decomposition schemes – OCD based scenario decomposition, OCD based two-stage decomposition, and two-stage mixed decomposition are proposed to decompose the overall problem into several subproblems, which makes the parallel implementation possible thereby reducing the computation time. Two fundamental classes of decomposition methods are briefly introduced and compared with the three proposed approaches in terms of convergence. The proposed mixed decomposition approach consisting of a Benders decomposition for the first-stage scenario-based decomposition and an optimality condition decomposition for the second-stage temporal-based decomposition outperforms all the other considered methods in the simulation.

In terms of the two OCD based methods, numerical results from both the WECC 9-bus system and the IEEE New England 39-bus system indicate that the scenario-based decomposition achieves a better trade-off between convergence speed and the number of subproblems for the considered optimal dispatch problem. The importance of line search on ensuring the convergence of those two methods is also highlighted via the simulation. In addition, we resolve the singularity issues that arise in the proposed OCD based decomposition approaches, which is applicable to the decomposition of general model predictive control problems.

# Chapter 5

# Conclusions and Future Work

In this closing chapter, the work of the dissertation is summarized and concluded, and possible directions of future work are pointed out.

## 5.1 Conclusions

This dissertation explains the basic problem of real power balancing control in power systems with high penetration of variable generation and proposes a two-level control approach consisting of advanced frequency control and stochastic optimal dispatch to tackle the problem with the objective of safe and optimal integration of energy storage devices in real power balancing control. The control actions of both the two levels are determined through optimization processes with consideration of the power and energy limits of energy storage devices. Extensive simulations on both the WECC 9-bus system and the IEEE New England 39-bus system verify the feasibility of the proposed approach.

The concept of time-scale matching for coordination between conventional generation and energy storage in real power balancing responsibilities is introduced and implemented. The proposed time-scale matching principle states that the conventional generators are mainly responsible to balance the low frequency components of the power variations whereas the energy storage devices because of their fast response capability are employed to alleviate the relatively high frequency components. The time-scale matching is ensured in the advanced frequency control level via frequency dependent weighting functions and the stochastic optimal dispatch level achieves the principle by including quadratic ramping cost terms.

In terms of the advanced frequency control level, a structure-preserving dynamic model for interconnected power systems is systematically derived based on component-level models and the DC power flow model for the control design. In addition, a model to estimate the local frequency at non-generator buses is developed to facilitate the decentralized control scheme for advanced frequency control in the design stage.

An $H_\infty$ optimization approach for enhanced frequency control with energy storage is then proposed. The problem of integrating energy storage and renewable generation with respect to real power balancing is constructed as a multi-objective $H_\infty$ optimization problem. In addition to frequency dependent weighting functions, the decentralized static output feedback is applied to achieve task-specific but easily-implementable controllers. We also show in the simulations that this $H_\infty$-based frequency control approach provides a promising means to design and coordinate decentralized proportional-integral (PI) controllers for multiple conventional generators which enables the return to the nominal frequency. As for the optimal $H_\infty$ controller gain calculation, an existing iterative linear matrix inequality algorithm involving a non-convex generalized eigenvalue minimization problem is improved by convexifying this minimization problem via heuristics.

In terms of the stochastic optimal dispatch level, the use of stochastic model predictive control for optimal dispatch considering energy storage in the future power systems is proposed to optimally and safely dispatch energy storage and conventional dispatchable generation under uncertainties for a certain period of look-ahead horizon. Due to the resulting large-scale and computationally demanding SMPC optimization problem, both the primal based (Benders decomposition) and dual based (Lagrangian relaxation decomposition and augmented Lagrangian decomposition) optimization decomposition techniques are extensively analyzed in terms of problem formulation and convergence speed. The value of decomposition is demonstrated in the simulations using the two test systems.

In order to speed up the process of solving the stochastic model predictive control based optimal dispatch problem, three decomposition approaches built upon the optimality condition decomposition are proposed and evaluated via numerical simulations. A temporal-based decomposition is introduced to achieve the tradeoff between convergence speed and subproblem size for the considered SMPC problem. Simulation results indicate that, among the three proposed approaches, the two-stage mixed decomposition scheme has the best performance record in terms of convergence speed. To the best of our knowledge, this is the first time the mixed decomposition algorithm is proposed for two-stage stochastic model predictive control problems. Under such a two-stage decomposition, each subproblem in the first stage is associated with a specific scenario for the stochastic process. The second stage further decomposes each of the scenario-based subproblems into even smaller subproblems where each corresponds to a set of time steps in the optimization horizon. In addition, we resolve the singularity issues that arise in the three proposed decomposition approaches, which is applicable to the decomposition of general model predictive control problems.

## 5.2 Future Work

In terms of the advanced frequency control level, one major concern is the increasing computational complexity in calculating the optimal controller gains for very large power systems. It is therefore worthwhile to investigate model reduction techniques to reduce the order of the system model. The caveat of using general model reduction techniques is that the stability of the original system may not be ensured. The yielding robust controllers computed based on the reduced system model must be plugged into the original model to check stability. Under certain conditions, the passivity control theory [73–75] could be employed to achieve such a goal where it is guaranteed that the calculated controllers based on the reduced model also stabilize the original system. However, this theory is not directly applicable to our case because the considered power system model including governor dynamics is not a passive network. Further research on developing model reduction techniques with stability guarantee for the decentralized static output feedback robust control is in high demand.

In addition, more research is needed to deal with the issue of network topology changes. Different network topologies are very likely to result in very different optimal controller gains for the same set of generating units, storage devices, and demands. Offline simulation and machine learning can be utilized in order for the proposed advanced frequency control to quickly adapt to the possible network topology changes. Offline simulation is used to generate training data including optimal controller gains with respect to various power network topologies whereas machine learning is employed to learn and predict the intrinsic relation between network topologies and optimal controller gains.

More importantly, the uncertainties in the parameters of the structure-preserving power system model need to be taken into consideration because in reality the task to obtain a system model with reasonable accuracy for a very large scale power network is quite challenging. One possible solution is to use the Small Gain Theorem [22] in the robust control theory to deal with the model inaccuracy where the model uncertainties are represented by an unstructured model set, which is typically a norm bounded disk uncertainty around the nominal system model.

As for the stochastic optimal dispatch level, the proposed mixed decomposition method with the best performance in terms of convergence speed needs to be further tested under a more realistic environment by implementing the algorithm on a computer cluster via message passing. In addition, while the focus of this dissertation is on the convergence aspect of the resulting computationally demanding SMPC problem at a specific time step, future work needs to evaluate the value of stochastic solution as well as the value of energy storage in terms of actual monetary cost savings by using more realistic system data and implementing the receding horizon concept, i.e. repeatedly solving the SMPC problem with a prediction horizon which keeps being shifted forward over a certain period of time.

The scaling performance of the proposed decomposition approaches with respect to the power system size is also worthwhile to investigate for the purpose of testing and anticipating their performance for very large power systems. The three proposed approaches need to be run and tested on multiple systems with different sizes so that the regression methods can then be applied to numerically determine their computational complexities in terms of the big O notation.

Last but not least, the interaction between the two proposed levels needs to be investigated. One possible way of doing this is to build a co-simulation platform that combines the stochastic decision making process and the real time frequency control so that the interaction can be numerically evaluated. The difficulty lies in the time scale difference between these two levels, which might result in a very slow simulation.

# Appendix A

# WECC 9-Bus Test System

## A.1 Dynamic and Static Generator Parameters

The dynamic and static generator parameters of the WECC 9-bus system in the simulations are modified based on [2, 42] and given in Table A.1. All the values are p.u. values, unless otherwise stated. Note that the ramp rate limits $\Delta P_G^{min}$ and $\Delta P_G^{max}$ shown below are in p.u. per minute. In addition, the nominal frequency $f_0$ is 60 Hz and the power base $S_N$ is 100 MVA and the droop coefficient $R$ for all the three generators is set to be 5%.

Table A.1: Generator parameters of the WECC 9-bus system.

| Gen # | Bus # | $S$ | $H$ (sec.) | $k_D$ | $T_{CH}$ (sec.) | $T_G$ (sec.) | $P_G^{min}$ | $P_G^{max}$ | $\Delta P_G^{min}$ | $\Delta P_G^{max}$ |
|---|---|---|---|---|---|---|---|---|---|---|
| 1 | 1 | 2.475 | 9.5515 | 2.9040 | 0.3 | 0.2 | 0.6 | 2.4 | $-0.4$ | 0.4 |
| 2 | 2 | 1.920 | 3.3333 | 2.3352 | 0.3 | 0.2 | 0.5 | 2.0 | $-0.5$ | 0.5 |
| 3 | 3 | 1.280 | 2.3516 | 2.1137 | 0.2 | 0.2 | 0.4 | 1.5 | $-0.6$ | 0.6 |

## A.2 Parameters of Transmission Lines

The transmission line parameters of the WECC 9-bus system are listed in Table A.2 [2]. All the values in Table A.2 are p.u. values.

Table A.2: Transmission line parameters of the WECC 9-bus system.

| From Bus# | To Bus# | $X$ | From Bus# | To Bus# | $X$ |
|---|---|---|---|---|---|
| 1 | 4 | 0.0576 | 5 | 7 | 0.1610 |
| 2 | 7 | 0.0625 | 6 | 9 | 0.1700 |
| 3 | 9 | 0.0586 | 7 | 8 | 0.0720 |
| 4 | 5 | 0.0850 | 8 | 9 | 0.1008 |
| 4 | 6 | 0.0920 | | | |

# Appendix B

# IEEE New England 39-Bus Test System

## B.1 Dynamic and Static Generator Parameters

The dynamic and static generator parameters of the IEEE New England 39-bus system in the simulations are modified based on [5, 42] and given in Table B.1. All the values are p.u. values, unless otherwise stated. Note that the ramp rate limits $\Delta P_G^{min}$ and $\Delta P_G^{max}$ shown below are in p.u. per minute. In addition, the nominal frequency $f_0$ is 60 Hz and the power base $S_N$ is 100 MVA and the droop coefficient $R$ for all the ten generators is set to be 5%.

Table B.1: Generator parameters of the IEEE New England 39-bus system.

| Gen # | Bus # | $S$ | $H$ (sec.) | $k_D$ | $T_{CH}$ (sec.) | $T_G$ (sec.) | $P_G^{min}$ | $P_G^{max}$ | $\Delta P_G^{min}$ | $\Delta P_G^{max}$ |
|---|---|---|---|---|---|---|---|---|---|---|
| 1 | 39 | 10.0 | 500.0 | 100.02 | 0.3 | 0.2 | 7.0 | 10.0 | −0.06 | 0.06 |
| 2 | 31 | 7.0 | 30.3 | 6.07 | 0.3 | 0.2 | 4.0 | 7.0 | −0.34 | 0.34 |
| 3 | 32 | 7.0 | 35.8 | 7.16 | 0.3 | 0.2 | 4.0 | 7.0 | −0.34 | 0.34 |
| 4 | 33 | 7.0 | 28.6 | 5.73 | 0.3 | 0.2 | 4.0 | 7.0 | −0.32 | 0.32 |
| 5 | 34 | 6.0 | 26.0 | 5.20 | 0.3 | 0.2 | 3.0 | 6.0 | −0.28 | 0.28 |
| 6 | 35 | 7.0 | 34.8 | 6.97 | 0.3 | 0.2 | 4.0 | 7.0 | −0.32 | 0.32 |
| 7 | 36 | 6.0 | 26.4 | 5.28 | 0.3 | 0.2 | 3.0 | 6.0 | −0.28 | 0.28 |
| 8 | 37 | 6.0 | 24.3 | 4.86 | 0.3 | 0.2 | 3.0 | 6.0 | −0.26 | 0.26 |
| 9 | 38 | 9.0 | 34.5 | 6.90 | 0.3 | 0.2 | 6.0 | 9.0 | −0.28 | 0.28 |
| 10 | 30 | 4.0 | 42.0 | 8.41 | 0.3 | 0.2 | 2.0 | 4.0 | −0.18 | 0.18 |

## B.2 Parameters of Transmission Lines

The transmission line parameters of the IEEE New England 39-bus system are listed in Table B.2 [5]. All the values in Table B.2 are p.u. values.

Table B.2: Transmission line parameters of the IEEE New England 39-bus system.

| From Bus# | To Bus# | $X$ | From Bus# | To Bus# | $X$ |
|---|---|---|---|---|---|
| 1 | 2 | 0.0411 | 14 | 15 | 0.0217 |
| 1 | 39 | 0.0250 | 15 | 16 | 0.0094 |
| 2 | 3 | 0.0151 | 16 | 17 | 0.0089 |
| 2 | 25 | 0.0086 | 16 | 19 | 0.0195 |
| 2 | 30 | 0.0181 | 16 | 21 | 0.0135 |
| 3 | 4 | 0.0213 | 16 | 24 | 0.0059 |
| 3 | 18 | 0.0133 | 17 | 18 | 0.0082 |
| 4 | 5 | 0.0128 | 17 | 27 | 0.0173 |
| 4 | 14 | 0.0129 | 19 | 20 | 0.0138 |
| 5 | 6 | 0.0026 | 19 | 33 | 0.0142 |
| 5 | 8 | 0.0112 | 20 | 34 | 0.0180 |
| 6 | 7 | 0.0092 | 21 | 22 | 0.0140 |
| 6 | 11 | 0.0082 | 22 | 23 | 0.0096 |
| 6 | 31 | 0.0250 | 22 | 35 | 0.0143 |
| 7 | 8 | 0.0046 | 23 | 24 | 0.0350 |
| 8 | 9 | 0.0363 | 23 | 36 | 0.0272 |
| 9 | 39 | 0.0250 | 25 | 26 | 0.0323 |
| 10 | 11 | 0.0043 | 25 | 37 | 0.0232 |
| 10 | 13 | 0.0043 | 26 | 27 | 0.0147 |
| 10 | 32 | 0.0200 | 26 | 28 | 0.0474 |
| 11 | 12 | 0.0435 | 26 | 29 | 0.0625 |
| 12 | 13 | 0.0435 | 28 | 29 | 0.0151 |
| 13 | 14 | 0.0101 | 29 | 38 | 0.0156 |

# Bibliography


[1] G. Andersson, "Lecture notes on dynamics and control of electric power systems," ETH Zurich, 2012.

[2] P. M. Anderson and A. A. Fouad, *Power System Control and Stability*, Wiley - IEEE Press, 2nd edition, 2003.

[3] "Product manual 82560: EG-3P actuator," Woodward Company, 2014.

[4] P. Kundur, *Power system stability and control*, McGraw-Hill, USA, 1994.

[5] M. A. Pai, *Energy Function Analysis for Power System Stability*, Springer, 1989.

[6] C. Monteiro, R. Bessa, V. Miranda, A. Botterud, J. Wang, and G. Conzelmann, "Wind power forecasting: State-of-the-art 2009," Tech. Rep. ANL/DIS-10-1, Argonne National Laboratory, 2009.

[7] Peder Bacher, Henrik Madsen, and Henrik Aalborg Nielsen, "Online short-term solar power forecasting," *Solar Energy*, vol. 83, no. 10, pp. 1772–1783, 2009.

[8] J. P. Barton and D. G. Infield, "Energy storage and its use with intermittent renewable energy," *IEEE Trans. Energy Convers.*, vol. 19, no. 2, pp. 441–448, 2004.

[9] V. Vittal, "The impact of renewable resources on the performance and reliability of the electricity grid," *The bridge*, vol. 40, no. 1, pp. 5–12, 2010.

[10] M. Beaudin, H. Zareipour, A. Schellenberglabe, and W. Rosehart, "Energy storage for mitigating the variability of renewable electricity sources: An updated review," *Energy for Sustainable Development*, vol. 14, no. 4, pp. 302–314, 2010.

[11] R. Fioravanti, Vu Khoi, and W. Stadlin, "Large-scale solutions," *IEEE Power Energy Mag.*, vol. 7, no. 4, pp. 48–57, 2009.

[12] S. Chu and A. Majumdar, "Opportunities and challenges for a sustainable energy future," *Nature*, vol. 488, no. 7411, pp. 294–303, 2012, 10.1038/nature11475.

[13] J. M. Carrasco, L. G. Franquelo, J. T. Bialasiewicz, E. Galvan, R. C. P. Guisado, Ma A. M. Prats, J. I. Leon, and N. Moreno-Alfonso, "Power-electronic systems for the grid integration of renewable energy sources: A survey," *IEEE Trans. Ind. Electron.*, vol. 53, no. 4, pp. 1002–1016, 2006.

[14] D. Lew, G. Brinkman, N. Kumar, P. Besuner, D. Agan, and S. Lefton, "Impacts of wind and solar on fossil-fueled generators," in *Proc. IEEE Power and Energy Society General Meeting*, 2012.

[15] A. Oudalov, T. Buehler, and D. Chartouni, "Utility scale applications of energy storage," in *Energy 2030 Conference*, 2008.

[16] S. C. Smith, P. K. Sen, and B. Kroposki, "Advancement of energy storage devices and applications in electrical power system," in *Power and Energy Society General Meeting - Conversion and Delivery of Electrical Energy in the 21st Century, 2008 IEEE*, 2008, pp. 1–8.

[17] K. C. Divya and Jacob Østergaard, "Battery energy storage technology for power systems–an overview," *Electric Power Systems Research*, vol. 79, no. 4, pp. 511–520, 2009.

[18] Ioannis Hadjipaschalis; Andreas Poullikkas; Venizelos Efthimiou, "Overview of current and future energy storage technologies for electric power applications," *Renewable and Sustainable Energy Reviews*, vol. 13, no. 6-7, pp. 10, 2008.

[19] P. F. Ribeiro, B. K. Johnson, M. L. Crow, A. Arsoy, and Y. Liu, "Energy storage systems for advanced power applications," *Proceedings of the IEEE*, vol. 89, no. 12, pp. 1744–1756, 2001.

[20] M. L. Lazarewicz and T. M. Ryan, "Integration of flywheel-based energy storage for frequency regulation in deregulated markets," in *Proc. IEEE Power and Energy Society General Meeting*, 2010.

[21] J. Cleary, M. L. Lazarewicz, L. Nelson, R. Rounds, and J. Arsenault, "Interconnection study: 5MW of Beacon Power flywheels on 23 kV line – Tyngsboro, MA," in *Proc. Conf. on Innovative Technologies for an Efficient and Reliable Electricity Supply*, 2010.

[22] K. Zhou, J.C. Doyle, and K. Glover, *Robust and Optimal Control*, Prentice Hall, 1995.

[23] K. Zhou and J.C. Doyle, *Essentials of robust control*, Prentice Hall, 1998.

[24] D. Rerkpreedapong, A. Hasanovic, and A. Feliachi, "Robust load frequency control using genetic algorithms and linear matrix inequalities," *IEEE Trans. Power Syst.*, vol. 18, no. 2, pp. 855–861, 2003.

[25] H. Bevrani, Y. Mitani, and K. Tsuji, "Robust decentralised load-frequency control using an iterative linear matrix inequalities algorithm," *IEE Generation, Transmission and Distribution*, vol. 151, no. 3, pp. 347–354, 2004.

[26] J. Liu, B. H. Krogh, and B. E. Ydstie, "Decentralized robust frequency control for power systems subject to wind power variability," in *Proc. IEEE Power and Energy Society General Meeting*, 2011.

[27] W. Katzenstein and J. Apt, "Air emissions due to wind and solar power," *Environ. Sci. Technol.*, vol. 43, no. 2, pp. 253–258, 2009.

[28] S. Dechanupaprittha, K. Hongesombut, M. Watanabe, Y. Mitani, and I. Ngamroo, "Stabilization of tie-line power flow by robust SMES controller for interconnected power

system with wind farms," *IEEE Trans. Appl. Supercond.*, vol. 17, no. 2, pp. 2365–2368, 2007.

[29] B. C. Pal, A. H. Coonick, I. M. Jaimoukha, and H. El-Zobaidi, "A linear matrix inequality approach to robust damping control design in power systems with superconducting magnetic energy storage device," *IEEE Trans. Power Syst.*, vol. 15, no. 1, pp. 356–362, 2000.

[30] R. de Castro, R. E. Araujo, J. P. F. Trovao, P. G. Pereirinha, P. Melo, and D. Freitas, "Robust DC-link control in EVs with multiple energy storage systems," *IEEE Trans. Veh. Technol.*, vol. 61, no. 8, pp. 3553–3565, 2012.

[31] F. Liu, S. Mei, D. Xia, Y. Ma, X. Jiang, and Q. Lu, "Experimental evaluation of nonlinear robust control for SMES to improve the transient stability of power systems," *IEEE Trans. Energy Convers.*, vol. 19, no. 4, pp. 774–782, 2004.

[32] T. Goya, E. Omine, Y. Kinjyo, T. Senjyu, A. Yona, N. Urasaki, and T. Funabashi, "Frequency control in isolated island by using parallel operated battery systems applying H infinity control theory based on droop characteristics," *IET Renewable Power Generation*, vol. 5, no. 2, pp. 160–166, 2011.

[33] M. Chawla, R. Naik, R. Burra, and H. Wiegman, "Utility energy storage life degradation estimation method," in *Proc. Conf. on Innovative Technologies for an Efficient and Reliable Electricity Supply*, 2010.

[34] G. Lalor, J. Ritchie, S. Rourke, D. Flynn, and M. J. O'Malley, "Dynamic frequency control with increasing wind generation," in *Proc. IEEE Power and Energy Society General Meeting*, 2004.

[35] J. Nutaro and V. Protopopescu, "Calculating frequency at loads in simulations of electro-mechanical transients," *IEEE Trans. Smart Grid*, vol. 3, no. 1, pp. 233–240, 2012.

[36] S. Skogestad and I. Postlethwaite, *Multivariable feedback control: analysis and design*, John Wiley & Sons, 2nd edition, 2005.

[37] P. Gahinet and P. Apkarian, "A linear matrix inequality approach to H infinity control," *International Journal of Robust and Nonlinear Control*, vol. 4, pp. 421–448, 1994.

[38] Y. Y. Cao, J. Lam, and Y. X. Sun, "Static output feedback stabilization: An ILMI approach," *Automatica*, vol. 34, no. 12, pp. 1641–1645, 1998.

[39] M. Grant and S. Boyd, "CVX: Matlab software for disciplined convex programming," 2011.

[40] K. W. Cheung, "Ancillary service market design and implementation in north america: From theory to practice," in *Proc. Conf. Electric Utility Deregulation and Restructuring and Power Technologies*, 2008.

[41] PJM, *Manual 11: Energy and Ancillary Services Market Operations*, 2014.

[42] J. Liu, *Decentralized robust frequency control for power systems subject to wind power variability*, Ph.D. thesis, Carnegie Mellon University, 2011.

[43] R. N. Anderson, A. Boulanger, W. B. Powell, and W. Scott, "Adaptive stochastic control for the smart grid," *Proceedings of the IEEE*, vol. 99, no. 6, pp. 1098–1115, 2011.

[44] A. Tuohy, P. Meibom, E. Denny, and M. O'Malley, "Unit commitment for systems with significant wind penetration," *IEEE Trans. on Power Systems*, vol. 24, no. 2, pp. 592–601, 2009.

[45] P. Patrinos, S. Trimboli, and A. Bemporad, "Stochastic MPC for real-time market-based optimal power dispatch," in *Proc. Conf. Decision and Control and European Control*, 2011.

[46] M. Goonewardena and Le Long Bao, "Charging of electric vehicles utilizing random wind: A stochastic optimization approach," in *IEEE Globecom Workshops*, 2012, pp. 1520–1525.

[47] L. Xie and M. D. Ilic, "Model predictive dispatch in electric energy systems with intermittent resources," in *Proc. Conf. Systems, Man and Cybernetics*, 2008.

[48] X. Xia, J. Zhang, and A. Elaiw, "A model predictive control approach to dynamic economic dispatch problem," in *Proc. IEEE PowerTech*, 2009.

[49] M. D. Ilic, L. Xie, and J. Y. Joo, "Efficient coordination of wind power and price-responsive demand - part i: Theoretical foundations," *IEEE Trans. Power Systems*, vol. 26, no. 4, pp. 1875–1884, 2011.

[50] A. Hooshmand, M. H. Poursaeidi, J. Mohammadpour, H. A. Malki, and K. Grigoriads, "Stochastic model predictive control method for microgrid management," in *Proc. IEEE ISGT*, 2012.

[51] D. Phan and S. Ghosh, "A two-stage non-linear program for optimal electrical grid power balance under uncertainty," in *Proc. Conf. Simulation*, 2011.

[52] M. Lubin, C. G. Petra, M. Anitescu, and V. Zavala, "Scalable stochastic optimization of complex energy systems," in *Proc. Conf. High Performance Computing, Networking, Storage and Analysis*, 2011.

[53] J. Dupacova, N. Gröwe-kuska, and W. Römisch, "Scenario reduction in stochastic programming: An approach using probability metrics," *Math. Program.*, vol. 95, no. 3, pp. 493–511, 2003.

[54] N. Growe-Kuska, H. Heitsch, and W. Romisch, "Scenario reduction and scenario tree construction for power management problems," in *Proc. IEEE Power Tech*, 2003, vol. 3.

[55] N. Z. Shor, Krzysztof C. Kiwiel, and Andrzej Ruszcayǹski, *Minimization Methods for Non-differentiable Functions*, Springer-Verlag New York, Inc., New York, NY, USA, 1985.

[56] J. E. Kelley, "The cutting plane method for solving convex programs," *Journal of the SIAM*, vol. 8, pp. 703–712, 1960.

[57] Jack Elzinga and ThomasG. Moore, "A central cutting plane algorithm for the convex programming problem," *Mathematical Programming*, vol. 8, no. 1, pp. 134–145, 1975.

[58] J. F. Benders, "Partitioning procedures for solving mixed-variables programming problems," *Numerische Mathematik*, vol. 4, no. 1, pp. 238–252, 1962.

[59] A. M. Geoffrion, "Generalized Benders decomposition," *Journal of Optimization Theory and Applications*, vol. 10, no. 4, pp. 237–260, 1972.

[60] M. J. Bagajewicz and V. Manousiouthakis, "On the generalized Benders decomposition," *Computers & Chemical Engineering*, vol. 15, no. 10, pp. 691–700, 1991.

[61] A. J. Conejo, E. Castillo, R. Minguez, and R. Garcia-Bertrand, *Decomposition Techniques in Mathematical Programming*, Springer, 2006.

[62] G. Cohen, "Auxiliary problem principle and decomposition of optimization problems," *Journal of Optimization Theory and Applications*, vol. 32, no. 3, pp. 277–305, 1980.

[63] David Luenberger and Ye, *Linear and Nonlinear Programming*, Springer, third edition, 2008.

[64] Dimitri P. Bertsekas and Dimitri P. Bertsekas, *Nonlinear Programming*, Athena Scientific, 2nd edition, Sept. 1999.

[65] R. T. Rockafellar and R. J.-B. Wets, "Scenarios and policy aggregation in optimization under uncertainty," *Mathematics of Operations Research*, vol. 16, no. 1, pp. 119–147, 1991.

[66] A. J. Conejo, F. J. Nogales, and F. J. Prieto, "A decomposition procedure based on approximate newton directions," *Mathematical Programming*, vol. 93, no. 3, pp. 495–515, 2002.

[67] G. Tognola and R. Bacher, "Unlimited point algorithm for OPF problems," *IEEE Trans. Power Systems*, vol. 14, no. 3, pp. 1046–1054, 1999.

[68] Y. Saad, *Iterative Methods for Sparse Linear Systems*, Society for Industrial and Applied Mathematics, 2nd edition, 2003.

[69] G. Hug-Glanzmann and G. Andersson, “Decentralized optimal power flow control for overlapping areas in power systems,” *IEEE Trans. on Power Systems*, vol. 24, no. 1, pp. 327–336, 2009.

[70] J. E. Dennis and R. B. Schnabel, *Numerical Methods for Unconstrained Optimization and Nonlinear Equations*, Classics in Applied Mathematics. Society for Industrial and Applied Mathematics, 1996.

[71] W. H. Press, S. A. Teukolsky, W. T. Vetterling, and B. P. Flannery, *Numerical Recipes: The Art of Scientific Computing*, Cambridge University Press, 3rd edition, 2007.

[72] Panos Parpas and Berç Rustem, “Computational assessment of nested benders and augmented lagrangian decomposition for mean-variance multistage stochastic problems,” *INFORMS Journal on Computing*, vol. 19, no. 2, pp. 239–247, Apr. 2007.

[73] J. C. Willems, “Dissipative dynamical systems part I: General theory,” *Archive for Rational Mechanics and Analysis*, vol. 45, no. 5, pp. 321–351, 1972.

[74] J. C. Willems, “Dissipative dynamical systems part II: Linear systems with quadratic supply rates,” *Archive for Rational Mechanics and Analysis*, vol. 45, no. 5, pp. 352–393, 1972.

[75] J. Bao and P. L. Lee, *Process Control: The Passive Systems Approach*, Springer-Verlag London, 2007.